Electronic and Magnetic Properties of trans-Polyacetylene

by

Luis R. Cruz-Cruz

B.S. University of Puerto Rico, 1985.
M.S. University of Puerto Rico, 1989.

Submitted to the Department of Physics
in partial fulfillment of the requirements for the degree of
Doctor of Philosophy
at the

MASSACHUSETTS INSTITUTE OF TECHNOLOGY

May 1994

Author .....
Department of Physics
May 9, 1994

Certified by .....
Philip Phillips
Professor of Physics
Thesis Supervisor

Certified by .....
Boris L. Altshuler
Professor of Physics
Thesis Co-Supervisor

Accepted by .....
George F. Koster
Chairman of the Physics Graduate Committee

Electronic and Magnetic Properties of trans-Polyacetylene

by

Luis R. Cruz-Cruz

Submitted to the Department of Physics
on May 9, 1994, in partial fulfillment of the
requirement for the degree of
Doctor of Philosophy

Abstract

In the first part of this work we present a study of the stability of soliton and polaron excitations in a single strand of trans-polyacetylene. We proceed by first solving exactly the continuum version of the SSH Hamiltonian for the single particle states that arise when n-doped electrons are added to a single polymer chain. The role of on-site (U), nearest-neighbor (V), and bond repulsion (W) Coulomb interactions are obtained from a first-order perturbative calculation with the exact single-particle states. By minimizing the total energy we show that, at a fixed doping level, a polaron lattice is favored over a soliton configuration provided that U and V exceed critical values. However, as the doping level is increased, we show that these critical values increase beyond experimentally-accepted estimates. Our work then supports the view of a soliton lattice that persists into the metallic phase of polyacetylene. In addition, we show that the bound state soliton levels merge to fill the gap sufficiently that the magnetic susceptibility becomes non-zero and comparable to the corresponding experimental values. This picture also accounts for the onset of a Pauli susceptibility at a doping level of 6% in terms of the rate of closure of the gap.

In the second part, the transport properties in the highly doped regime are analyzed considering the density of states of an impurity in the chain. It is calculated as a function of the atomic impurity level and the hybridization energy. The inclusion of a gap in the spectrum of the chain takes into account the remaining charge alternation pattern observed in this high doping regime. It is shown that a Kondo-like resonance exists at the top of the gap and that a $\log T$ behavior should be exhibited in the resistivity of the sample, as experiments have revealed. It is shown that in order to observe the Kondo resonance, the gap must be smaller than the Kondo Temperature of the system without the gap.

Thesis Supervisor: Philip Phillips
Title: Professor of Physics

Acknowledgements

I want to express my sincere thanks to my advisor Prof. Philip Phillips for his continuous support throughout the time that the research leading to this thesis was in progress. His commitment to serious and dedicated research is a model to me and to the ones surrounding him. Not only in the professional aspects has he shown concern but also in the more personal level he demonstrated real commitment towards my work and well being.

I also want to extend my gratitude to the Department of Physics for their service and support through all these five years at MIT. I want to thank my thesis co-supervisor, Prof. Boris Altshuler for his patience and service and also my thesis committee for their comments and corrections. The support of all my close friends has been invaluable to me specially of my class-mate Robin Côte and my office-mate Günter Schmid. Also, the department of Chemistry deserves my thanks and all the people in the "zoo" for their friendship and laughs.

My family has always supported me and their continuing concern and care have definitely played a decisive role. I want to thank them for keeping me in their prayers that undoubtedly pulled me through these years. Lastly, but most importantly, I want to thank my wife Sandra for her continuing understanding, patience, warmth, and love throughout the hardships and labor of this thesis. Without her support this thesis would have been impossible.

Contents

List of Figures

Chapter 1

Introduction.

The doping dependence of the electronic and magnetic properties of trans Polyacetylene (PA) have challenged experimentalists and theoreticians for quite some times. At the heart of the PA story are the onset of a Pauli susceptibility at a doping level of 6%, and the nature of the log$T$ behavior in the resistivity of heavily doped samples. It is precisely these two problems that we focus on here in this thesis. As a consequence, this work will help illuminate a key outstanding problem regarding PA, namely, the nature of the charge carriers in the system in the highly doped regime.

The interest in PA stems from the fact that its conductivity as a function of doping ranges from $\sigma \sim 10^{-6}$ to $\sigma \sim 10^{5}$S/cm [1]. In addition to the high conductivity, PA is useful technologically because it can be reversibly doped [2]. Also, the lack of metallic temperature behavior in the conductivity at the highly doped regime ($p \sim 10\%$) indicates that perhaps the measured properties are not intrinsic and still higher values of σ could be attained [3]. Theoretically, this activated behavior in the conductivity is problematic because such high conductivity is generally not associated with activated transport. This discrepancy poses questions as to the origin of its high conductivity in the highly doped regime. In addition, the magnetic properties exhibit an onset of a metallic magnetic susceptibility at around a doping level of $p \sim 6\%$ [4]. At this doping level the conductivity is on the

order of 100S/cm. At low doping, charged soliton excitations have been shown to be the predominant species that dominate the physics and chemistry [5]. However, because charged solitons are spinless, the onset of the magnetic susceptibility at $p \sim 6\%$ would be difficult to be attributed to such charge carriers. A key result that is established in the present work is that the soliton level distribution can lead to an emergence of a Pauli susceptibility as a function of doping.

In this chapter a brief account of the basic experimental and theoretical aspects of PA is given. The four sections deal with the most important aspects that are relevant and of interest in PA. The four topics are the morphology of the system and its relevance to the physical properties, the excitations that dominate the physics, magnetic properties as studied by measurements of the magnetic susceptibility, and the conductivity.

1.1. Morphology.

A key to the understanding of the physical phenomena involved in PA is its morphology. PA a planar molecule with carbon atoms in an sp_2 hybridization constituting its backbone. This type of hybridization gives rise to one dangling p_z-bond per atomic site that associate in pairs to form π-bonds. The σ-electrons, forming tighter bonds than the π-electrons, are responsible for the strong intrachain forces that maintain the integrity of the chains even as doping is achieved (figure 1.1). The distribution of these two alternating and different lengths (arising from the alternation of σ- and π-bonds) creates an insulator of what otherwise would have been a 1-d half-filled metal. In most samples, PA strands tend to arrange in a crystalline structure depicted in figure 1.2(a) [6]. The interchain spaces will play a major role in the doping dynamics and overall properties of the doped material because the impurities will gather and diffuse through them. The crystalline phases are themselves encompased in superstructural fibrils of about $\sim$ 200A in diameter (figure 1.2(b)).

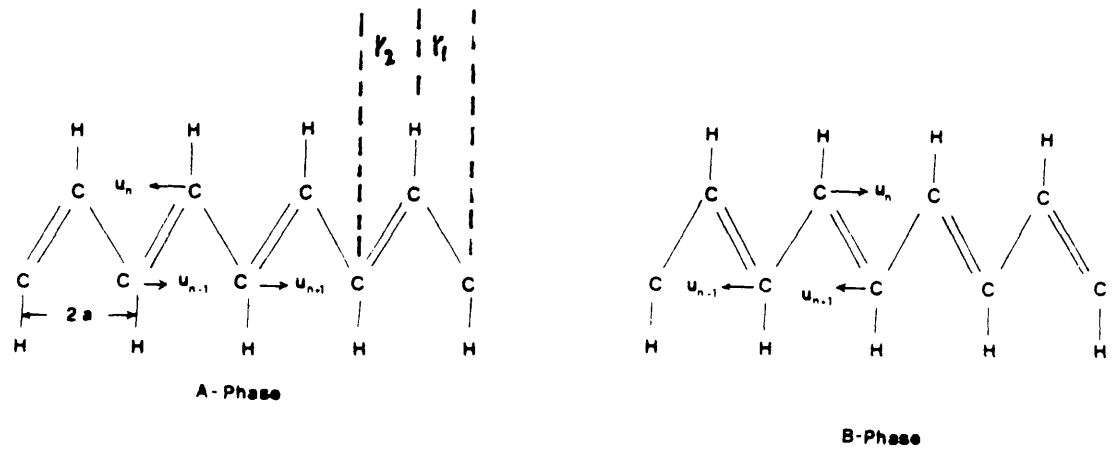

Figure 1.1. Sketch of the two degenerate phases of PA. The u_n represent the relative shift from the equillibrium position of the carbon atoms due to the double bond. The distances r_1 and r_2 indicate this relation where $r_1 > r_2$.

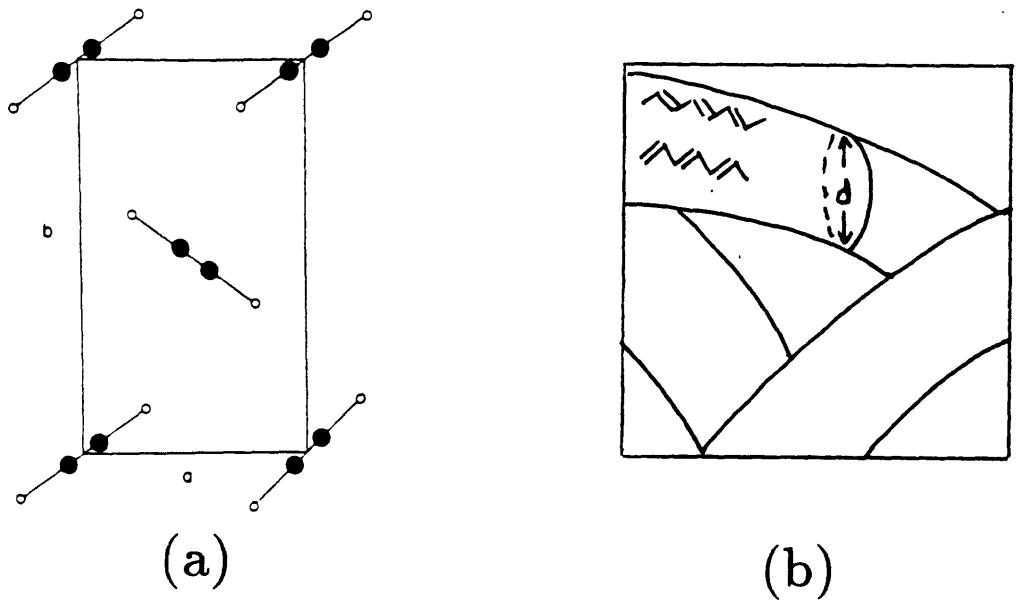

Figure 1.2. (a) Schematic projection of the structure of PA where $a = 4.24A$ and $b = 7.32A$. (b) Superstructural fibrils containing the PA chains.

This complex arrangement locks the system with an open morphology (high surface area) while weak interchain forces permit a reversible doping mechanism at room temperature. Because dopants have to travel at most 100A to get to any chain, this also yields fast doping dynamics. Regarding the role of the impurities in PA, studies show that there is complete charge transfer between the dopant atom and the PA chains and that charge carriers reside on the chains [7]. However, the role of the dopant atoms do not end there, adding point sources of Coulombic electrical fields to the system. In the light of this hierarchy of structures then one concludes that in order to account for the macroscopic transport properties, interfibrilar transport, interchain hoping, and breaks in single chains should be taken into account [5].

The alternating distribution of the two inter-site distances described previously renders the pristine or undoped system an insulator with a gap. This undoped π-electron band can be very simply accounted for by considering a simple tight-binding model of the backbone containing two different hopping electron probabilities t_1 and t_2. Usual values for these are $t_1 = 3.65$eV and $t_2 = 2.75$eV. This alternating arrangement can be mapped into a uniformly periodic atomic chain with site energies $\epsilon = (t_1^2 + t_2^2)/E$ and intersite hopping $V = t_1 t_2/E$. Solving the eigenvalue equation

$$(E - E_n)C_n = V(C_{n+1} + C_{n-1}) \tag{1.1}$$

where C_n are the electronic amplitudes at site n, we get for the energy as a function of wavenumber

$$\begin{aligned} E(k) =& \epsilon + 2V\cos(2ka) \\ =& \pm\sqrt{t_1^2 + t_2^2 + 2t_1 t_2 \cos(2ka)}. \end{aligned} \tag{1.2}$$

This spectrum is depicted in figure 1.3. Usual values for the size of the band and gap are $W = 12.8$eV $(4t_o)$ and $2\Delta_o = 1.8$eV. The gap of $2\Delta_o$ renders the undoped phase of PA an insulator.

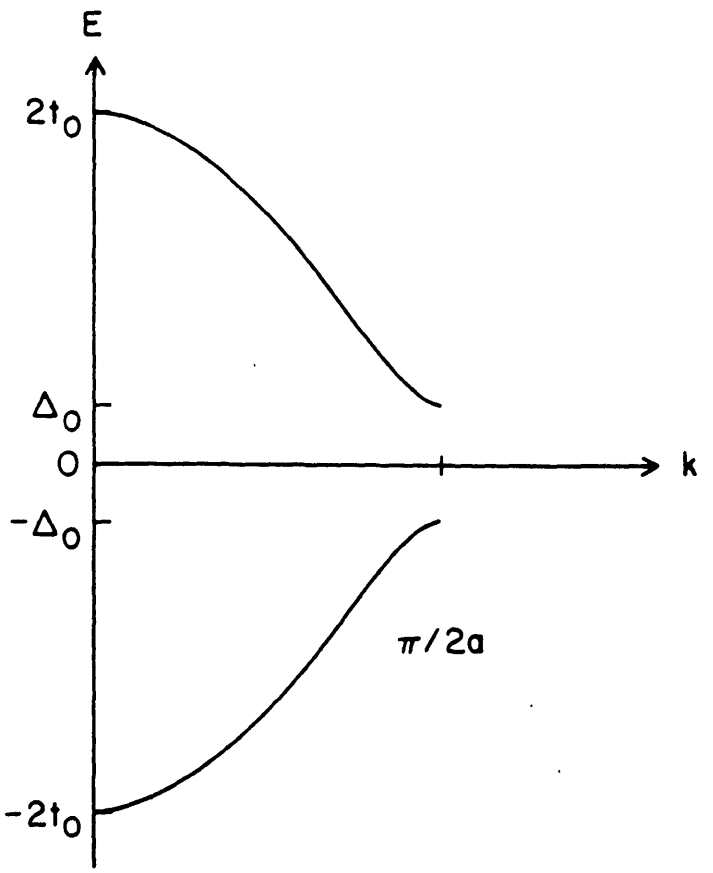

Figure 1.3. One-dimensional tight-binding band structure. The total gap $2\Delta_o$ arises from the electron-phonon interaction. t_o is the electron hopping term and a the lattice constant.

1.2. Excitations.

In addition to electrons and holes as elementary excitations in PA, there are also polarons and solitons. A polaron consists basically of a self localized charge distribution. This charge is distributed over a series of adjacent sites. Solitons can also exist as stable excitations forming the domain wall separating the two degenerate ground states of PA [8]. In the same way as polarons, solitons have a charge density that extends over a series of neighboring sites. On the other hand, only odd or even numbered sites will actually have some of this charge density allocated to them. A point of further distinction is the fact that solitons exhibit opposite charge-spin relations to the ones exhibited by normal charges. These points will be made clearer in what follows.

Consider the two degenerate phases A and B where each one corresponds to having the π-electons in one of the two sides of the backbone (figure 1.1). These two phases can be joined together by a domain wall which can be considered as a topological defect, or soliton. To this defect there is associated a width 2ξ that is of the order of $\xi \sim 7a$, where a is the lattice constant [8]. An order parameter can also be defined as being the relative distance from site to site. If site n is displaced a distance u_n from equillibrium, let us define then the order parameter by $\Delta_n \equiv (-1)^n u_n$. This makes the order parameter a measure of the displacement away from equillibrium of the set of sites in the chain. For a uniformly dimerized PA chain $|u_n - u_{n+1}| = 2u_o$. This prompts us to define $u_n = (-1)^n u_o$ which results in an order parameter $\Delta_n = \pm u_o$ (+ for phase A and − for phase B). In this way the order parameter for a chain of a single phase is given by a constant value of magnitude $|u_o|$. Because $\Delta_n = \pm u_o$, then having the two phases in a chain implies figure 1.4(a), where 2ξ is the region of "transition" between each phase. Studies show that $\Delta(x) = \Delta_o \tanh(kx)$ where $\Delta(x)$ is the continuum version of the order parameter. The parameter k is the wavenumber associated to the soliton.

To every domain wall or soliton there can be assigned a midgap state. There

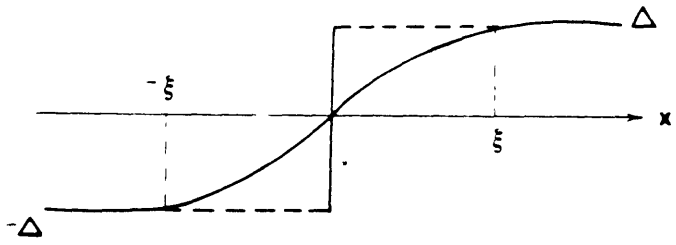

(a)

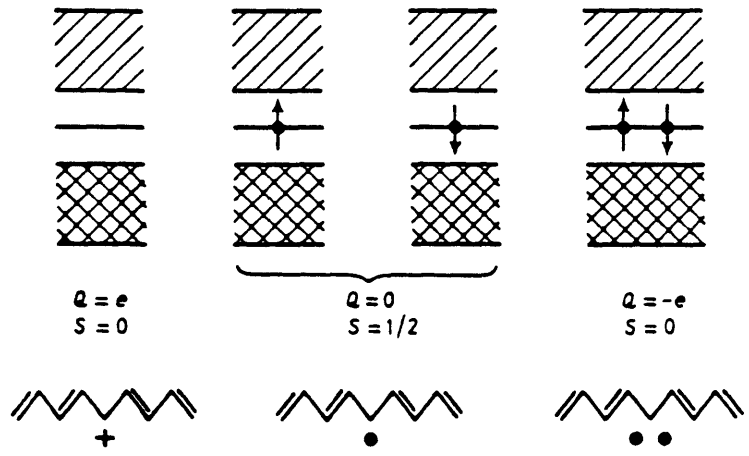

(b)

Figure 1.4. (a) Order parameter for the soliton of width ξ. At large values of x away from the domain wall the order parameter assumes the constant value corresponding to the relevant phase. (b) shows the three possible soliton configurations with their respective occupation numbers and the molecular analog for each.

are three basic possibilities for a soliton, as is depicted in figure 1.4(b). The inverse charge-spin relations make this excitation a very interesting one. The neutral soliton can be realized in practice by considering an odd-numbered chain. Because chains prefer to end with a double bond at both ends, an odd-numbered chain will have by definition two distinct phases at each extreme. Somewhere in the middle they have to join, thus forming the neutral soliton. It is neutral because no charge has been added to it, but possesses spin 1/2 which belongs to the "extra" π orbital (net spin 1/2) of net charge zero. The two other realizations are possible by either adding (negative soliton) or taking (positive soliton) a charge from the chain already containing a neutral soliton, for example. In the case of adding one electron, the extra electron would pair with the existing π-electron thus cancelling out the spin, but adding a charge $-e$. The same argument applies as well for the case of extracting a charge $-e$. The creation energy for a soliton is calculated to be $E_s = 2\Delta_o/\pi$ [9].

Consider now the case of polarons. Because a polaron is simply a localized charge with a width, there will be a local distortion of the distribution of bonds around the polaron. Because the charge spreads over a region without causing any phase change, the polarons are non-topological excitations. Therefore, they can exists in chains that are in a single phase. The order parameter for a polaron is represented in the same way as in the soliton case (figure 1.5(a)). The distortion of the π-electron cloud is seen only locally. The lack of any topological constraint makes the polaron formation in a chain the preferred one when a single electron is introduced into the chain. The energy levels for a polaron are a distance $\Delta_o/\sqrt{2}$ from the center of the gap (figure 1.5(b)). The creation energy for a polaron is calculated to be $E_p = 2\sqrt{2}\Delta_o/\pi$ [10, 11].

Experiments can confirm the existence of polarons. This comes from the fact that the charge transferred from the impurity to the chains is pinned to the impurity. This is the situation to be expected if one considers the charge transfer to be localized in polaron excitations. Further doping indicates a "de-pinning" of the charges in the chain. This "de-pinning" is closely related to the formation of

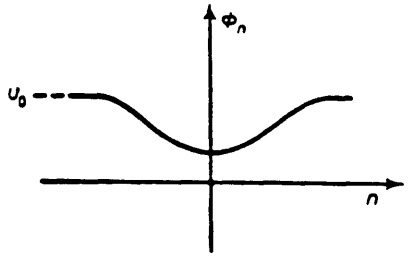

(a)

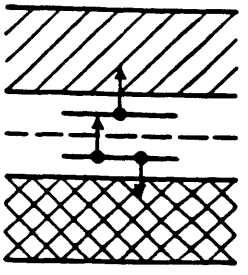

(b)

Figure 1.5. (a) Order parameter and (b) band diagram for a polaron. An electron is missing from the upper state for an electron polaron, and only a single electron occupies the lower state for a hole polaron.

solitons. It is remarkable that present experimental techniques support the subsequent formation of solitons with as much certainty as in the polaronic case. Solitons may be generated by photoexcitation [12] and doping experiments [13]. As experimental proof of the existence of solitons is the midgap absorption upon doping as illustrated in figure 1.6 [14]. In photoexcitation experiments charge carriers are generated with $\hbar\omega < 1$eV. Quantum fluctuations can be shown to supply the other .8eV to create an electron-hole pair across the gap. This two-particle complex in turn decays into a soliton-antisoliton pair and some other "breathers" (neutral solitons). The small decay time $\tau \sim 10^{-3}$s confims the small calculated effective mass ($m^* \sim 6m_e$) and the strong short range repulsion between equally charged solitons. This has been simulated by molecular dynamics calculations. The mechanism of decay of an electron-hole pair into soliton-antisoliton is confirmed by the infrared active vibrational (IRAV) modes, the midgap absorption, and electron spin resonance (ESR) experiments during photogeneration [5]. Perhaps the strongest experimental support for solitons in PA is the fact that PA exhibits photoconductivity but not photoluminescence. This is due to the mobile character of the solitons that diffuse the charge away from the hole, therefore suppresing the photoluminescence that would occur if the electron and hole were to recombine again. In general, photoluminescence (but not photoconductivity) can be observed in polymers with non-degenerate ground state [5]. This comes about because polymers without a degenerate ground state cannot exhibit the domain wall between the two degenerate phases, thus precluding the existence of solitons. As evidence to the delocalization of the spin, electron spin resonance (ESR), nuclear magnetic resonance (NMR), and electron-nuclear double resonance (ENDOR) experiments can be used to estimate that the spins for neutral solitons are spread over 15–20 lattices.

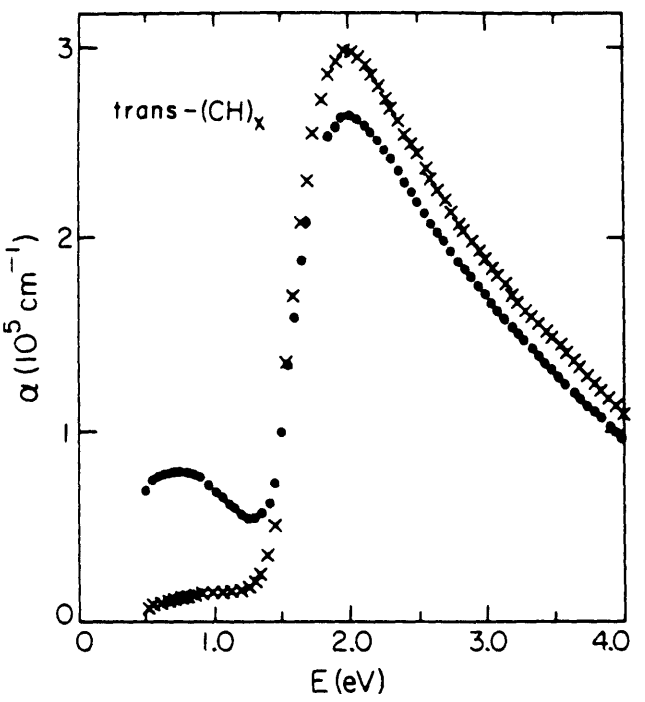

Figure 1.6. Absorption spectra for neutral (crosses) and doped PA (dots). The peak at around 2eV indicates the band absorption and the peak-induced one at around .7eV indicates the midgap absorption from the soliton level. Taken from reference [14].

1.3. Magnetic Susceptibility.

Experiments concerned with the magnetic susceptibility have been performed that show perhaps the most interesting property of PA [15]. The most dramatic results are presented in figure 1.7(a) [4]. The results appear to characterize three regions in the magnetic susceptibility as a function of doping; the very low doping regime ($p << 1\%$) where a decrease of localized spins is observed, the intermediate doping regime ($1\% < p < 6\%$) where there is roughly a constant number of about 1/2 spins per chain, and the highly doped regime ($p > 6\%$) where there is the appearance of a temperature independent magnetic susceptibility (figure 1.7(b)). Initially, ESR measurements indicate that in the $p = 0$ (no doping) region there is roughly one spin per chain.

The low doping region can be explained in a consistent fashion with a soliton picture. First, consider a sample of undoped PA. Experiments indicate roughly one spin per chain. This fact can be explained by observing that a macroscopic sample is expected to contain approximately equal amounts of even-numbered and odd-numbered chains. Because odd chains intrinsically possess the two degenerate phases, there is automatically a neutral soliton formed in them. This means that there is going to be at least 1 spin per every odd-chain as a result of the spin-charge relations for solitons. Then, the decay in spins at the very light doping regime ($p < 1\%$) can be explained considering that the neutral solitons already existing in the chains get charged. Thus, the population of neutral solitons with spin decreases giving rise to charged solitons with no spin.

The intermediate doping region ($1\% < p < 6\%$), where experiments show a constant 1/2 spins per chain, poses other conceptual problems. If we were to explain the existence of this 1/2 spin per chain by merely charging up the neutral solitons we would face the problem that we should have ran out of these neutral solitons at $p \sim 10^{-5}$. However, the appearance of the dopant induced IRAV modes (but dopant independent) seems to indicate that charged solitons are present in this

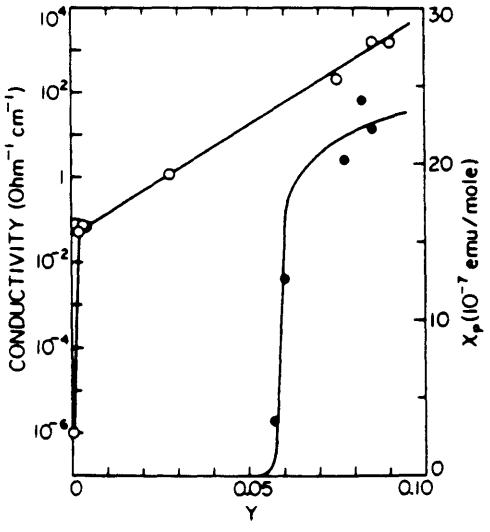

(a)

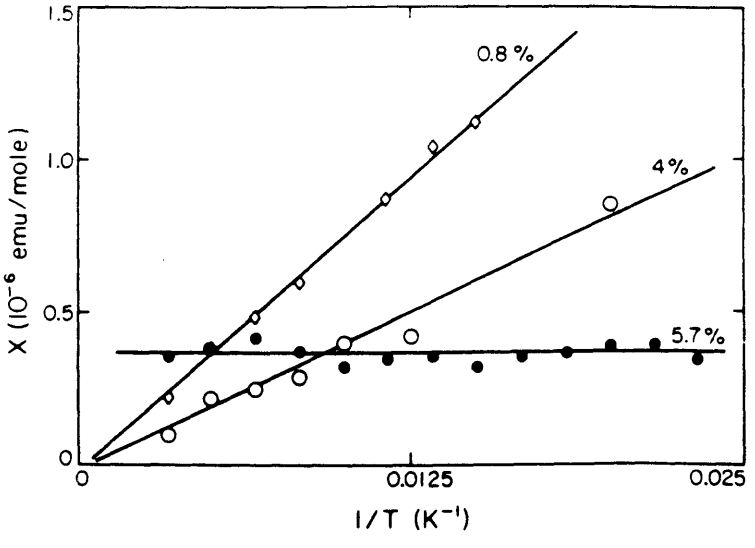

(b)

Figure 1.7. (a) Measurements for the magnetic susceptibility (filled dots) and conductivity (empty dots) for PA at room temperature. (b) Temperature dependence of the magnetic susceptibility for different doping levels. Taken from reference [4].

doping regime. IRAV modes are the signature of charged localized structural distortions with localized phonons (breathers). Also, the midgap transition at $\hbar\omega \sim \Delta_o$ and the fact that $N_s/N_{ch} << 1$ (N_s is the number of spins obtained from ESR experiments and N_{ch} is the number of charges obtained from the intensity of the IRAV modes), which is a key signature of reverse spin-charge numbers, truly point to solitons as the key players in the susceptibility. The explanation comes from the long range attraction between polarons indicated by the reaction $P + P \rightarrow S + \overline{S}$ [16]. This means that as we dope the system, the number of polarons in the chains increases, but that their long range attraction will recombine them into charged soliton-antisoliton pairs. This reaction limits the number of polarons in a chain to at most one, thus accounting for the observed spins per chain in the intermediate region. Furthermore, because the system can be reversibly doped, experiments can determine that the doping occurs through the formation of polarons and that the undoping is realized through the uncharging of solitons.

The highly doped region ($p > 6\%$) exhibits the rapid onset of the magnetic susceptibility χ to a T-independent one. Its value is roughly what one could expect for a metal. The form of the transition is dopant dependent (Na shows a very sharp transition). X-ray data suppport some kind of structural order that could be interpreted as a lattice or a highly correlated soliton liquid [5]. In chapter 2 we give a simple account to the possible origin or this magnetic susceptibility.

1.4. Conductivity.

The results presented in section 1.1 regarding the decrease of the conductivity σ as the temperature is increased at high doping levels ($p \sim 10\%$), suggest that PA is not an intrinsic material. A contributing factor to not having an intrinsic material is the interfibrillar contacts that act as "series resistances". However, charge carriers can be shown to have relatively long mean free paths (several hundred

angstroms) because by slightly increasing the precentage of sp_3 defects lowers σ by an order of magnitude. Also, the highest value of σ at this level ($\sigma \sim 1.5 \times 10^5(\Omega cm)^{-1}$) [17] indicates that the intrinsic properties of PA should be better than simple metals. In contradistinction to simple metals, however, transport seems to be highly anisotropic hinting that the main mechanisms involved in the physics are of one-dimensional character [18,19]. Also, the pressure dependence of σ is anisotropic yielding for example $\sigma_{\|}/\sigma_{\perp} \sim 80$ at .7kbar [5]. The fact that $\sigma_{\|}$ increases with the pressure while $\sigma_{\perp}$ remains constant confirms the small overlap of neighboring chains.

Another aspect of utmost importance is the high value that the conductivity can achieve as a function of doping (figure 1.7(a)). It has two main doping regions that are of interest. In the dilute doping limit ($p < 10^{-5}$) the conductivity exhibits a behavior $\sigma(T) \sim T^n$ ($n \sim 13$). This causes a rapid onset of condutivity that seems to slow down at approximately $p \sim 1\%$. Variable Range Hopping theory does not quite account for this behavior nor the pressure dependence [20]. By electrochemical voltage spectroscopy (EVS) measurements it is known that the charge transport is carried out through a narrow band about midgap at this low doping [21]. This result automatically rules out any model on hopping from states near the edges of the bands. The model that correctly accounts for this is the intersoliton hopping model (ISM) that indicates that the transport is intrinsic for $p \sim 1\%$ and does not depend on the complex morphology [22]. The ISM considers hopping at midgap at equal energies. That is, the hopping is realized between pinned charged solitons to neutral mobile solitons. This model of transport by mobile charged solitons is consistent with the susceptibility measurements as well as with the absorption measurements. It is also consistent with the Infrared modes, which indicate charge in spinless gap states.

The highly doped regime (metallic state) exhibits a very high value for the conductivity ($10^3 - 10^5$S/cm) but in contrast with metals, it decreases with temperature. The nature of the charge carriers is still the topic of debate. The highly doped regime is strongly correlated and hence cannot be described by non-interacting mod-

els. χ_p is what roughly one might expect from a nearly half-filled π-band in the absence of any Peierl's distortion, nontheless there is evidence of bond alternation even at this doping level [23]. Suggestions as to the consideration of other interactions may be important, such as electron-electron interactions and interchain couplings [24]. Recently developed Highly Conducting PA (HCPA) exhibits such high value for the conductivity even at very low temperatures (mK region) [25]. One of the interesting properties addressed in chapter 3 will be the log$T$ behavior at the very low T region of the conductivity measurements (figure 1.8).

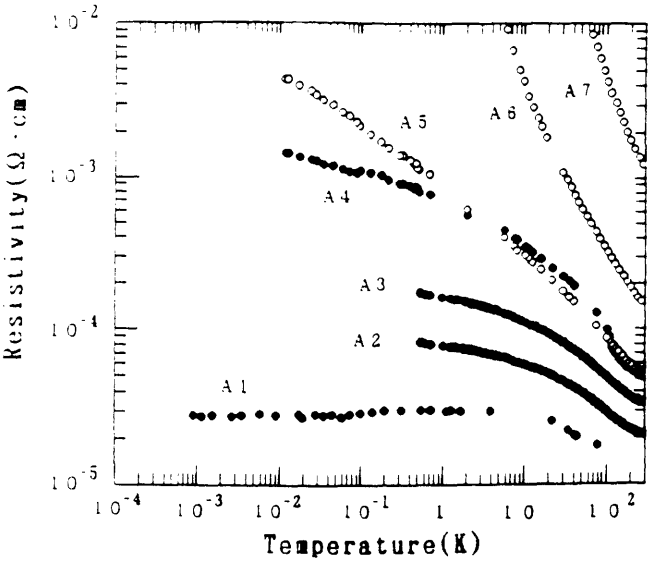

(a)

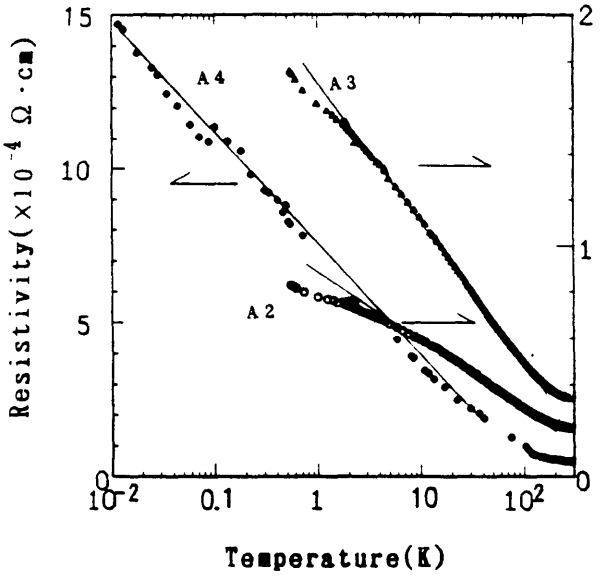

(b)

Figure 1.8. (a) Temperature dependences of the resistivity for various heavily I-doped PA samples represented in a logρ vs logT plot. The data from A1 to A7 where attained in the same sample as a function of aging. Sample A1 corresponds to the cleanest sample. (b) shows a blow-up of samples A2-A4 that correspond to intermediate aging. The logT characteristics are shown by the straight lines.

References for Chapter 1.

1. H. Naarmann, N. Theophilou, *Synth. Met.*, **22**, 1 (1987).
2. Y.-B. Moon, M. Winokur, A.J. Heeger, J. Baker, D.C. Bott, *Macromolecules*, **20**, 2457 (1987).
3. N. Basescu, Z.-X. Liu, D. Moses, H. Naarmann, N. Theophilou, *Electronic Properties of Conjugated Polymers*, eds. H. Kuzmany, M. Mehring, S. Roth, Springer Series in Solid State Sciences, No. 76 (Springer Berlin), p.156 (1988).
4. F. Moraes, J. Chen, T.-C. Chung, A.J. Heeger, *Synth. Met.*, **11**, 271 (1985).
5. A.J. Heeger, S. Kivelson, J.R. Schrieffer, W.P. Su, *Rev. Mod. Phys.*, **60**, 781 (1988).
6. C.R. Fincher, C.E. Chen, A.J. Heeger, A.G. MacDiarmid, J.B. Hastings, *Phys. Rev. Lett.*, **48**, 100 (1982).
7. J. Fink, G. Leising, *Phys. Rev. B*, **34**, 5320 (1986).
8. W.-P. Su, J.R. Schrieffer, A.J. Heeger, *Phys. Rev. B*, **22**, 2099 (1980).
9. H.Takayama, Y.R. Lin-Liu, K. Maki, *Phys. Rev. B*, **21**, 2388 (1980).
10. S.A. Brazovskii, N. Kirova, *Sov. Phys. JETP Lett.*, **33**, 4 (1981).
11. D.K. Campbell, A.R. Bishop, *Nucl. Phys. B*, **200**, 297 (1982).
12. Z. Vardeny, J. Orenstein, G.L. Baker, *Phys. Rev. Lett.*, **50**, 2032 (1983).
13. S. Etemad, A. Pron, A.J. Heeger, A.G. MacDiarmid, E.J. Mele, M.J. Rice, *Phys. Rev. B*, **23**, 5137 (1981).
14. H. Suzuki, M. Ozaki, S. Etemad, A.J. Heeger, A.G. MacDiarmid, *Phys. Rev. Lett.*, **45**, 1209 (1980).
15. S. Ikehata, J. Kaufer, T. Woerker, A. Pron, M.A. Druy, A. Sivak, A.J. Heeger, A.G. MacDiarmid, *Phys. Rev. Lett.*, **45**, 1123 (1980).
16. Y. Onodera, S. Okuno, *J. Phys. Soc. Jpn.*, **52**, 2478 (1983).
17. N. Basescu, Z.-X. Liu, D. Moses, A.J. Heeger, H. Naarmann, N. Theophilou, *Nature*(London), **327**, 403 (1987).

18. G. Leising, talk given at the Symposium on Conducting Polymers: their Emergence and Future, Americal Chemical Society Meeting, Denver, CO (to be published).

19. C.R. Fincher, M. Ozaki, M. Tanaka, D.L. Peebles, L. Lauchlan, A.J. Heeger, A.G. MacDiarmid, *Phys. Rev. B*, **20**, 1589 (1979).

20. D. Moses, J. Chen, A. Denenstein, A.J. Heeger, A.G. MacDiarmid, *Sol. State Commun.*, **40**, 1007 (1981).

21. J.H. Kaufman, T.-C. Chung, A.J. Heeger, *J. Electrochem. Soc.*, **131**, 2847 (1984).

22. S. Kivelson, *Phys. Rev. Lett.*, **46**, 1344 (1981).

23. Y.H. Kim, A.J. Heeger, *Phys. Rev. B*, **40**, 8393 (1989).

24. D.K. Campbell, T.A. DeGrand, S. Mazundar, *Phys. Rev. Lett.*, **52**, 1717 (1984).

25. T. Ishiguro, H. Kaneko, Y. Nogami, H. Ishimoto, H. Nishiyama, J. Tsukamoto, A. Takahashi, M. Yamaura, T. Hagiwara, K. Sato, *Phys. Rev. Lett.*, **69**, 660 (1992).

Chapter 2

Properties as a Function of Doping.

2.1. Statement of the Problem.

Because the ground state of trans-polyacetylene is two-fold degenerate, polyacetylene is a Peierls band gap insulator at half filling. The degeneracy arises from the periodic arrangement of alternating double and single bonds (which constitute a commensurate charge density wave) along the polymer backbone. Su, Schrieffer, and Heeger (SSH) have shown that the dimerization of the ground state of this polymer can be accounted for by a one-electron phonon model with a periodic lattice distortion [1]. On physical grounds, one would suspect that because an on-site Hubbard U favors a uniform charge density, the tendency to dimerization at half-filling would desist if Hubbard-type of interactions were turned on. A curious feature of trans-polyacetylene, however, is that electron correlations enhance dimerization at half-filling [Ref. 2 and references therein]. This result, first established within the context of the extended Peierls-Hubbard models [see for example Ref. 3], certainly hinted that the phonon SSH model can only partially account for the ground as well as conducting states of this polymer. Subsequent perturbative calculations [4,5], Monte Carlo [2,6], selfconsistent numerical [7], and exact studies [8] on finite systems have substantiated the finding that short-range electron correlations most

likely dominate the dimerization process in the ground state.

Away from half-filling, there have been relatively few studies on the role of electron correlations in trans-polyacetylene. Such studies are of utmost importance if the precise mechanism of the insulator-metal transition in polyacetylene is to be understood. In this chapter, we address two questions: 1) what are the stable excitations as single strands of polyacetylene are doped into the metallic regime? and 2) can the resultant excitations explain the onset of a Pauli susceptibilty at the insulator-metal transition (IMT)? This work is motivated by the lack of concensus on the operative mechanism for the IMT in trans-polyacetylene [9,10,11,12,13, 14,15].

A key experimental feature that a successful mechanism for the IMT in polyacetylene must explain is the onset of the Pauli susceptibility at a doping level of 6% [16]. Below this doping level only a residual Curie susceptiblilty is observed. The virtual lack of spins below the IMT supports the view that charged solitonic rather than electron or hole-like excitations form in the lightly-doped form of the polymer. Charged solitonic excitations populate the mid-gap states and are spinless. One of the early suggestions for the IMT in polyacetylene is the polaron model of Kivelson and Heeger [9]. Although this model would account for the Pauli susceptibility, it is inconsistent with the intense IRAV modes observed in the experiments of Kim and Heeger [17]. Kim and Heeger have observed that the intensity of the IRAV mode (a signature of solitonic excitations) increases as the doping level is increased. Nonetheless, a transition to some kind of polaron lattice must obtain if itinerant spins are to form in the metallic state of trans-polyacetylene. Within the SSH one-electron phonon model, only soliton excitations are stable, however at all doping levels. Consequently, recent work on the metal transition in polyacetylene has focused on extensions of the SSH model that support polaron formation [10,18,19]. For example, Mizes and Conwell [19] have shown that interchain coupling as well as chain breaks stabilize polaron formation in trans-polyacetylene. These results were established for short chains containing at most one polaron. Attempts to explore the

stability of polarons in single strands of polyacetylnene have focused on perturbative studies of the SSH model [5,20] appended with an on-site Hubbard U [21]. For values of U as large as 4.2eV it was found that solitons were favored over polarons regardless of the doping level. However, such studies treated the interactions at the Hartree level and hence could not definitively answer the question as to the fate of polarons in single strands of trans-polyacetylene. Other studies that point to this solitonic characteristic are those on optical data [22], vibrational features [23,24], crystal orbital calculations [25], and transport properties[26]. An alternative scheme which skirts the IRAV mode problem, as well as some of the other features, is the polson model of Tanaka, et. al. [11, 12]. In this model it is argued that a hybrid polaron-soliton excitation exists in the metal state of polyacetylene[11]. As a hybrid excitation, a polson can explain both the soliton characteristics of the metallic phase as well as the Pauli susceptibility.

Given the obvious variety of proposals for the stable excitations in polyacetylene, we begin our investigation addressing the issue of the role of short-range correlations along single strands of trans-polyacetylene as a function of doping. In this way we will determine precisely whether solitons, polarons or some hybrid state exists in the metallic phase of polyacetylene. To this end, the starting point of our analysis is a Hamiltonian which incorporates both phonon interactions as well as electron correlations [27]. The phonon interactions will be described by the Takayama, Lin-Liu , and Maki (TLM) [28] continuum version of the Su, Schrieffer, and Heeger Hamiltonian [1], which is known to support both, polarons and solitons as stable excitations [29]. Short-range electron correlations will be modeled with an on-site Hubbard U, a nearest neighbor repulsion V and a bond-repulsion W. Although it is well accepted [2, 3,4,5,6,7, 8,30] that electron correlations play a significant role in the ground-state properties of polyacetylene, few studies of their influence away from half-filling have been conducted [5, 20,21,31]. In fact, what studies have been completed have been confined to at most two extra electrons [20,21,31] in a single polymer chain.

In this chapter it will be shown that even in isolated chains a transition towards a polaron lattice can be achieved as the interaction strength increases. We find moreover, that doping appears to favor a soliton state. In addition, we consider the role of a bond-charge Coulomb repulsion term, W. It has been suggested [4] that W stabilizes a polaron lattice. Exact numerical calculations of the ground state of short chains using this term at half filling have demonstrated a transition from a dimerized to a ferromagnetic phase [32]. We have performed calculations including this term in the total Hamiltonian and show that contrary to accepted wisdom W favors a soliton lattice over a polaron lattice as a function of its strength and doping level in the chain.

In the first part of this chapter we present a formalism [33] we have developed recently that allows for a systematic study of electron correlations in so far as they influence the stability of polaron and soliton configurations that result when a single polymer strand is doped. The doping dependence will be determined by calculating the energy levels of localized excitations that form in the mid gap region when electrons are added to a single strand. The energy levels and wavefunctions for these states will be obtained by using an Inverse Scattering Theory for reflectionless bound states [31]. Because the resulting wavefunctions extrapolate smoothly from soliton to polaron excitations when the position of the bound state energies in the gap is tuned, we will minimize the total energy (which will include the short-range Coulomb repulsion terms) with respect to these discrete energies in order to determine the stable configuration of solitons or polarons. First order perturbation theory on the full Hamiltonian will then be used to determine the role of correlations [34,35].

The key results from this study are as follows. At a particular doping level, a transition to a polaron lattice in an isolated chain certainly occurs provided that U and V exceed critical values. However, as the doping level is increased, a soliton lattice is favored. This conclusion is shown to be valid well into the metallic phase. Within a soliton model for the metallic phase, we show that a Pauli susceptiblity

can arise simply from the spreading of the bound state soliton levels across the gap. The resultant Pauli susceptibility is shown to be consistent with the experimental values.

2.2. Model Hamiltonian.

Before we present our model Hamiltonian, let us explain what happens when one and two electrons are added to a single polyacetylene chain in the absence of electron correlations. Consider first the addition of a single electron. The particle-hole symmetry in the ground state of polyacetylene guarantees that each electron added will produce two states symmetrically located around the Fermi energy, $\epsilon = 0$. The lower states are donated from the valence band and the upper states emerge as bound states just above mid-gap. For a single electron [2], the energy levels are located at $\frac{\pm\Delta_o}{\sqrt{2}}$ where Δ_o is the order parameter for the ground state. The lower level will be doubly-occupied while the upper level will be singly occupied and hence it will carry a spin of $s = \pm 1/2$ and a charge of Q=-e. The resultant excitation is then an electron-polaron with a creation energy of $E_p = \frac{2\sqrt{2}\Delta_o}{\pi}$ where Δ_o . Consider now the case of two electrons. In this case four levels form with energies $\pm\Delta_o$ and 0. The two extra electrons can either doubly occupy the bound state at 0 or they can singly occupy the Δ_o and 0 energy states. The former case corresponds to the formation of a soliton-antisoliton pair with a creation energy of $E_s = 2(\frac{2\Delta_o}{\pi})$. The singly-occupied case corresponds to the creation of two polarons. The difference in energy between the soliton and polaron configurations is $\delta E = 2E_p - E_s = \frac{4(\sqrt{2}-1)\Delta_o}{\pi} > 0$. Consequently, in the case of two extra electrons, the soliton-antisoliton pair is more stable than two polarons. The formation of two solitons from a polaron and an electron is mediated by the formation of and subsequent dissociation of two polarons. This is an indication that the long-range interaction between two polarons is sufficiently attractive and ultimately renders the

two-soliton configuration as the lowest energy state [31]. It stands to reason then that if on-site correlations are included, polarons could become stabilized relative to the corresponding soliton-antisoliton configurations. It is precisely this issue that we now address.

To this end, we start our analysis by considering the extended Peierls-Hubbard model

$$\mathcal{H} = \mathcal{H}_{TLM} + \mathcal{H}_U + \mathcal{H}_V + \mathcal{H}_W \tag{2.1}$$

where $\mathcal{H}_{TLM}$ is the continuum TLM hamiltonian [20]

$$\mathcal{H}_{TLM} = \frac{1}{2\pi\lambda v_f}\int dx\Delta(x)^2 + \int dx\Psi^\dagger[-iv_f\sigma_2\partial_x + \Delta(x)\sigma_1]\Psi. \tag{2.2}$$

In equation (2.2), $\Psi = (u, v)$ is the two-component spinor, v_f the fermi velocity, $\Delta(x)$ the order parameter, and σ_i are the Pauli matrices. The parameter λ denotes the elastic energy coupling constant and the convention $\hbar = 1$ has been used. The numerical values for the parameters are taken from Ref. 1. With our use of σ_2 instead of the conventional σ_3, u and v correspond directly to the amplitudes for the even and odd sites of the chain, respectively [31]. On-site and nearest-neighbor electron correlations are described by

$$\mathcal{H}_U = U\sum_j n_{j\uparrow}n_{j\downarrow} \tag{2.3}$$

and

$$\mathcal{H}_V = V\sum_j n_j n_{j+1}, \tag{2.4}$$

where $n_{js} = c^\dagger_{js}c_{js}$ is the number of electrons with spin s on site j, c_n is the annihilation electron operator, and $n_j = n_{j\uparrow} + n_{j\downarrow}$. The inclusion of off-diagonal terms has been restricted in our calculations to the bond-charge repulsion term

$$\mathcal{H}_W = W\sum_l (B_{l,l+1})^2 \tag{2.5}$$

where $B_{l,l+1} = \sum_s(c^\dagger_{ls}c_{l+1,s} + c^\dagger_{l+1,s}c_{ls})$. We have ignored the other usually considered "mixed" term involving both on-site and bond-charge effects primarily because

W appears to play a more relevant role than the mixed term [4]. However, the main conclusions of this article will be based primarily on on-site and nearest-neighbor interactions. The W term will only introduce minor corrections.

Consider the generalized Hartree-Fock wavefunction for the valence band $|\mathcal{V}\rangle = \prod c^{\dagger}_{l\uparrow} c^{\dagger}_{m\downarrow}|0\rangle$ where l and m refer to the continuum states. The total state containing n polarons or solitons can be represented simply as $|\Phi\rangle = \prod c^{\dagger}_{\alpha\uparrow} c^{\dagger}_{\beta\downarrow}|\mathcal{V}\rangle$ where α and β refer to the bound states inside the gap. The expectation value of equation (2.1) with respect to $|\Phi\rangle$, according to the atomic orbital representation used in obtaining (2.2), is given by

$$\langle \mathcal{H}_{TLM} \rangle = \frac{1}{2\pi\lambda v_f} \int dx \Delta(x)^2 + \sum_{k,s} n_{k,s} \int dx \Psi^{\dagger} \big[-iv_f \sigma_2 \partial_x + \Delta(x)\sigma_1 \big] \Psi, \quad (2.6)$$

$$\langle \mathcal{H}_U \rangle = Ua \int dx \big[\mathcal{Z}_{\downarrow 0} \mathcal{Z}_{\uparrow 0} + \mathcal{Z}_{\downarrow 3} \mathcal{Z}_{\uparrow 3} \big], \quad (2.7)$$

$$\langle \mathcal{H}_V \rangle = Va \int dx \sum_s \big[\mathcal{Z}_{s0}(\mathcal{Z}_{s0} + \mathcal{Z}_{\bar{s}0}) - \mathcal{Z}^2_{s1} - \mathcal{Z}^2_{s2} - \mathcal{Z}_{s3}(\mathcal{Z}_{s3} + \mathcal{Z}_{\bar{s}3}) \big], \quad (2.8)$$

$$\langle \mathcal{H}_W \rangle = 2Wa \int dx \sum_s \big[-\mathcal{Z}^2_{s0} + \mathcal{Z}^2_{s1} + \mathcal{Z}^2_{s3} + \mathcal{Z}_{s2}(\mathcal{Z}_{s2} + 2\mathcal{Z}_{\bar{s}2}) \big] + 2WN, \quad (2.9)$$

where $\mathcal{Z}_{si} = \sum_k n_{k,s} \Psi^{\dagger}_k \sigma_i \Psi_k$ with σ_0 the identity matrix, $n_{k,s}$ the occupation number for state (k, s), N the total number of electrons in the chain, and a the intersite distance. The intermediate steps in the calculations leading to equations (2.7) through (2.9) are given in Appendix F.

For a chain of arbitrary length, we must find u and v. Inverse scattering is ideally suited for calculating u and v for a chain of infinite length. This procedure determines the wavefunctions for an arbitrary number of excitations as well as the distortion in the wavefunctions of the electrons forming the valence band. Results for finite chains will be obtained by imposing appropriate boundary conditions on the order parameter $\Delta(x)$ at the chain ends. The primary hurdle in obtaining the non- interacting states is in determining the gap energy levels as the filling is varied. These energies will be obtained uniquely by demanding that when n electrons are added to a single chain, the gap energy levels variationally yield a minimum in the

total energy. Note that because the total energy contains the Coulomb repulsion terms, the subsequent energies of the bound states will depend on U, V and W in a non-trivial way. As will be seen, to incorporate the electron correlations into the single particle levels will have a profound effect on the subsequent Pauli susceptibility. We also note that there have been other attempts to implement the Inverse Scattering procedure to obtain the single particle states for the TLM Hamiltonian. In all previous works, however, a particular choice was made for the order parameter that favored either soliton or polaron states [13,14]. No such restrictions will be imposed here.

We now outline briefly how the exact solution can be obtained for the non-interacting part of the Hamiltonian. The eigenvalue equation for the TLM Hamiltonian

$$\begin{aligned} -v_f \partial_x v_k(x) + \Delta(x) v_k(x) &= \epsilon_k u_k(x) \\ v_f \partial_x u_k(x) + \Delta(x) u_k(x) &= \epsilon_k v_k(x) \end{aligned} \tag{2.10}$$

involves the site amplitudes for the even and odd-numbered sites, respectively. The energies $\epsilon_k = \pm\sqrt{\Delta_o^2 + k^2 v_f^2}$ refer to the conduction and valence band states. Electrons added to the system will occupy states which lie in the gap region. Electron-hole symmetry guarantees that each electron added will produce two states symmetrically located with respect to $\epsilon = 0$. These discrete states also satisfy (2.10) but with their respective energies $\omega_n = \pm\sqrt{\Delta_o^2 - k_n^2 v_f^2}$. For all cases, u and v satisfy the normalization constraint,

$$\int dx \left[|u|^2 + |v|^2\right] = 1 \,. \tag{2.11}$$

The expectation value of $\mathcal{H}_{TLM}$ can now be written as,

$$E_{TLM} = \frac{1}{2\pi\lambda v_f} \int dx \Delta(x)^2 + \sum_{k,s} n_{k,s} \epsilon_k \,. \tag{2.12}$$

The sum has to be carried out over continuum as well as discrete states of the chain. For a chain of length L, periodic boundary conditions [36] are imposed such that $kL = 2m\pi + \phi_k$, where $\phi_k = \sum_i^n 2\tan^{-1}\frac{k}{k_i}$ for n excitations in the chain. Details

on the derivation of this boundary condition are given in Appendix B. In order to calculate equation (2.12) for the n-excitation state we need the order parameter $\Delta(x)$. The following development leads to the solution. Equation (2.10) can be decoupled straightforwardly as

$$\begin{aligned} -\partial_x^2 v_n(x) + U_o(x)v_n(x) &= \lambda_n v_n(x) \\ -\partial_x^2 u_n(x) + U_e(x)u_n(x) &= \lambda_n u_n(x) \end{aligned} \tag{2.13}$$

where

$$\begin{aligned} U_o &= \frac{1}{v_f}\frac{\partial\Delta(x)}{\partial x} + \frac{1}{v_f^2}[\Delta(x)^2 - \Delta_o^2] \\ U_e &= -\frac{1}{v_f}\frac{\partial\Delta(x)}{\partial x} + \frac{1}{v_f^2}[\Delta(x)^2 - \Delta_o^2] \end{aligned} \tag{2.14}$$

the parameter $\lambda_n = \frac{1}{v_f^2}[\omega_n^2 - \Delta_o^2]$, and e, o stand for even and odd, respectively. These 1-dimensional Schrodinger equations can be solved by the Inverse Scattering technique [37,38]. In this account, the $U_{o,e}$ are determined in terms of the set of λ_n defined in equation (2.13). Then we can proceed to find the minimum of E_{TLM} by

$$\frac{\partial E_{TLM}}{\partial\vec{\omega}} = 0, \tag{2.15}$$

where $\vec{\omega} = \{\omega_1, \ldots \omega_n\}$. The minimizing set of $\{\omega_i\}_{min}$ will be used to calculate the minimum energy of the stable configuration of electronic excitations. The order parameter is given then by inverting equation (2.14),

$$\begin{aligned} \frac{\partial\Delta(x)}{\partial x} &= \frac{v_f}{2}(U_o - U_e) \\ \Delta(x)^2 &= \Delta_o^2 + \frac{v_f^2}{2}(U_o + U_e). \end{aligned} \tag{2.16}$$

For very long chains Inverse Scattering Theory yields [37]

$$U_{o,e} = -2\frac{d^2}{dx^2}\ln\det(A + I) \tag{2.17}$$

where $A_{m,n}^{e,o} = e^{\alpha_{e,o}^m} e^{\alpha_{e,o}^n} \frac{e^{(k_n+k_m)x}}{k_n+k_m}$. Because a requisite of equation (2.17) is that the potentials $U_{o,e}$ vanish at the ends of the chain, long chains are required. On physical grounds, $U_{o,e}$ are the potentials that confine the excitation states. Consequently, they vanish at distances larger than the width of the excitations. Thus,

the solution in (2.17) is valid as long as the chain is longer than the combined width of all the excitations in it. A relation between the set of $\{\alpha^n_{o,e}\}$ and the set of $\{\omega_i\}$ is developed in Appendix C. Once this is achieved the $\{\omega_i\}$ will be the only undetermined set of parameters which are subsequently fixed by applying equation (2.15). The determinant in equation (2.17) has been evaluated explicitly for the n-excitation case. The expression is given in Appendix C where we have defined $W_{o,e} \equiv \det(A + I)$.

With the order parameter in hand, we can now solve explicitly for E_{TLM}. We are particularly interested in the creation energies for excitations introduced into the gap. Let E^o_{TLM} be the energy of a uniformly dimerized undoped chain. The creation energy for an arbitrary number of excitations in the gap is

$$\delta E = \frac{4v_f\rho}{\pi} + \frac{4}{\pi}\sum_i \omega_i tan^{-1}\frac{\omega_i}{k_i v_f} + \sum_i (n^i_+ - n^i_-)\omega_i \qquad (2.18)$$

where $\delta E \equiv E_{TLM} - E^o_{TLM}$, $\rho = \sum_i k_i$, and $k_i v_f = \sqrt{\Delta_o^2 - \omega_i^2}$ where ω_i are the energies of the levels in the gap. The notation $n^i_\pm$ denotes the occupation number for the negative and positive ith level in the gap. The energy E^o_{TLM} is calculated from equation (2.12) using $\Delta(x) = \Delta_o$ and carrying out the summation over k with the corresponding boundary condition $kL = 2m\pi$. In this way the quantity in equation (2.18) is the creation energy for the excitations introduced in the gap.

Let us analyze expression (2.18) in the case of a single electron. When an extra electron is added, two levels form in the band gap. One is donated from the conduction band and the other from the valence band. The electronic occupations correspond to $n^1_- = 2$, $n^1_+ = 1$ for the lower and upper levels, respectively. In this case a minimization of the energy with respect to this single parameter (both levels are symmetrically located at $\pm\omega_1$) $\frac{\partial \delta E}{\partial \omega_1} = 0 = \frac{4}{\pi} tan^{-1}\frac{\omega_1}{k_1 v_f} + (n^1_+ - n^1_-)$ yields $\omega_1 = \frac{\Delta_o}{\sqrt{2}}$. When substituted into equation (2.18) we obtain that $\delta E = \frac{2\sqrt{2}\Delta_o}{\pi}$, the well-known polaron creation energy for trans-polyacetylene [39]. Similarly, for two electrons, four levels form with energies $\omega_2 = \Delta_o$ and $\omega_1 = 0$ and occupation numbers $n^2_- = 2$, $n^1_- = 2$, $n^1_+ = 2$, and $n^2_+ = 0$. Using these values for ω_1 and ω_2,

we find that the total creation energy is $\delta E = 2(\frac{2\Delta_o}{\pi})$ which is the creation energy for two solitons. The formation of two solitons from a polaron and an electron is mediated by the formation of and subsequent dissociation of two polarons. This is an indication that the long-range interaction between two polarons is sufficiently attractive and ultimately renders the two-soliton configuration as the lowest energy state [31]. Note that by choosing $n_+^1 = n_+^2 = 1$ instead, we would have forced the system into a two-polaron state thereby suppresing dissociation. The corresponding energy would be equivalent to the energy of two isolated polarons. This fact will be important because then we have a way of constructing both soliton and polaron states with the same amount of electrons in the chain.

Due to electron-hole symmetry only negative type excitations will be considered. The distinction between polaron and soliton excitations will be introduced, as outlined in the above development, by noting that polarons carry singly occupied levels above the center of the gap meanwhile solitons are obtained by doubly occupying those same states. These fillings may be verified by carrying out (2.15) and further examining the corresponding order parameters and charge densities of each excitation. By calculating the energy of each configuration then, we will be able to choose that configuration that has the lowest energy, or equivalently the stable configuration.

In order to calculate the energy of the full interacting Hamiltonian (2.1) we now have to determine the amplitudes u_n and v_n that describe the bound states in the gap region. To this end, we must solve the eigenvalue equations (2.10) for the bound state energies instead of the continuum energies ϵ_k. In analogy with Inverse Scattering for reflectionless potentials [38], the wavefunctions of the bound states in the gap are given by

$$u_m(x) = e^{-k_m x}[1 - \sum_n \frac{2k_n e^{2\alpha_\epsilon^n} u_n(x) e^{-k_n x}}{k_n + k_m}] \tag{2.19}$$

where $v_m(x) = \text{sign}(\omega_m)(-1)^{m+1} u_m(-x)$. The distorted valence and conduction

band states are given by

$$u_k(x) = e^{ikx}[1 - \sum_n \frac{2k_n e^{2\alpha_e^n} u_n(x) e^{-k_n x}}{k_n - ik}] \tag{2.20}$$

A useful approximation that much facilitates calculations is given by inserting (2.20) in the second equation of (2.10) and considering that the wave functions are slowly varying functions of the distance. In this limit

$$v_k(x) \cong \text{sign}\epsilon_k \frac{ikv_f + \Delta(x)}{|\epsilon_k|} u_k(x). \tag{2.21}$$

The above expressions define the amplitudes for the wavefunctions up to a normalization factor that is subsequently determined by applying equation (2.11). The amplitudes of the wavefunctions in the continuum as well as those in the gap are now solely determined by solving the system given by (2.19). Details of the calculation and explicit expressions for u_n in the n-excitation case are given in Appendix C.

We have provided thus far a means for calculating variationally the interacting creation energies of the n-excitation system for infinite chains. To consider finite chains, we proceed as follows. The condition for the vanishing of the potentials $U_{e,o}$ at the boundaries of the system imply that $\lim_{x\to\pm\infty} \Delta(x) = \pm\Delta_o$, as can be checked by equation (2.14). This means physically that at and near the boundaries, the system returns to the alternating bond configuration corresponding to the uniformly dimerized chain. In order then to be able to consider smaller chain lengths and still be able to use Inverse Scattering Theory we only need to impose $\lim_{x\to\pm L/2} \Delta(x) = \pm\Delta_o$, which is exactly the same condition but now L enters explicitly in the calculation of the order parameter. Imposing this boundary condition on the second equation of (2.16) and using the fact that $U_{o,e} = -2\frac{d^2}{dx^2} \ln W_{o,e}$ we obtain

$$\Delta(x)^2 - \Delta_o^2 = G(x) + D(L) \tag{2.22}$$

where $G(x) = -v_f^2 \frac{d^2}{dx^2} \ln(W_o W_e)$. The quantity $D(L)$ has to satisfy the conditions $D(L) = -G(\pm\frac{L}{2})$ and $\lim_{L\to\pm\infty} D(L) = 0$. The first condition defines D and the

second condition follows directly from the properties of $W_{o,e}$ as outlined in Appendix C. Now applying the boundary condition on the first equation of (2.16) we obtain the relation

$$\Delta(x) = \frac{v_f}{2}\int dx(U_o - U_e) = f(x) + C(L) \tag{2.23}$$

where $f(x) = -v_f[\frac{\dot{W}_o}{W_o} - \frac{\dot{W}_e}{W_e}]$. Again, from the boundary conditions it follows that $C(L) = \Delta_o - f(\pm\frac{L}{2})$. A relation can be found between D and C using the above equations, namely $D(L) = C(L)^2 - \Delta_o^2$.

Because our objective in this chapter is to determine to what extent polarons are stable given their intrinsic attractive long-range interactions, we concern ourselves with an even number of extra electrons in the chain. Also, for simplicity we will only consider even numbered chains. Thus, having even number of excitations and sites in a chain restrict further the boundary condition to $\Delta(\pm\frac{L}{2}) = \Delta_o$. Incorporating the modifications on the order parameter given by equations (2.22) and (2.23) into equation (2.12) we obtain for the energy of the non-interacting part of the full Hamiltonian

$$\begin{aligned}\delta E =& \frac{-v_f}{\pi\lambda}\left[\frac{\dot{W}_o(\frac{L}{2})}{W_o(\frac{L}{2})} + \frac{\dot{W}_e(\frac{L}{2})}{W_e(\frac{L}{2})}\right] + \frac{L}{2\pi\lambda v_f}(C^2 - \Delta_o^2) + \frac{2v_f}{\pi}(2 + \frac{1}{\lambda})\sum_i k_i \\ &+ \frac{4}{\pi}\sum_i \omega_i tan^{-1}\frac{\omega_i}{k_i v_f} + \sum_i (n_+^i - n_-^i)\omega_i.\end{aligned} \tag{2.24}$$

Details of the calculation leading to equation (2.24) are given in Appendix E. Note that from the limiting properties of the $W_{o,e}$, as outlined and shown in Appendix C, $\lim_{L\to\infty}[\frac{\dot{W}_o(\frac{L}{2})}{W_o(\frac{L}{2})} + \frac{\dot{W}_e(\frac{L}{2})}{W_e(\frac{L}{2})}] = 2\sum_i k_i$, reducing to equation (2.18) as expected. The energy of the full interacting Hamiltonian (2.1) as a function of the length of the chain can now be calculated (Appendix F) by inserting the wavefunctions described above into equations (2.7) through (2.9) and adding the contribution from the non-interacting part as given by (2.24). The configuration of the energy levels that render the energy a minimum will be given by equation (2.15) using the total interacting energy instead of E_{TLM}. The nature of the final state, either a polaron or soliton state, will be determined by the lowest energy of the two configurations.

A comment on equation (2.22) is in order. Because the Inverse Scattering Formalism requires that $U_{o,e}(L/2) \rightarrow 0$ then the vanishing of the potential at the boundaries is true as long as $\Delta(x) \rightarrow \Delta_o$ and $\frac{\partial \Delta(x)}{\partial x} \rightarrow 0$ at $x = \frac{L}{2}$. By adding the parameter $D(L)$ in equation (2.22) we are effectively adding the parameter D/v_f^2 to the potentials $U_{o,e}$, as can be checked by direct substitution of equation (2.22) into equation (2.14). This means that the parameter D has to be a small number. Because $D(L)$ is a decreasing function of the length of the chain L, in order to maintain D small, L cannot be taken to be arbitrarily small. As a consequence of this, the calculations presented here cannot be applied to arbitrarily high concentrations (small L). A criterion that gives good numerical results is that the minimum value of L should not be smaller than the combined widths of the excitations in the chain. That is, if there are n polarons of width d each in a chain, L should satisfy $L \geq nd$. This condition puts a lower bound on L and can be related to the width of the polarons or solitons in the chain. The relation between the lower bound on L and the width of the excitation in the chain can be rationalized in the following way. As we make the chain shorter the excitations will tend to get closer to each other. This shortening will also bring the excitations closer to the ends of the chains. By doing this the derivative of the order parameter in the neighborhood of the boundaries will deviate from the value of the dimerized chain Δ_o.

2.3. Phase Diagram.

Because of the complexity of the expressions for the functions $W_{o,e}$ and the wavefunctions for both continuum and bound states, the minimization calculations as well as the calculations for the energy were carried out numerically. In the doping process, each added electron will introduce a new bound-state energy parameter ω_i. This means that for n added electrons there will be an n-dimensional set of ω_i's on which the energy must be minimized. Such a multidimensional minimization

is far from straightforward numerically. We have chosen to use algorithms that make use of the derivatives of the function to be minimized. Though time consuming, this procedure exceeds the efficiency of convergence reached by interpolation methods. Also, because we are concerned with doping of two electrons at a time for each chain, the computational time for the minimizations in each subsequent doping step more than doubles. Results will be presented for two, four, and six added electrons to a chain. For comparison purposes, all results will be presented in terms of the concentration n/N, where N is the number of sites in the chain. We will only consider in the doping process the addition of extra electrons to the chain. Electron-hole symmetry guarantees that hole doping will yield identical results. As is well known, the occupations of the soliton and polaron states differ. This fact will prove to be relevant because the interactions will contribute in each case according to their occupations. For negative doping, the polaron state possesses a half filled uppermost state while the soliton state has a doubly-filled state.

For comparison purposes we define $\Delta E \equiv E_p - E_s$ where E_p and E_s are the corresponding interacting creation energies for a polaron and soliton configurations, as described at the end of the previous section. The point at which $\Delta E = 0$ marks the transition from one to the other configuration. In figure 2.1 we present ΔE as a function of U for the cases of two, four, and six extra electrons in an $N = 200$ chain. It is calculated for the case of $V = W = 0$. The value for U at which $\Delta E = 0$ indicates a point beyond which a polaron state has lower creation energy than a soliton one. We call this critical value for U, U_c. The fact that the soliton state reaches a point at which its creation energy surpasses that of the corresponding polaron state can be undestood in the sense that an on-site repulsion term will be most costly for those configurations containing double occupancy of the same site, or in our case to the same state. Thus, after the interaction strength increases beyond U_c the polaron configuration of singly occupied states has lower total energy than the doubly occupied one for the solitons. An alternative way of thinking about these results is that electronic repulsions are needed in order to stabilize a polaron

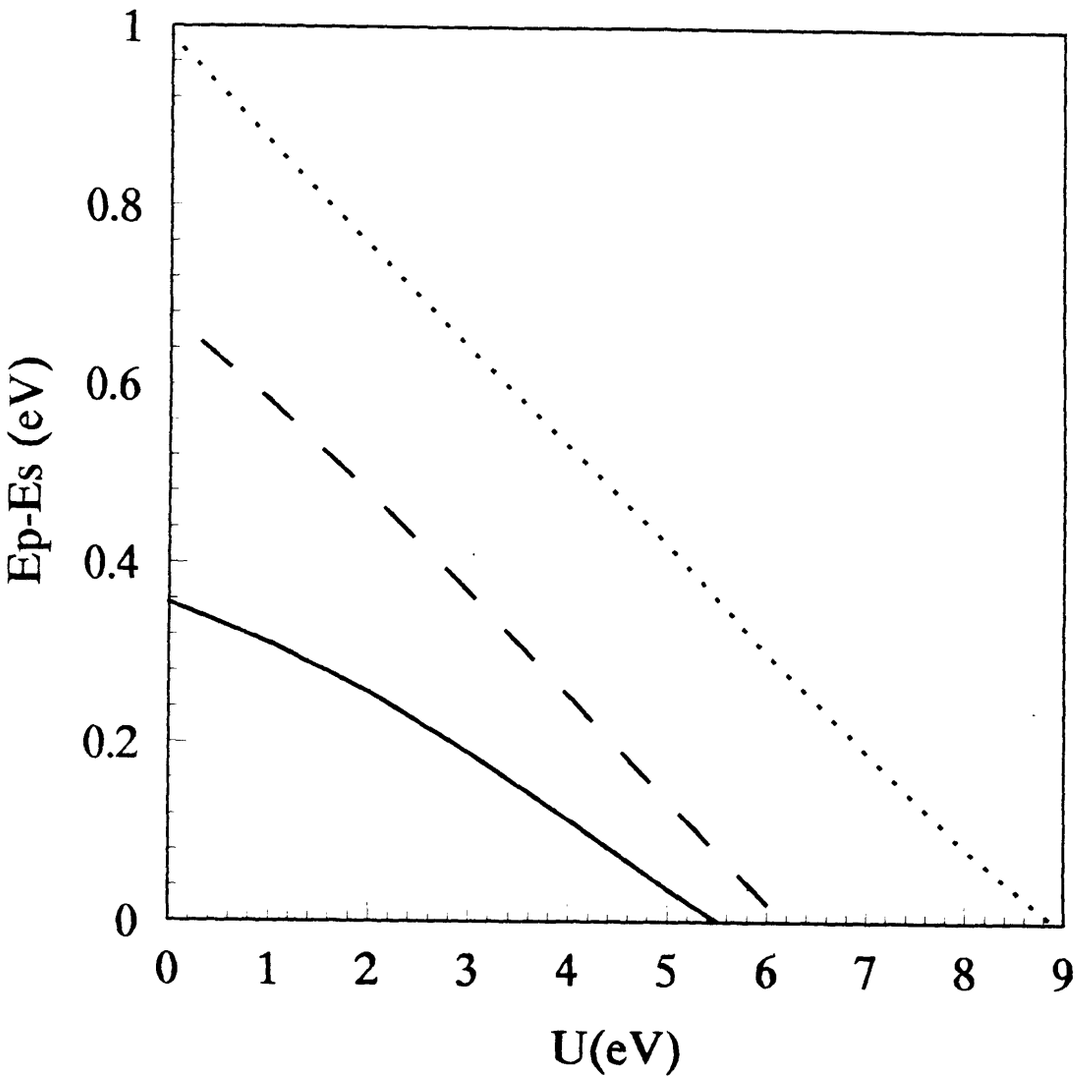

Figure 2.1. Difference between the polaron and soliton configuration energies ΔE as a function of on-site energy U for two (solid), four (dashed), and six (dotted) electrons in a chain of $N = 200$. ($V = W = 0$)

lattice because the interaction between polarons is intrinsically attractive and long-range. One point to note is that U_c increases as the number of added electrons increases. This is the same as saying that for increasing concentration (from 1% to 3%) the on-site repulsion needed to drive a transition increases. One might expect the contrary by noting that the slope of ΔE for greater numbers of electrons seems to increase. The crucial relationship, however, is that the value of ΔE at $U = 0$ increases much faster as the doping increases.

The values of U_c can be collected and plotted as a function of decreasing N, as in figure 2.2 where the x-axis is n/N (= %). Nearest neighbor interactions have been included in this figure for values of $V = 0.2$ and $0.4eV$. The results presented are only for the case of two electrons in the chain, but the general trend is true for any amount of doping. The upper region marked I and the one marked II correspond to regions where polarons and solitons are favored, respectively. The trend of increasing U_c as a function of concentration is clear demonstrating that given some value of U at 0% in phase II the soliton phase will persist. If one were to start in phase I, there will be a concentration beyond which solitons are favored, however. The result that V shifts the curves downward, therefore favoring polarons, can be explained in terms of charge distributions. Because the charge distribution for a soliton is more localized than in polarons and is only distributed in either even or odd sites, an overlaping soliton-antisoliton pair will gain more interaction energy from the V term than the corresponding polaron system. Thus V as well as U favor the polaron systems as a function of their strength.

In figure 2.3 we have considered the case of $V = W = 0$ for two, four, and six electrons in the chain. The pattern shown in figure 2.3 as the number of electrons is increased suggests that there is a limiting boundary for large n and N (but fixed n/N). We have extrapolated this behavior and presented a limiting curve as a dashed line. The limiting curve seems to exhibit the same behavior as do the others. This means that increasing concentration will not yield a polaron phase, if we had started in the soliton phase. We conclude then that it is unlikely that on-site

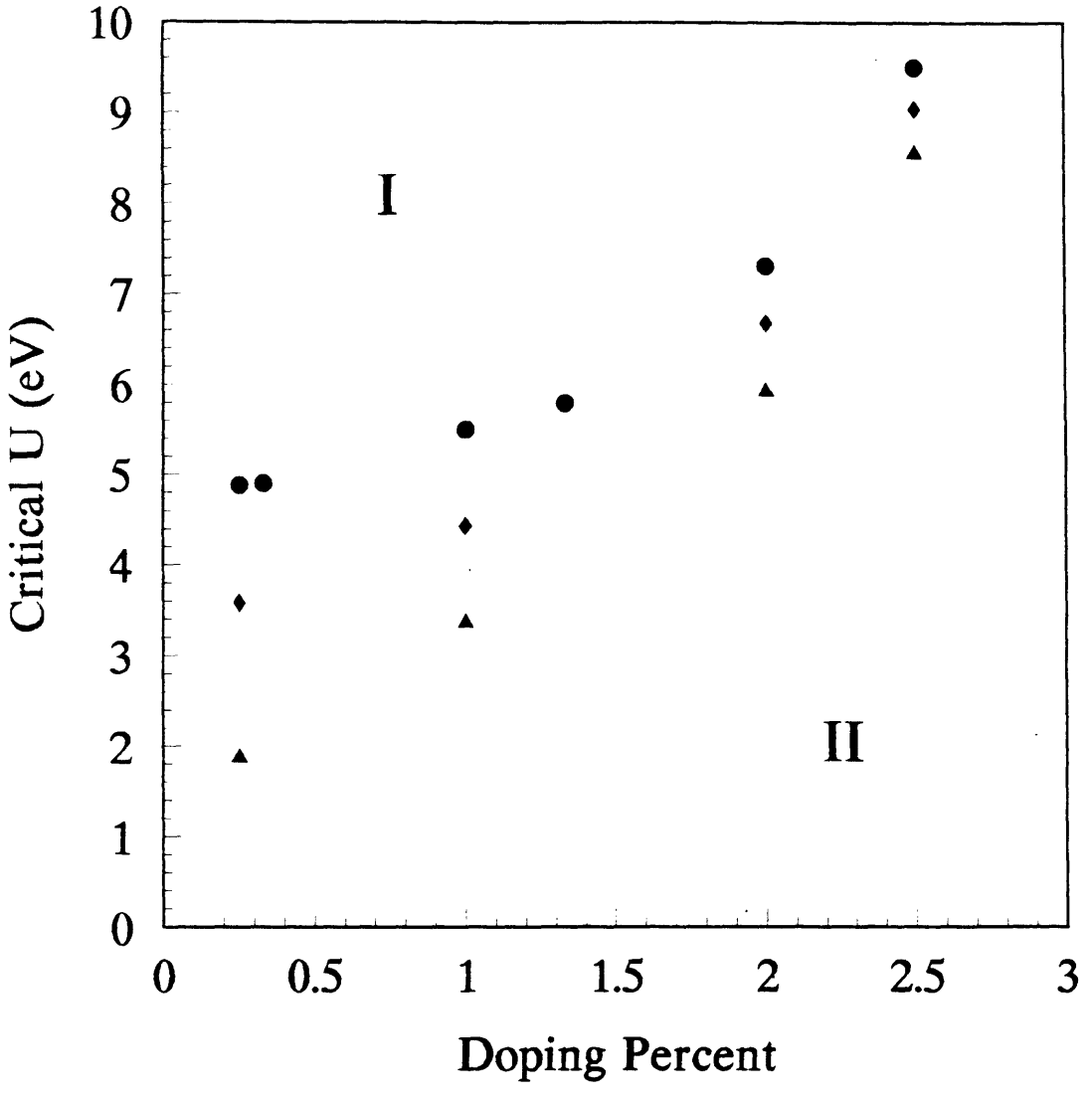

Figure 2.2. Critical on-site repulsion U_c versus concentration for two electrons in the chain. The results presented are for $V = W = 0$ (cirlces), $V = .2eV, W = 0$ (diamonds), and $V = .4eV, W = 0$ (triangles). Phase I and II stand for stable regions of polarons and solitons, respectively.

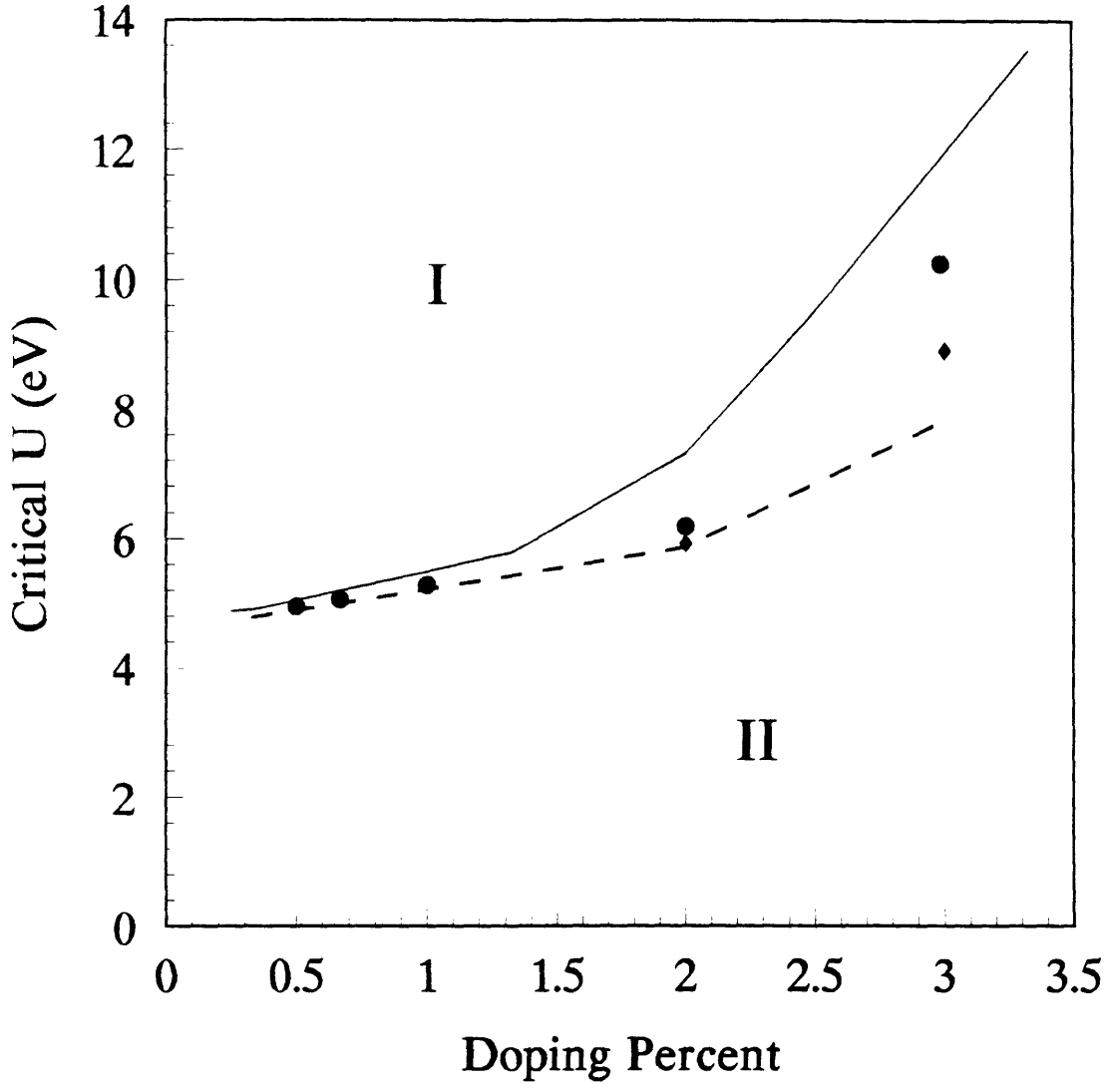

Figure 2.3. Critical on-site repulsion U_c versus concentration for $V = W = 0$. Solid line corresponds to two electrons, circles to four, and diamonds to six electrons. The dashed line represents an extrapolation to a system with an infinite number of doped electrons.

repulsion is responsible for the metal transition as a function of doping, although it *does* yields a transition as a function of its strength. Also, from figure 2.2 we see that for increasing nearest neighbor repulsion V, a smaller U_c can be achieved. However, nearest-neighbor repulsions ultimately stabilize the soliton phase once the doping is considered.

The non-diagonal term W has been considered in figure 2.4 where we present a phase diagram of W_c vs V at a value of $U = 4eV$ for $N = 200$. The values for W_c have been calculated in the same way as was done for the values of U_c. At a fixed value of U and V, the value of W at which $\Delta E = 0$ is W_c. The bond-charge W term is seen to give a different behavior from the other two terms. As a function of its strength the system if in phase I, is driven into phase II, that is, it breaks the polaron state into a soliton phase. On the other hand, W follows the same behavior as a function of the number of electrons in the chain, as do V and U. That is, it moves the boundary towards higher V, thereby destabilizing the polaron phase as a function of doping.

To further establish the robustness of the soliton phase, we can investigate if this phase is destroyed simply by increasing U but retaining the soliton occupation numbers of the bound states. In order to answer this question the order parameter is calculated as a function of U. In figure 2.5(a) we plot the order parameter of a chain containing two electrons in a solitonic level occupation. The length of the chain is $N = 600$. The corresponding charge density distributions are plotted in figures 2.5(b) and (c) for $U = 0$ and $U = 5$eV, respectively. In the plots of the charge densities the solid line and dashed line correspond to the charge densities in odd and even site numbers, respectively. This is accounted by the fact that solitons only reside on sites of a given parity. The corresponding antisoliton will be on the opposite parity as that of the soliton. The only apparent effect of the on-site repulsion on the order parameter seems to be the fact that the relative distance between the soliton-antisoliton pair gets smaller. The graphs of the corresponding charge density distributions indicate that no apparent change is observed between

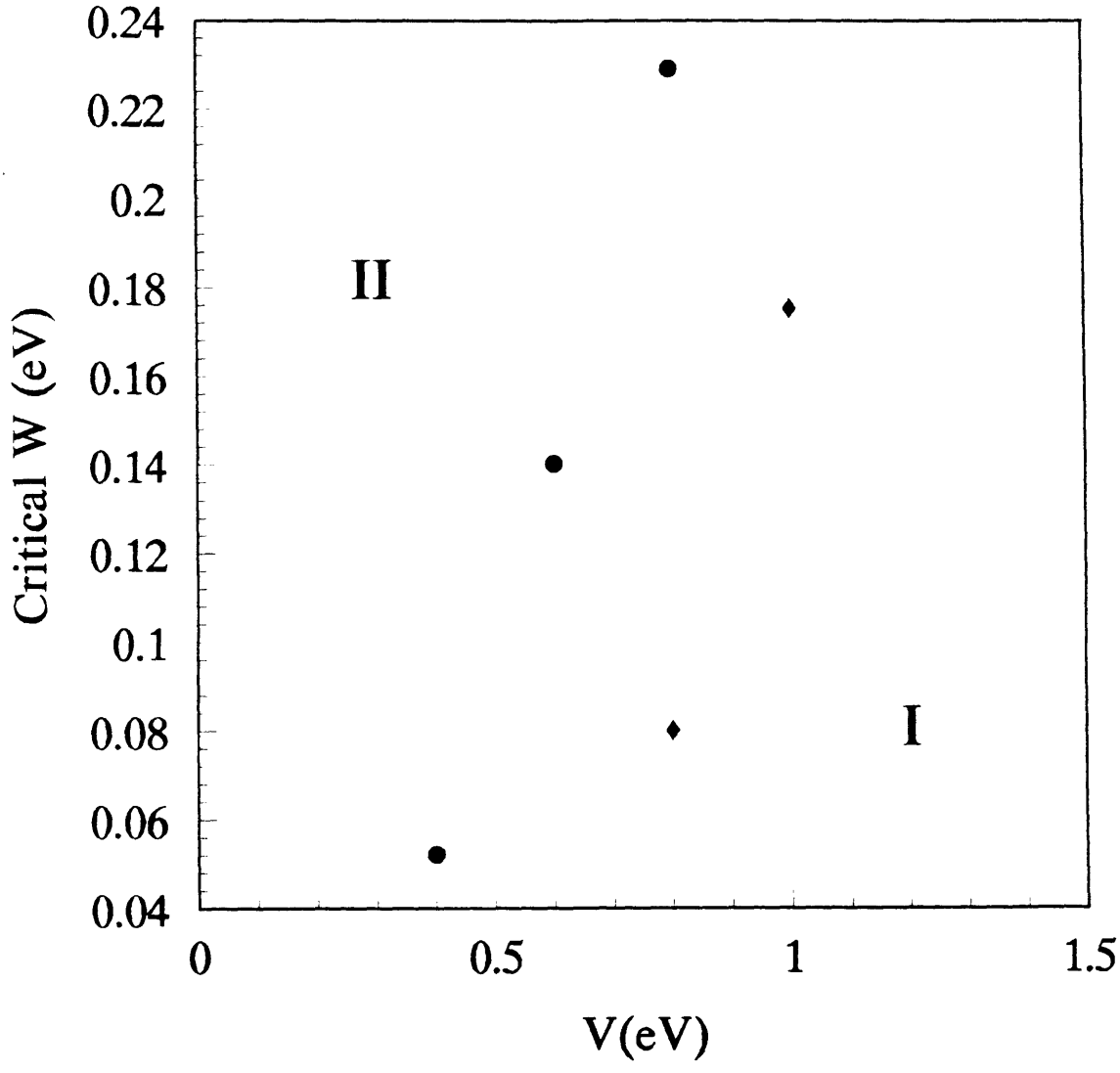

Figure 2.4. Critical value of W versus V at $U = 4$ for $N = 200$. Circles correspond to 2 electrons (1%) and diamonds to 4 electrons (2%).

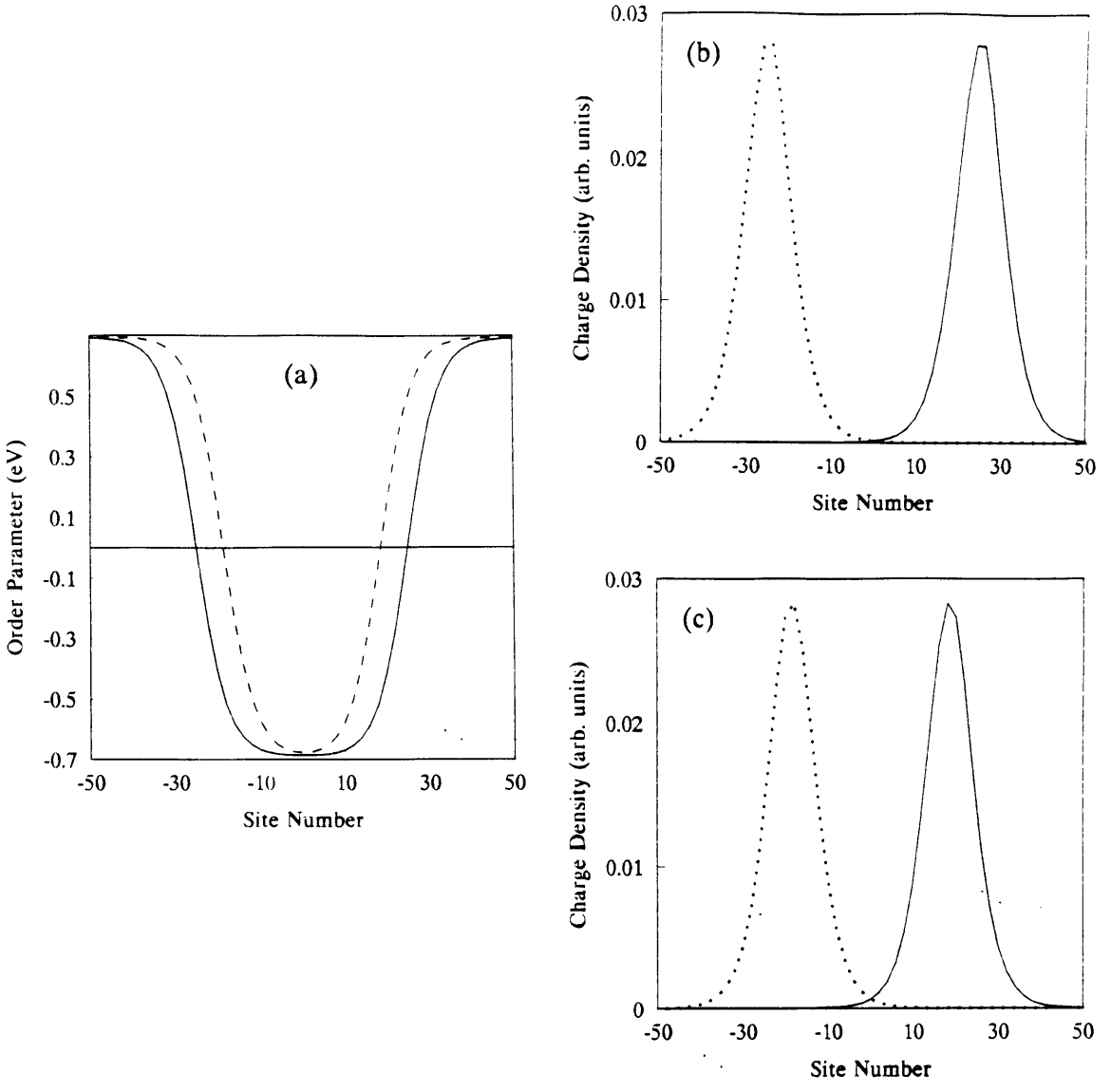

Figure 2.5. (a) Order parameter for a chain with two electrons in a solitonic configuration. The length of the chain is of $N = 600$. *The solid line corresponds to* $\Delta(x)$ *with* $U = 0$, *and the dashed line corresponds to* $U = 5eV$. *Note that the solitons in the* $U = 0$ *case get as far as necessary for their interaction energy to be zero, which is measured by the slope of the order parameter between them. (b) and (c) are the corresponding charge densities at odd (dotted) and even (solid) sites as a function of the position in the chain for the two U cases of 2.5(a). Case (b) is for* $U = 0$ *and (c) for* $U = 5eV$.

the two cases. Figure 2.6 corresponds to the same situation as presented in figure 2.5, but now for the case of a polaronic occupation number. The effect of the on-site repulsion is dramatically different in this polaronic case. The case for $U = 0$ (2.6(a) solid) shows the normal appearance of the two-polaron order parameter in the absence of any interactions. The dashed line shows how the on-site energy spreads the electronic charge throughout the chain in order to achieve a lower energy. That is, because double occupancy of a site costs energy, the system will try to spread as much as it can in order to get in average the least charge density per site. The plots of the charge densities (figures 2.6(b),(c)) illustrate this point. Figure 2.6(b) shows the normal equal distribution of the charge among both the odd and even numbered sites. Figure 2.6(c) explicitly illustrates how this same charge density is spread for $U = 5$eV. The fact that this arrangement is possible for the polarons but not for the solitons (figure 2.5) is the one responsible for the increase of the solitonic energy as a function of on-site energy repulsion. In general, the inability of the solitons to spread their charge distributions throught the chain, in contrast to the polarons, will drive the transition from a solitonic to a polaronic configuration as a function of U. This statement was already shown in figures 2.1 to 2.4.

To asses the influence that the length of the chain (the doping percent) has on the order parameter we again examine the above two cases, but for a much shorter chain. The cases presented in figure 2.5 and figure 2.6 correspond to a doping percent of about .3%. In the following we examine the highest doping allowed in our calculations which is of about 3%. In figure 2.7 the results are presented for two electrons in a solitonic configuration in a chain of $N = 70$. The order parameter in figure 2.7(a) shows a big difference from the behavior displayed in figure 2.5. Now the trend of the soliton-antisoliton pair to get closer has ceased. They attained a minimum distance and the greatest change is now in the form of the order parameter. For the values of U shown ($U = 0$ dashed-dotted, $U = 5$ dotted, $U = 8$ dashed, and $U = 11$ solid) the trend looks like we start from a solitonic order parameter and end up with a polaronic-like order parameter. This would imply that we are

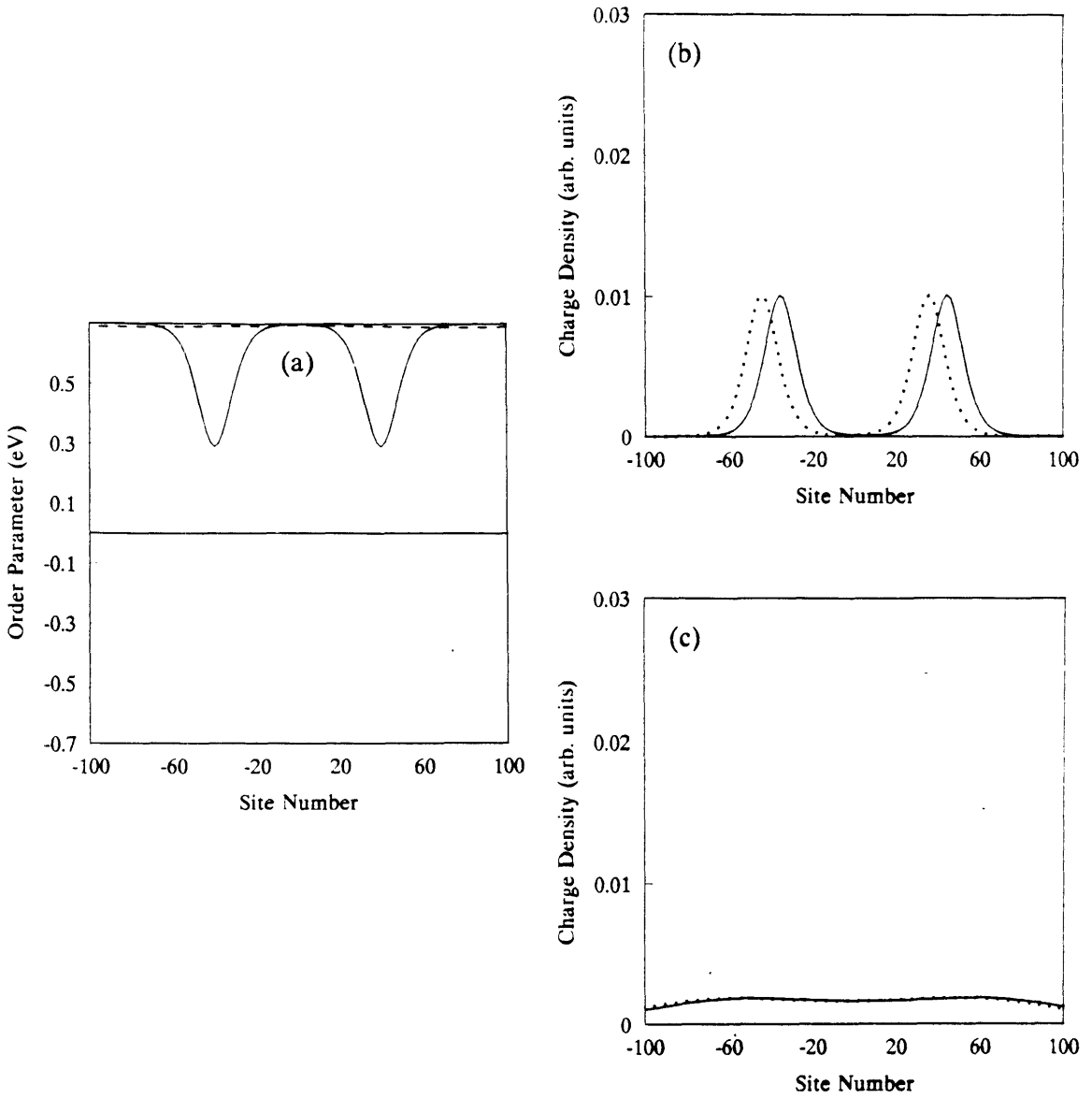

Figure 2.6. (a) Order parameter for a chain with two electrons in a polaronic configuration. The length of the chain is taken as $N = 600$. The solid line corresponds to the case of $U = 0$ and the dashed line to $U = 5eV$. (b) and (c) are the plots of the charge densities corresponding to $U = 0$ and $U = 5eV$, respectively. The line types indicate the charge densities at odd (dotted) and even (solid) sites.

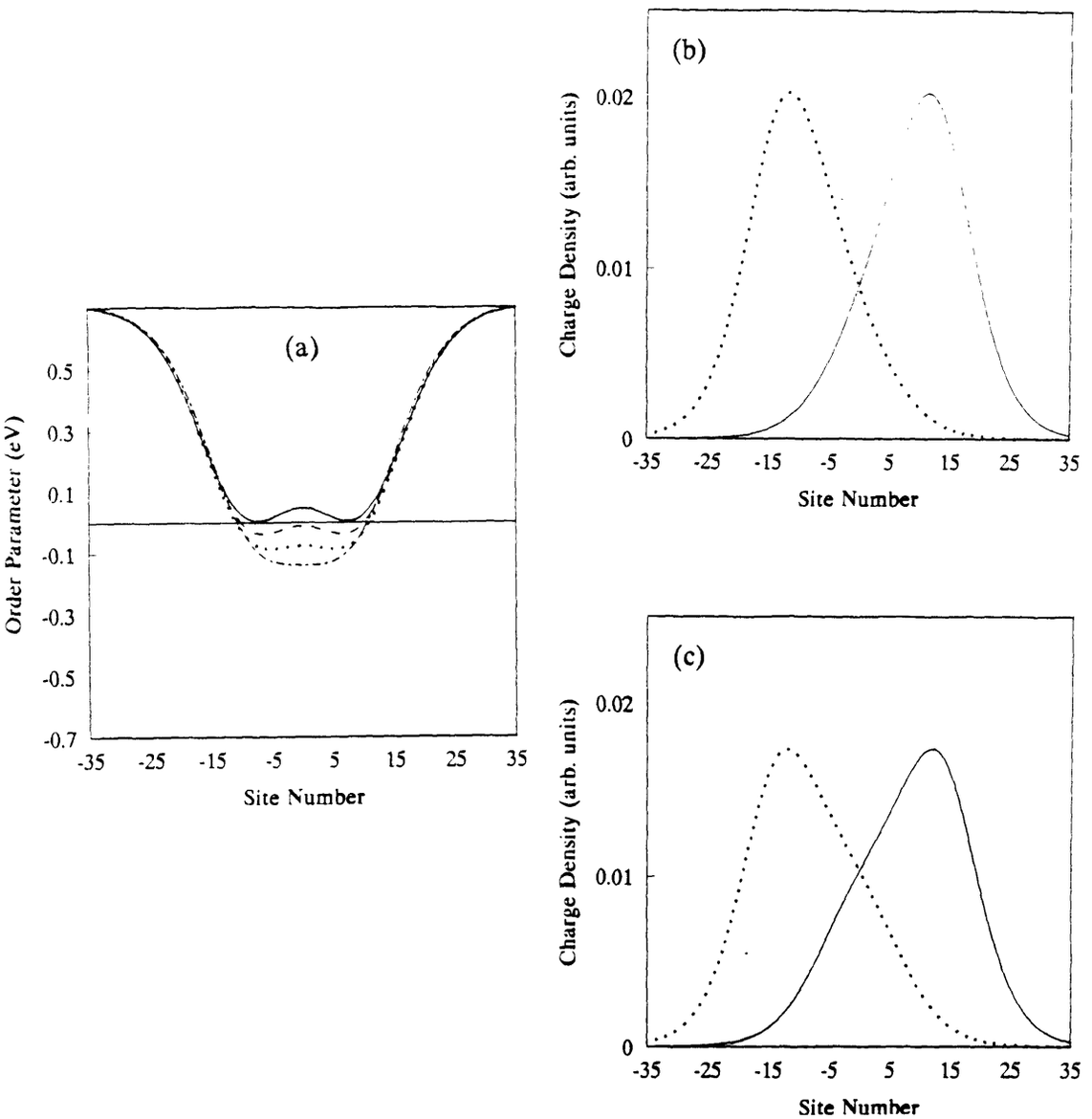

Figure 2.7. (a) Order parameter for a chain with two electrons in a solitonic configuration. The length of the chain is taken as $N = 70$. The dash-dot line corresonds to $U = 0$, the dotted to $U = 5eV$, the dashed to $U = 8eV$, and the solid to $U = 11eV$. (b) and (c) are the plots of the charge densities corresponding to $U = 0$ and $U = 11eV$, respectively. The line types indicate odd (dotted) and even (solid) sites.

reversing the reaction $P + P \rightarrow S + \overline{S}$ and transforming the solitons into polarons. This conjecture is refuted immediately by examining figures 2.7(b) and (c). Here the charge densities show no apparent change as a function of the on-site energy. The solitonic configuration of $U = 11\text{eV}$ is as robust as that for $U = 0$. This graph clearly shows that the solitonic character is preserved even at high electron-electron interactions. Now we look at the effect of the on-site repulsion on the corresponding polaronic configuration. In figure 2.8 results for $U = 0$ and $U = 11\text{eV}$ are shown for the case of the polaronic excitations. The main conclusion to be drawn from figure 2.8 is that the order parameter, as well as the charge densities show no significant change as a function of the on-site energy U. This is clearly in contrast to the case shown in figure 2.6 where the polarons spread throughout the chain in the presence of U. Now this is not possible due to the shortness of the chain. As a consequence, the average charge density per site will be more or less the same and the energy gain as a function of U will be large. That is, the polarons get much more expensive for higher dopings. This is precisely the trend obtained in figure 2.3 where for higher doping levels the U_c needed to break the solitons was much greater than that for smaller doping levels.

It is also an interesting question whether the above described effects are visible also for a higher number of electrons in the chain. In figure 2.9 we plot the order parameter of a chain with 6 electrons in a solitonic configuration for several values of the on-site energy. Figures 2.9(b) and (c) show their corresponding charge density distributions. The general trend is that the order parameter retains a solitonic characteristic, keeping both positive and negative values for $\Delta(x)$ for the values of U ranging from $U = 0$ to $U = 9\text{eV}$. The charge densities in (b) and (c) clearly show that the solitonic odd-even separation also persists.

Because one of the most important questions in the transition exhibited by PA has been whether a closing of the gap is obtained, we briefly comment on that respect in the following. By examining the set of $\{\omega_i\}$ that minimizes the energy for the non-interacting as well as the interacting cases the expected general trend that

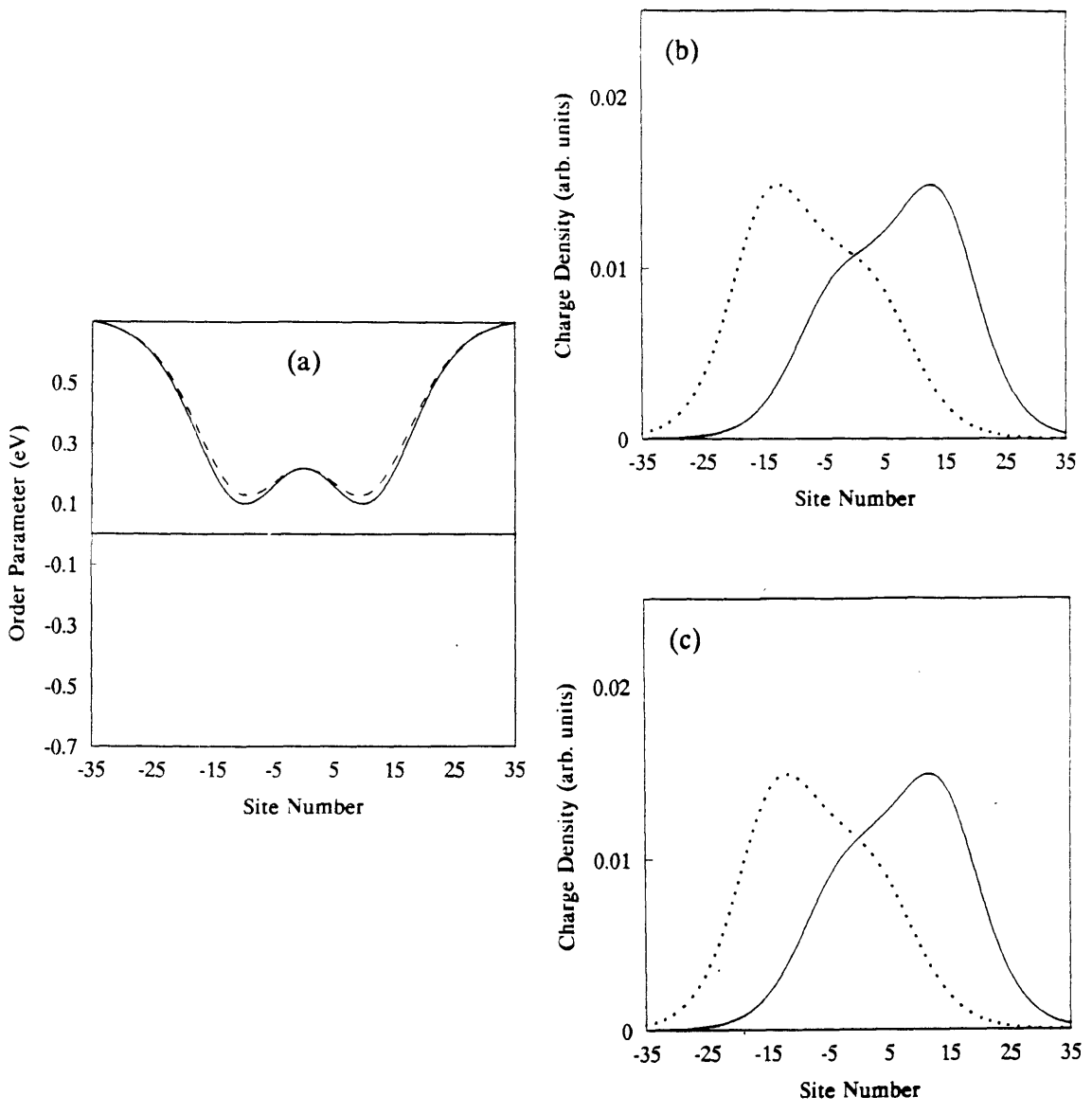

Figure 2.8. (a) Order parameter for a chain with two electrons in a polaronic configuration. The length of the chain is taken as $N = 70$. The solid line corresponds to the case of $U = 0$ and the dashed line to $U = 11eV$. (b) and (c) are the plots of the charge densities corresponding to $U = 0$ and $U = 11eV$, respectively. The line types correspond to odd (dotted) and even (solid) sites.

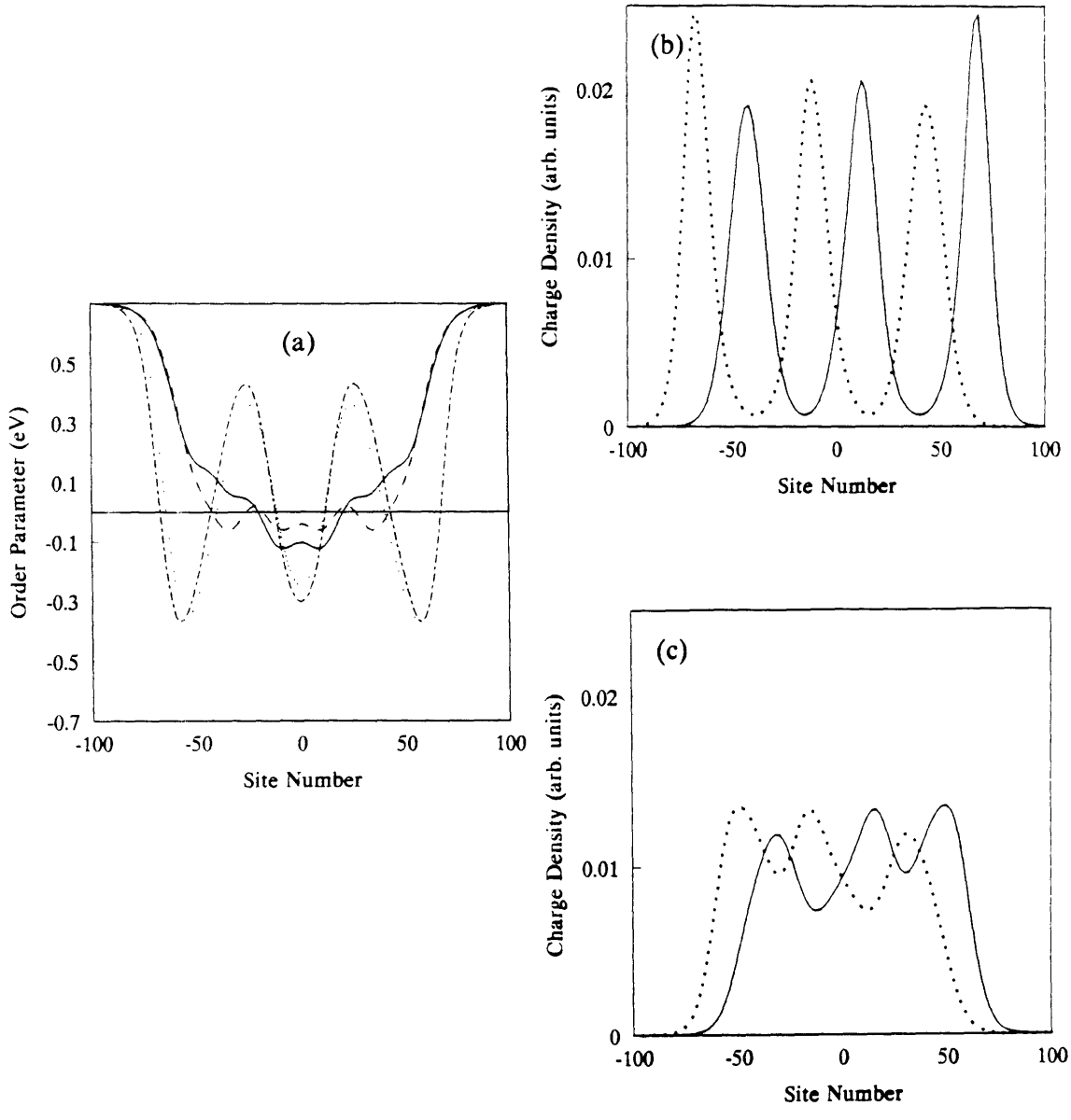

Figure 2.9. (a) Order parameter for a chain with six electrons in a solitonic configuration. The length of the chain is taken as $N = 200$. The dash-dot line corresonds to $U = 0$, the dotted to $U = 1eV$, the dahed to $U = 8eV$, and the solid to $U = 9eV$. (b) and (c) are the plots of the charge densities corresponding to $U = 0$ and $U = 9eV$, respectively. The line types correspond to odd (dotted) and even (solid) sites.

the levels start to form bands is observed. There are bands in the middle of the gap and at the symmetrically located levels for the soliton and polaron configurations, respectively. Up to the doping levels achieved in this work (around 3%) the levels seem to reduce the gap down to a value of the order of .3eV. The widening of the bands as a function of doping seem to obey a power law. On the next section we consider the magnetic susceptibility making use of a more detailed analysis of the rate of closure of the gap as a function of doping.

In conclusion, in this section we have shown how a transition from solitons to polarons in trans-polyacetylene can be achieved as a function of U alone, or U and V. W seems to break or dissociate polarons into solitons. This is related to other findings at half filling in which W increases dimerization [32]. In all the cases shown above an increase in concentration, via the decrease of the length of the chain or by increasing the number of electrons in the chain, ultimately favors solitons up to the concentration of 3%. However, we have no reason to believe that this trend will not continue to doping levels beyond 3% and into the metallic regime. We are then faced with the original question: what drives the onset of spins in polyacetylene? It has been proposed by several authors that interchain coupling effects must be included to describe the onset of the metal state in polyacetylene. Current estimates of the interchain hopping matrix element are around .15eV [19]. Based on our calculations, we can now estimate if an effect of this magnitude is sufficient to destabilize the soliton lattice at 5%. At a doping level of 5%, U=4eV, and V=.4eV, we estimate that a soliton lattice is more stable than the corresponding polaron one by .6eV. Interchain coupling effects of .6eV or higher would certainly then be sufficient to break up solitons on single chains. However, based on the estimates in the literature of $t_\perp$, it is unlikely if such effects are ultimately responsible for the transition from a soliton to a polaron lattice in trans-polyacetylene at the metal-insulator transition.

2.4. Pauli Susceptibility.

Given that we have established the robustness of the soliton lattice and its persistence at metallic concentrations (see figure 2.2), it is appropriate to investigate if a Pauli susceptibility emerges. Because charged solitons are spinless, it seems as if such an endeavor is doomed at the outset. However, reflection on the definition of the Pauli susceptibility indicates otherwise. Physically the Pauli susceptibility is proportional to the number of electrons within k_BT of the Fermi temperature. It is the electrons occupying these states that can flip their spins and allign with an external magnetic field. For a set of overlapping states the ratio $\frac{k_BT}{T_F}$ is proportional to the density of states. Because the Fermi level in polyacetylene lies at midgap, the Pauli susceptibility is expected to vanish. However, as the doping level increases, the bound state soliton levels spread out in the gap and ultimately could provide a finite density of states at the Fermi level. Hence, we simply need to investigate how the single particle levels we have calculated fill the gap region.

Shown in figures 2.10 and 2.11 are the resultant soliton levels for $U = 0$ and $U = 4$eV, respectively, as a function of the doping level. The corresponding chain lengths used to compute the bound state energies are indicated on each respective curve. The lower curves shown in these figures (closest to the lower axis) are bound soliton states that originate at mid-gap. The upper states (at the top of the graph) arise from the conduction band. As is evident in both cases, these levels merge to fill the energy gap. In the U=0 case, the soliton levels merge as p^5 whereas when on-site repulsions are turned on (figure 2.11) a slower rise of p^2 is observed, where p is the doping level. The slower rate of filling the mid-gap states when $U \neq 0$ is consistent with the observations that U enhances dimerization in the ground state [10,11,13,14,16,17,28,34,35]. Because we perfomed calculations only up to a doping level of 3.3% we cannot predict definitively whether the gap closes at a doping level of 6%. Based on our calculations, however, we do not suspect the trend of gap closing to desist as the dopant level increases further. Hence, we extrapolate the

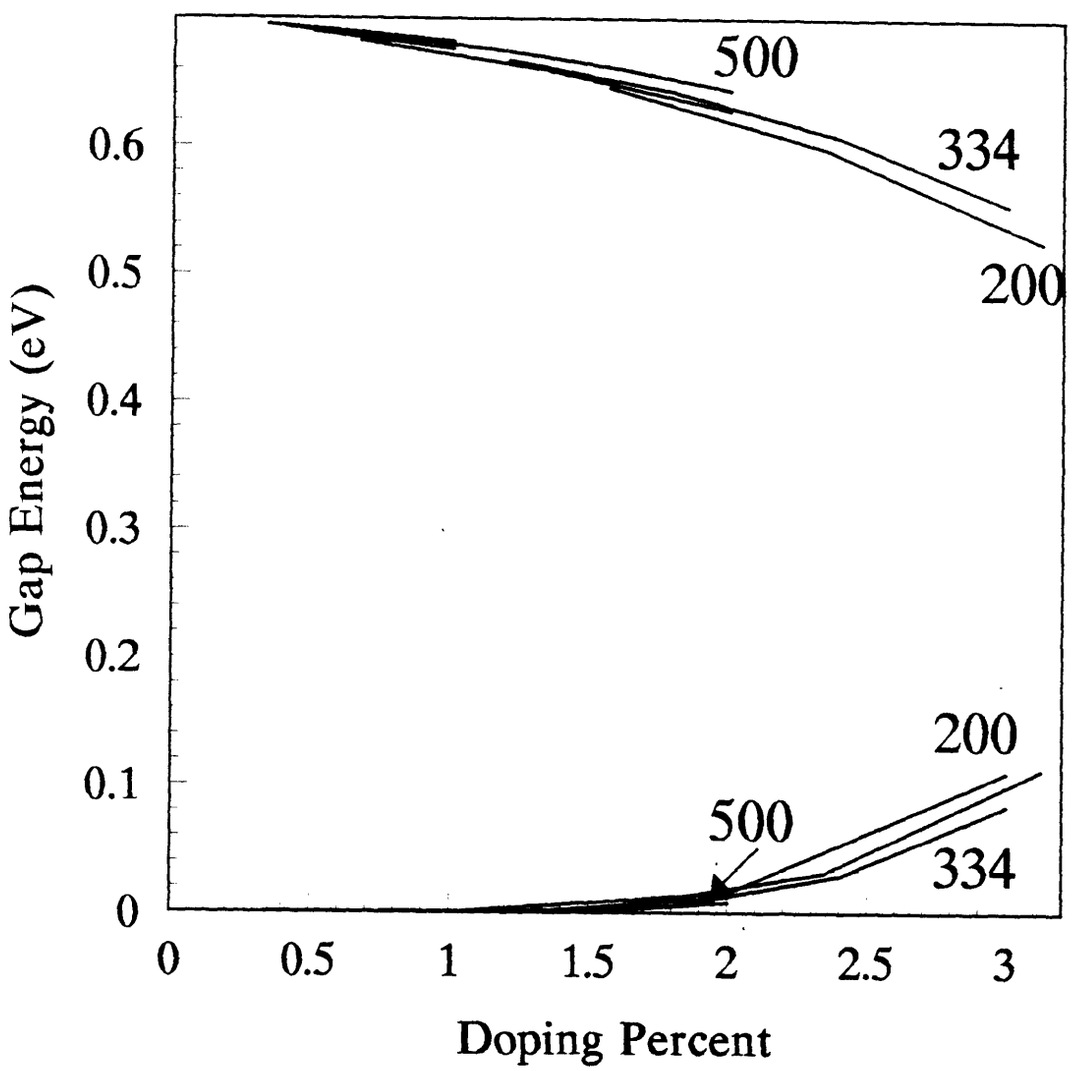

Figure 2.10. Soliton levels as a function of doping for several lengths of chains indicated in each case. The value of the on-site energy is taken as $U = 0$. The region in energy shown corresponds to the upper half of the gap (from $\epsilon = 0$ to $\epsilon = .7eV$). The trend of the levels to close the gap is shown.

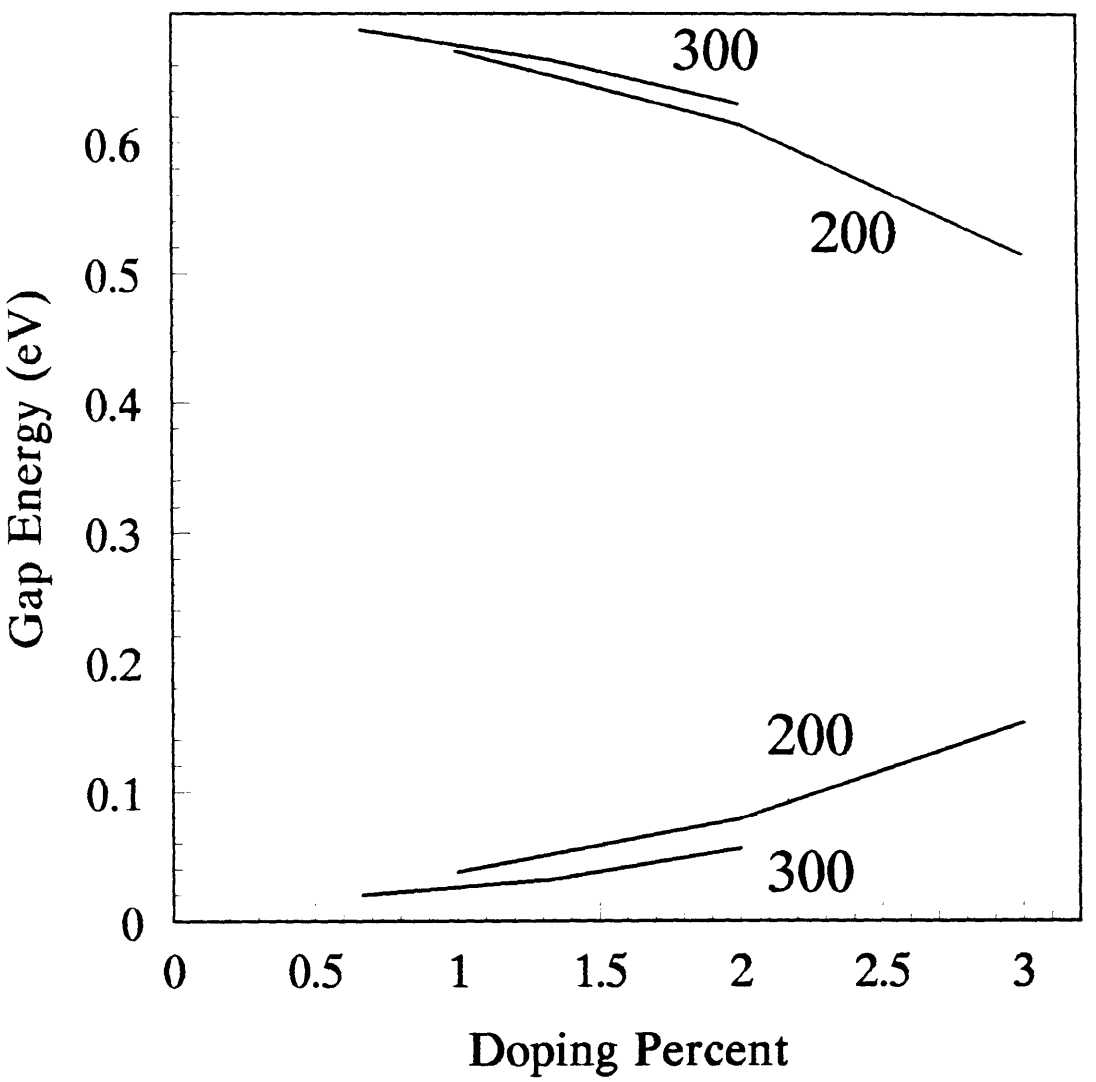

Figure 2.11. Soliton levels as a function of doping for two values of the lengths of the chains. The value of the on-site energy is taken as $U = 4eV$. The region in energy shown corresponds to the upper half of the gap (from $\epsilon = 0$ to $\epsilon = .7eV$). The rate of closing of the gap is smaller than that one shown in figure 2.10.

trends shown in figures 2.10 and 2.11 to arbitrary concentrations keeping in mind that we cannot conclude based on our results that the gap ultimately closes. We find that the upper and lower levels are best described by a function of the form $E_{l,h} = mp^x + C$, where l and h refer to the lower and upper soliton levels, m is the rate at which the gap closes and C is a constant. For the lower level $C \approx 1/N$ and in the upper level $C \approx \Delta_o$. These values were obtained from figures 2.10 and 2.11. In figure 2.12 we plot the form of $E_{l,h}$ for a chain of $N = 600$ and with $U = 4$eV. A residual gap of .08eV is seen to persist from $p > 6.5\%$ on. The Fermi level is depicted as the solid and dashed lines that lie between the upper and lower levels. The solid (100K) and dashed (300K) show the temperature dependence and relative position of the Fermi level, μ.

With the scaling function for $E_{l,h}$ in hand, we can now calculate the resultant magnetic susceptibility. We first must calculate the magnetization

$$M = \mu_B^2 B\beta \int d\epsilon g(\epsilon) f(\epsilon)[1 - f(\epsilon)]\,, \tag{2.25}$$

where $g(\epsilon)$ is the density of states and $f(\epsilon)$ is the Fermi distribution function. There are two contributions to $g(\epsilon)$, one from the continuum (valence) states and the other from the bound states in the gap. Because the continuum states are far away from the Fermi level, their contribution to the resultant magnetization is negligible. Also, we take the density of states for the bound levels, $g(\epsilon)$, as a delta-function located at the bound state energies, ω_i. Performing the integral in equation (2.25) and further taking the derivative with respect to the B-field, we will obtain the magnetic susceptibility

$$\chi \approx \frac{\mu_B^2 \beta}{2N} \sum_{i=1}^{n_b} [\cosh^{-2} \frac{\beta}{2}(\omega_i + \mu) + \cosh^{-2} \frac{\beta}{2}(\omega_i - \mu)]. \tag{2.26}$$

In equation (2.26) the parameter n_b corresponds to the number of bound states and the Fermi level μ is obtained by demanding that the integrated product of the density of states and the Fermi distribution function yield the number of added electrons. The complete derivation of equation (2.26) is given in Appendix G.

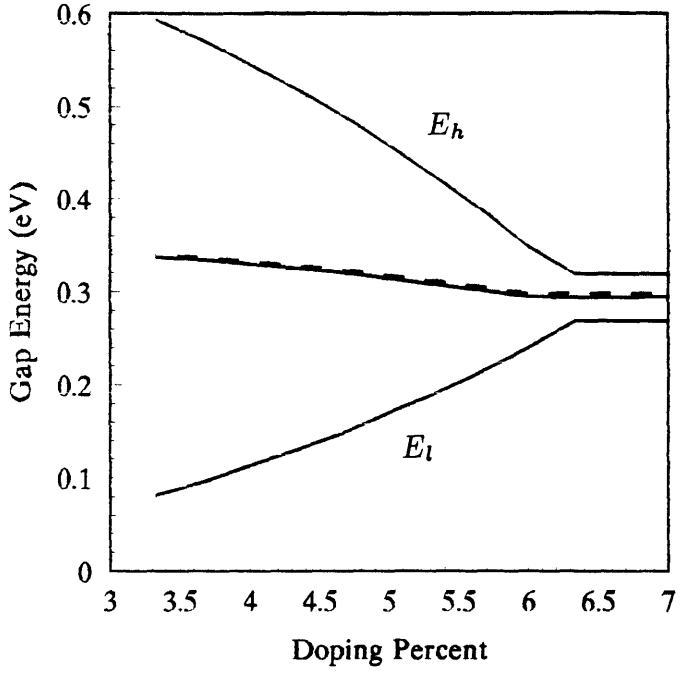

Figure 2.12. Plot of the levels E_l (lower) and E_h (higher) given by fitting the data from figures 2.10 and 2.11. The calculation is for $N = 600$, $U = 4eV$, and residual gap of $.08eV$. The energy axis represents the upper half portion of the gap. The upper solid line and the lower one represent E_h and E_l, respectively. The middle solid and dashed lines are the position of the fermi level for the temperatures of a 100K and 300K, respectively.

We have plotted equation (2.26) in figure 2.13 with $U = 0$ for chain lengths varying from N=400 to N=800. The residual gap is .05eV. The sudden rise in the calculated susceptibility arises from the form of equation (2.26). The hyperbolic functions cause there to be an exponential increase in the magnitude of χ as the levels get closer to each other. The apparent leveling of the curves at $p \sim 5\%$ comes from the fact that at that point the residual gap is the one ruling the position of the levels. Therefore, because the levels do not get any closer than this residual gap, the susceptibility retains a constant value. The fact that the curves depend on the length L of the chain may seem surprising since all the quantities appear to be parametrized by the concentration and not by the length. However, we believe that these results are correct and in Appendix H we give a brief explanation of why there should be an L dependence on the percentage at which the on-set is realized. In figure 2.14 results for the same parameters but using $U = 4$eV are presented. The effect of the on-site interaction on the on-set of the susceptibility is clearly distinct from the one depicted in figure 2.13. From figure 2.11 we know that the rate of closure of the gap diminishes with U. This is reflected now in a much later on-set of the magnetic susceptibility as a function of doping. This means that the effect of the interaction U is to move the point of on-set towards higher values of doping. In figures 2.15 and 2.16 we present the results for the same chain lengths and values of U. The only variation is in the size of the residual gap, that now is .08eV. This translates into a smaller value for the saturation of the susceptibility. Figure 2.16 shows for $N = 600$ and residual gap of .08eV the best fit to the experimental values.

Of great importance is also the temperature dependence of the magnetic susceptibility. Experiments show that the susceptibility changes from a Curie-like T-dependence to a T-independent region in the high doping regime. In order to asses the correctness of our calculations we plot in figure 2.17 the temperature dependence of the susceptibility at three different doping percents. The calculations are for a chain of $N = 600$, $U = 4$eV, and a residual gap of .08eV (best fit). The solid ($p = 4.67\%$) and dashed lines ($p = 5.67\%$) show a strong temperature depen-

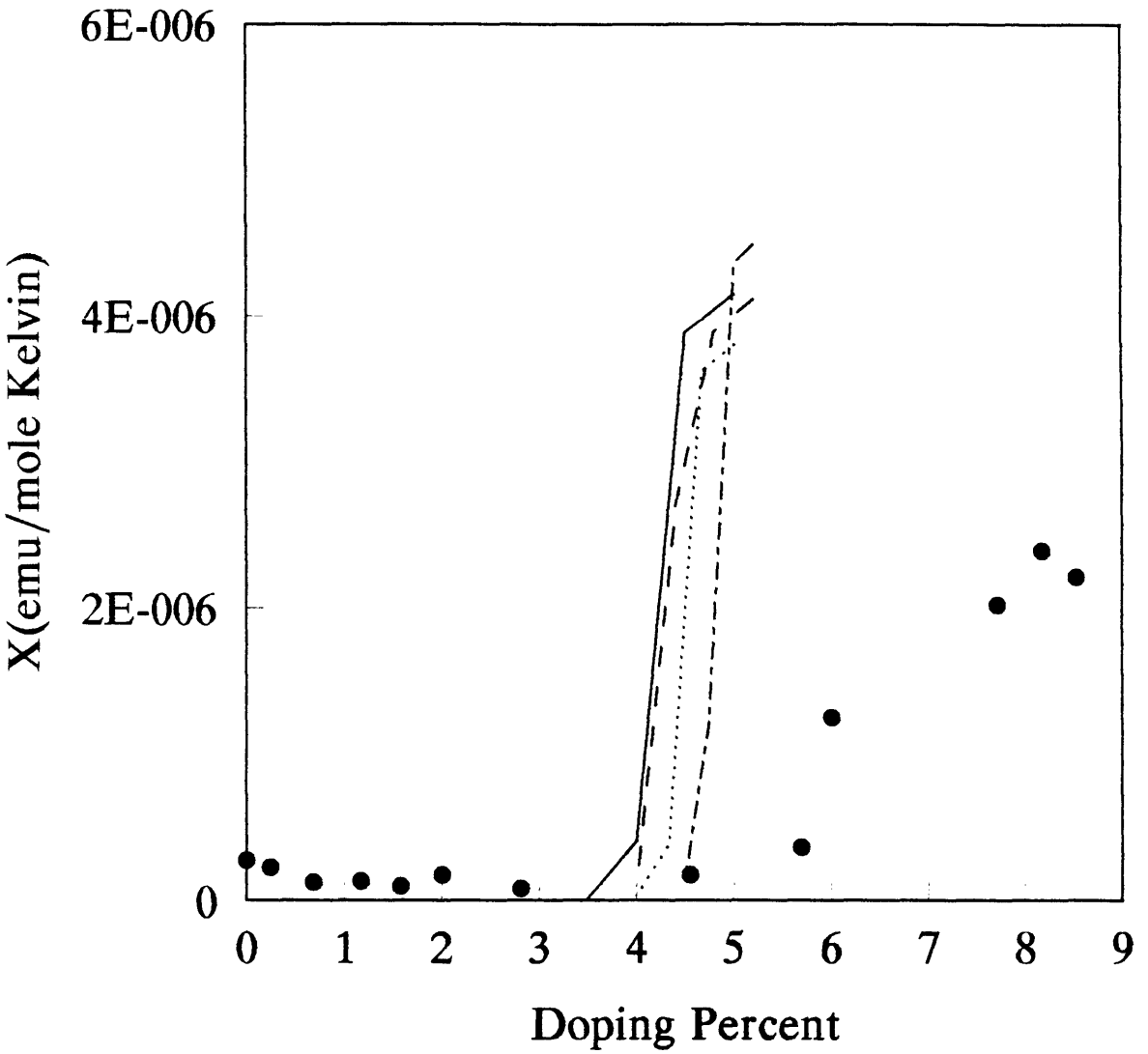

Figure 2.13. Magnetic susceptibility as a function of doping percent. The lines are from equation (2.26) with a residual gap of .05eV and a $U = 0$. The solid line corresponds to $N = 400$, the dashed to $N = 500$, the dotted to $N = 600$, and the dash-dotted to $N = 800$. The experimental data (big dots) are taken from ref. 16.

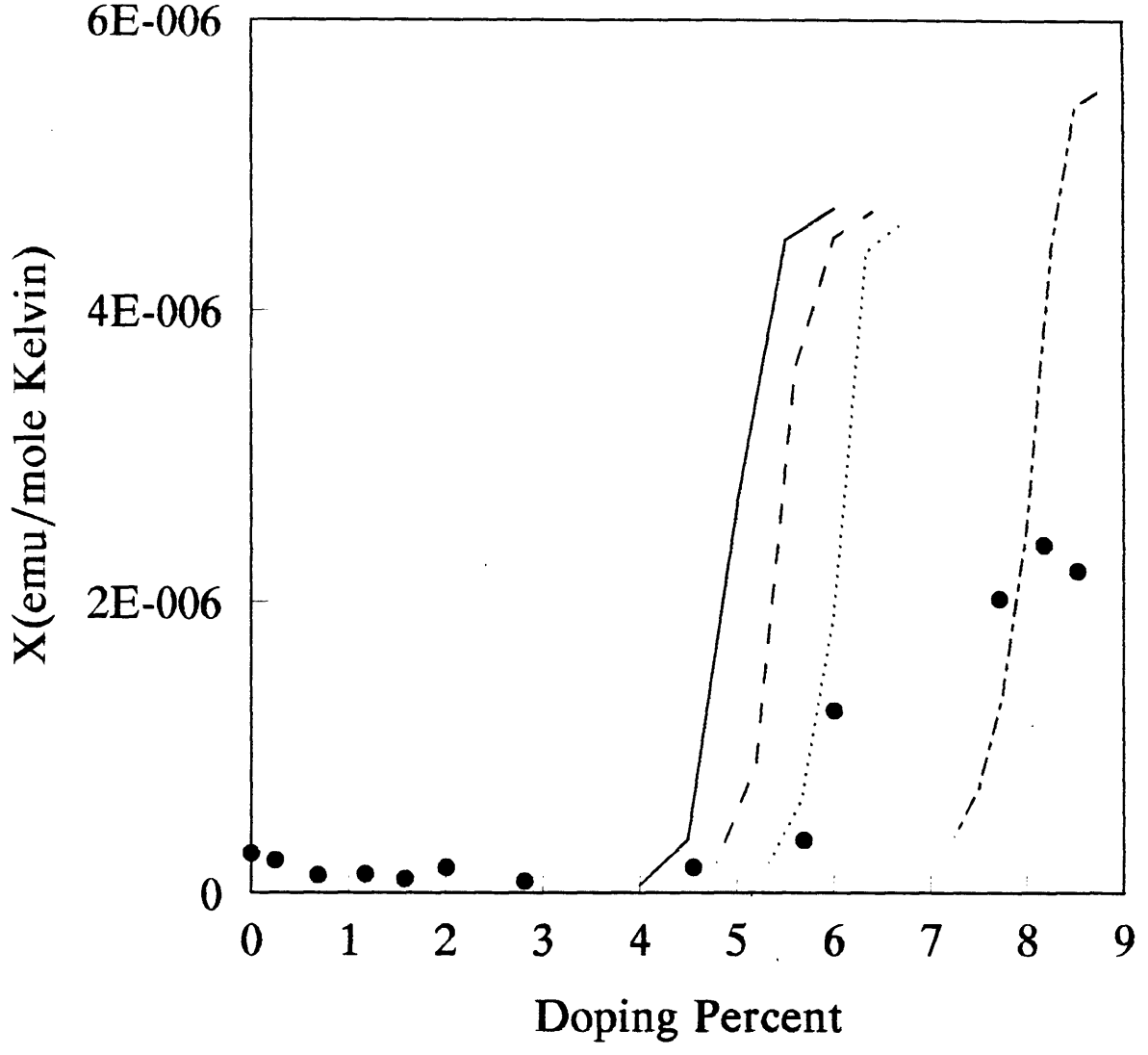

Figure 2.14. Magnetic susceptibility as a function of doping percent. The lines are from equation (2.26) with a residual gap of .05eV and a U = 4eV. The solid line corresponds to N = 400, the dashed to N = 500, the dotted to N = 600, and the dash-dotted to N = 800. The experimental data (big dots) are taken from ref. 16.

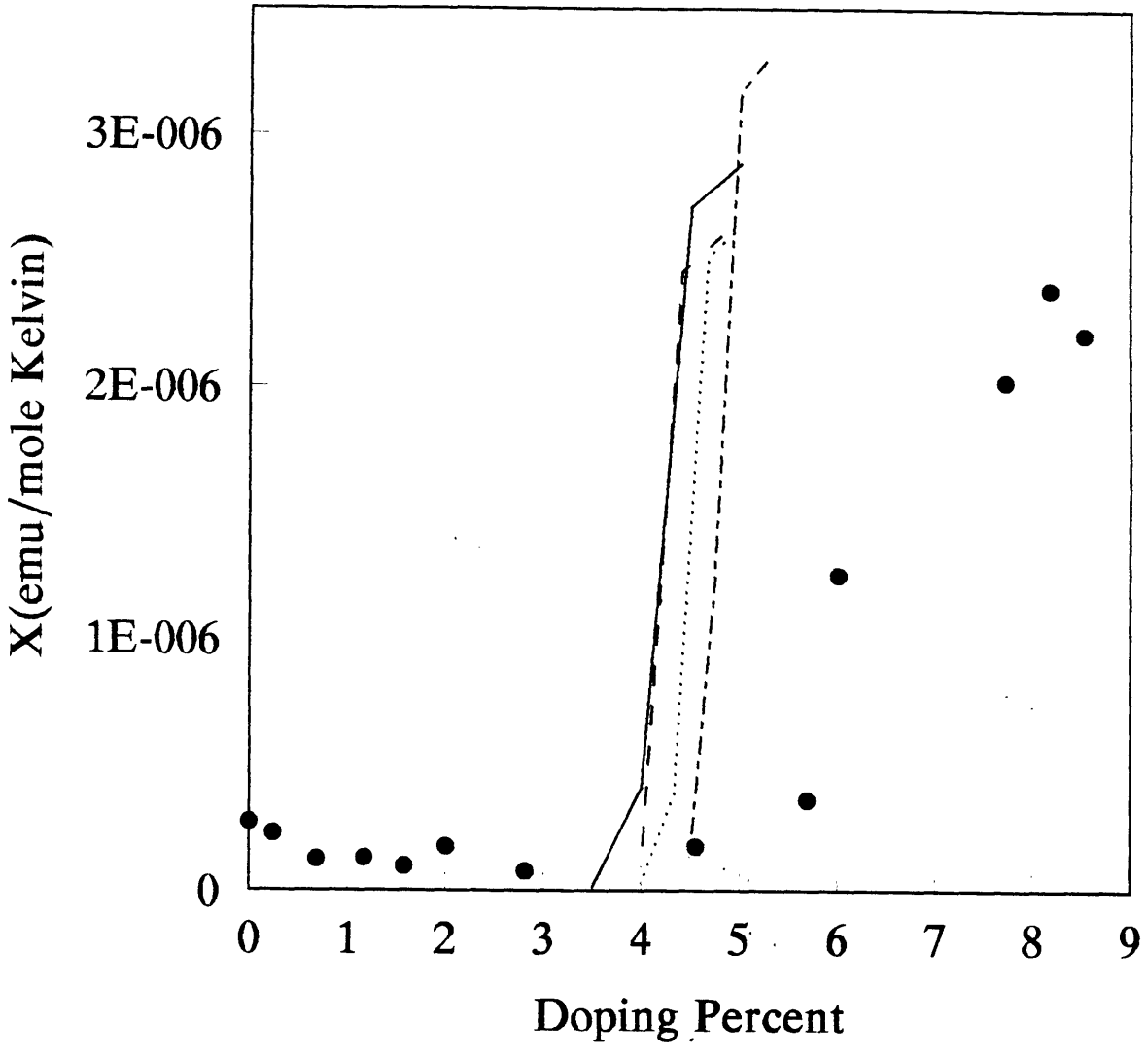

Figure 2.15. Magnetic susceptibility as a function of doping percent. The lines are from equation (2.26) with a residual gap of .08eV and a U = 0eV. The solid line corresponds to N = 400, the dashed to N = 500, the dotted to N = 600, and the dash-dotted to N = 800. The experimental data (big dots) are taken from ref. 16.

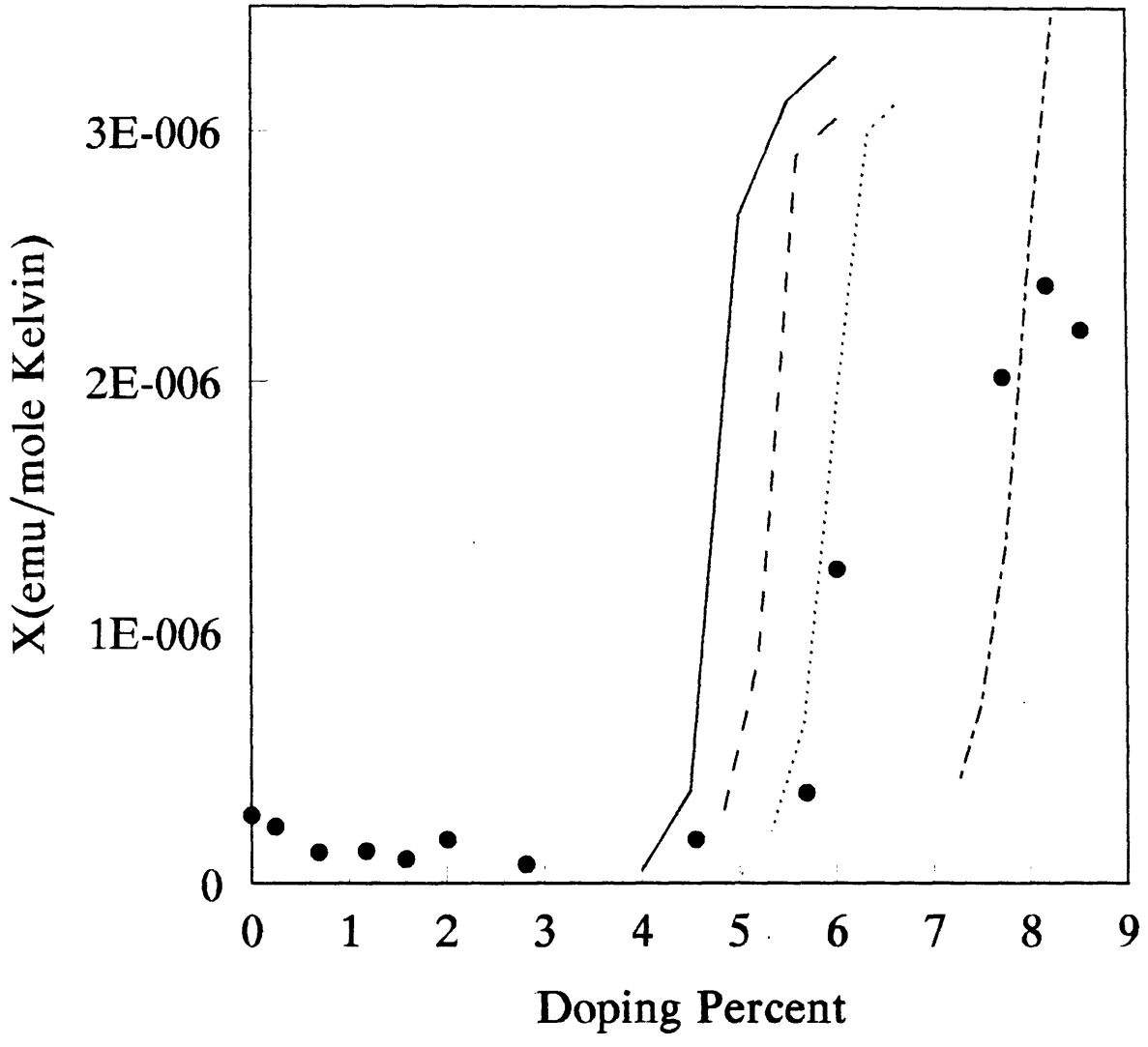

Figure 2.16. Magnetic susceptibility as a function of doping percent. The lines are from equation (2.26) with a residual gap of .08eV and a U = 4eV. The solid line corresponds to N = 400, the dashed to N = 500, the dotted to N = 600, and the dash-dotted to N = 800. The experimental data (big dots) are taken from ref. 16.

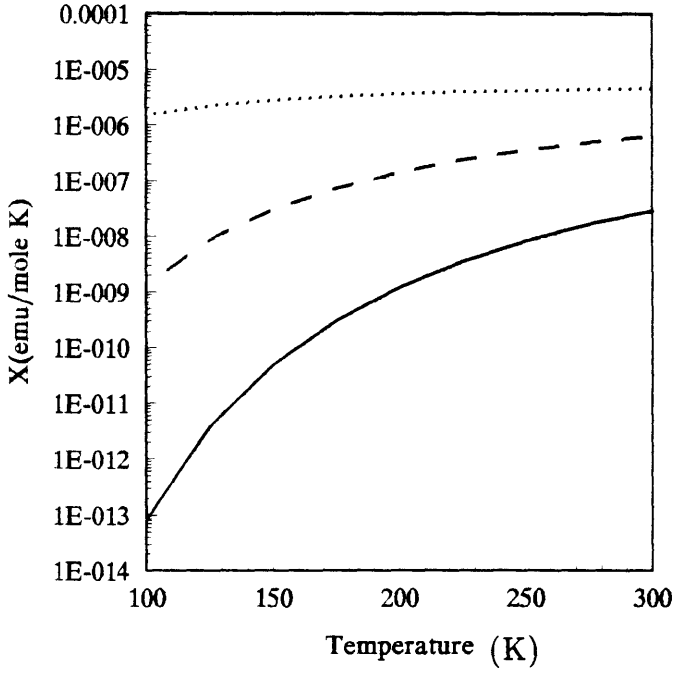

Figure 2.17. Temperature dependence of the magnetic susceptibility for three doping levels. The solid line corresponds to $p = 4.67\%$, the dashed to $p = 5.67\%$, and the dotted to $p = 6.67\%$. Of the three, only the dotted one is above the transition indicating that above the rapid onset the susceptibility is basicaly T-indenpendent. The calculations are for $N = 600$, $U = 4eV$, and a residual gap of $.08eV$.

dence. On the other hand, the dotted line ($p = 6.67\%$), above the transition, shows a T-independent behavior for the temperature range shown. The fact that the susceptibility decreases for low temperatures in the low doping cases is due to the fact that it is more difficult to flip the electrons close to the Fermi level. Although at a doping of $p = 6.67\%$ there is still a residual gap of .08eV (larger than $k_B T$), the probability of flipping, measured by the susceptibility, is considerably higher than for the other two cases and agrees remarkably well with experiments.

We now comment on the dependence of the on-set of the magnetic susceptibility to the length of the chain, as illustrated in figures 2.13 through 2.16. Our calculations propose that as the chains increase in length the on-set of a Pauli Susceptibility is delayed to higher values of the doping percent. This could be confirmed experimentally if for cleaner and more ordered systems (containing longer uninterrupted chains) the susceptibility exhibited this behavior. Exactly along this lines newly developed materials [40] when iodine doped exhibit higher conductivities which can be atributed to highly ordered structures. Also, measurements of the magnetic susceptibility have resulted in an on-set at a higher percent of approximately 10% [41]. Doubts could be raised as to the relation between the ordered structure and the conjugation lengths in these systems [42], arguing that definite experimental results are still missing. However, we strongly feel that the evidence is clear in showing a chain-length dependence in the magnetic properties. A brief and simple explanation to the rate of closure of the gap, which is the one giving rise to the length dependence, as a function of the length L of the chain is given in Appendix H.

2.5. Conclusions.

In conclusion, the dramatic rise in the susceptibility is a result of the soliton levels spreading to fill the gap. The susceptibility ceases to rise precipitously until the gap

has reached its minimum value, Γ. In the region where the upper and lower energy levels are separated by a residual gap of Γ, the susceptibility becomes independent of temperature. We then interpret the Pauli susceptibility in polyacetylene as a result of a closing of the upper and lower soliton levels to a narrow gap of width Γ. The function of the residual gap is two-fold. First it is responsible for the turn on of the Pauli susceptibility and secondly, it results in the vanishing of the temperature dependence of the susceptibility. We conclude then that a soliton lattice is stable in the metallic phase and consistent with a turn on of a Pauli susceptibility at a doping level of 6% in polyacetylene.

References for Chapter 2.

1. W.-P. Su, J.R. Schrieffer, A.J. Heeger, *Phys. Rev. B*, **22**, 2099 (1980).
2. D.K. Campbell, T.A. DeGrand, S. Mazundar, *Phys. Rev. Lett.*, **52**, 1717 (1984).
3. J.E. Hirsch, *Phys. Rev. Lett.*, **51**, 296 (1983).
4. S. Kivelson, W.-P. Su, J.R. Schrieffer, A.J. Heeger, *Phys. Rev. Lett*, **58**, 1899 (1987).
5. W.-K. Wu, S. Kivelson, *Phys. Rev. B*, **33**, 8546 (1986).
6. J.E. Hirsch, M. Grabowski, *Phys. Rev. Lett.*, **52**, 1713 (1984).
7. K.A. Chao, S. Stafström, *Mol. Cryst. Liq. Cryst.*, **118**, 45 (1985).
8. D.K. Campbell, J.Tinka Gammel, E.Y. Loh, *Synth. Met.*, **27**, A9 (1988).
9. S. Kivelson, A.J. Heeger, *Synth. Met.*, **17**, 183 (1987).
10. E.M. Conwell, H.A. Mizes, H.-Y. Choi, *Synth. Met.*, **41-43**, 3675 (1991).
11. S. Hasegawa, M. Oku, M. Shimizu, J. Tanaka, *Synth. Met.*, **38**, 371 (1990).
12. J. Tanaka, C. Tanaka, *Prog. Theor. Phys. Supp.*, No. 113, p. 61 (1993).
13. M. Dinter, *Phys. Rev. B*, **39**, 8423 (1989).
14. S. A. Brazovskii, S. A. Gordyunin, N. Kirova, *JETP Lett.* **31**, 456 (1980).
15. M.I.Salkola, S.A. Kivelson, *Prog. Theor. Phys. Supp.*, No.113, 53 (1993).
16. F. Moraes, J. Chen, T.-C. Chung, A.J. Heeger, *Synth. Met.*, **11**, 271 (1985).
17. Y.H. Kim, A.J. Heeger, *Phys. Rev. B*, **40**, 8393 (1989).
18. S. Stafström, *Phys. Rev. B*, **43**, 9158 (1991).
19. H.A. Mizes, E.M. Conwell, *Phys. Rev. Lett.*, **70**, 1505 (1993).
20. S.A. Kivelson, M.I. Salkola, *Synth. Met.*, **44**, 281 (1991).
21. S. Stafström, K.A. Chao, *Phys. Rev. B*, **30**, 2098 (1984).
22. X.Q. Yang, D.B. Tanner, A. Feldblum, H.W. Gibson, M.J. Rice, A.J. Epstein, *Mol. Cryst. Liq. Cryst.*, **117**, 267 (1985). X.Q. Yang, D.B. Tanner, M.J. Rice, H.W. Gibson, A. Feldblum, A.J. Epstein, *Solid State Commun.*, **61**, 335 (1987).
23. C. Benoit, O. Bernard, M. Palpawer, M. Rolland, M. J. M. Abadie, *J. Phys.* (Paris), **44**, 1307 (1983).

24. D.B. Tanner, G.L. Doll, A.M. Rao, P.C. Eklund, G.A. Arbuckle, A.G. MacDiarmid, *Synth. Met.*, **28**, D141 (1989).

25. K. Tanaka, M. Okada, T. Tamabe, *Synth. Met.*, **38**, 395, (1990). Ibid, **43**, 3509 (1991).

26. C.O. Yoon, Y.W. Park, K. Akagi, H. Shirakawa, *Mol. Cryst. Liq. Cryst.*, **224**, 69 (1993).

27. A.J. Heeger, S. Kivelson, J.R. Schrieffer, W.P. Su, *Rev. Mod. Phys.*, **60**, 781 (1988).

28. H.Takayama, Y.R. Lin-Liu, K. Maki, *Phys. Rev. B*, **21**, 2388 (1980).

29. S. Okuno, Y. Onodera, *J. Phys. Soc. Jpn.*, **52**, 3495 (1983).

30. D. Baeriswyl, D.K. Campbell, S. Mazundar, in H. Kiess (ed.), *Conjugated Conducting Polymers*, Springer Series in Solid State Sciences, **102**, 7 (1992).

31. Y. Onodera, S. Okuno, *J. Phys. Soc. Jpn.*, **52**, 2478 (1983).

32. D.K.Campbell, J. Tinka Gammel, E.Y. Loh, *Phys. Rev. B*, **38**, 12043 (1988).

33. L. Cruz, P. Phillips, *Phys. Rev. B*, **49**, 5149 (1994).

34. M. Grabowski, D. Hone, J.R. Schrieffer, *Phys. Rev. B*, **31**, 7850 (1985).

35. Yu.N. Garstein, *Synth. Met.*, **44**, 219 (1991).

36. S. Kivelson, T.-K. Lee, Y.R. Lin-Liu, I. Peschel, L. Yu, *Phys. Rev. B*, **25**, 4173 (1982).

37. I. Kay, H.E. Moses, *J. App. Phys.*, **27**, 1503 (1956).

38. V.E. Zakharov, A.B. Shabat, *Sov. Phys. JETP*, **34**, 62 (1972).

39. S.A. Brazovskii, N. Kirova, *Sov. Phys. JETP Lett.*, **33**, 4 (1981).

40. J. Tsukamoto, A. Takahashi, *Synth. Met.*, **41**, 7 (1991).

41. Y. Nogami, H. Kaneko, T. Ishiguro, A. Takahashi, *Solid State Commun.*, **76**, 583 (1990).

42. J. Tsukamoto, *Adv. Phys.*, **41**, 509 (1992).

Chapter 3

Conductivity at low Temperatures.

3.1. Statement of the Problem.

By far the most impressive and important property of doped Polyacetylene (PA) is its electrical conductivity [1]. As experimental methods have improved, conductivities comparable to copper are attained [2,3,4,5]. Metallic properties are also observed in quantities such as the thermoelectric power (linear T dependence) and the magnetic susceptibility (independent of temperature) at very high doping levels. However, the temperature dependence of the conductivity of these highly doped samples shows a disappointing non-metallic behavior as the temperature decreases [6]. Because PA is not a single crystal, various kinds of disorder are present ranging from local imperfections in conjugation bonds to higher order structures such as fibril configurations. These inhomogeneities can generally account for the decreasing T behavior in the conductivity. Within the framework of the Sheng model, for example, the conductivity [7] displays a good fit to the experimental data [6]. In the Sheng model it is assumed that there are ideal metallic parts with no resistivity and non-metallic barriers separating them, therefore accounting for the observed activated-type behavior in the conductivity. This thermally activated behavior is also supported by other experimental observations at high doping that sustain the

view that PA has a gap. In particular, IRAV modes in the highly doped phase confirm the existence of a remnant bond-charge alternation and a subsistent gap of at least 0.2eV [8]. Other studies based on optical data [9,10], vibrational features [11, 12,13], and crystal orbital calculations [14, 15] also support this view.

Recently, a highly conducting polyacetylene (HCPA) has been developed [16] whose dc electrical transport at low temperature surprisingly exhibits metallic behavior under certain conditions [17,18]. One important aspect of the properties shown in these new samples is that disorder has proven to yield a wide range of temperature variations in the samples [18,19]. Thermally activated behavior is found for the strongly disordered state, while a weak T-dependence down to the mK region is found for the weakly disordered state. An immediate explanation that comes to mind is transport carried out by a variable-range hopping mechanism. However, we can safely rule this mechanism out after considering the high value of the conductivity and the lack of thermally-activated behavior in the weakly disordered cases [20]. The other alternative would be the Sheng model, but it does not fit well to the conductivity measurements of the more ordered samples of HCPA. This lack of agreement arises because the Sheng model fails to consider temperature effects that should be important at low temperatures [6,17,21]. An explanation for the fan-like display of the different conductivities as a function of disorder is contained in a model that takes into account the complex fibrilar structure and the degree of disorder as parameters [22]. In this model, it is shown how the interfibrilar connections in PA are responsible for the apparent metal-insulator transition as a function of aging. This is shown even under the consideration that the individual chains forming the fibrils are taken as containing localized non-conducting states. As a conclusion of this model the conducting state of the whole sample is presented to be more sensitive to the disorder than to the strength of the interfibril coupling.

In this chapter we concern ourselves with the other curious feature exhibited in these iodine-doped HCPA samples. This feature is the anomalous log$T$ behavior in the conductivity at low temperatures [18]. Structural studies of the HCPA

samples show that, although they are better ordered compared to conventional materials, they are still far from being ideal crystals. The exact nature of the defects contributing to the log$T$ dependence is not known. Suggestions on this respect have proposed that these defects are due to chemical reactions between the chains and the impurities [18]. This interplay between the impurities and the chain then puts more relevance to the defects arising from the presence of the dopants, for example, over other scattering mechanisms that may come from chain breaks at the polymer ends. This conclusion is clearly illustrated in the fan-like spreading of the conductivity for different amounts of disorder that arise solely from aging at room temperature and not by changing the morphology of the chains. The natural conclusion is then that the sources of scattering in PA should come from local carbonyl (>C=O) defects that are naturally present in PA exposed to air [23]. Kondo-like behavior, the signature of which is a log$T$ dependence of the conductivity of normal metal (Appendix J), has been proposed to appear in HCPA [24]. However, as a result of the absence of localized moments in conducting polymers, a Kondo Hamiltonian where degenerate conduction electrons couple to localized spins [25], is unapplicable. A more realistic model would be the Anderson model in which the local spin is treated just as another electron. The scattering arises from the local spin becoming a conduction state and another conduction electron taking its place [26]. The on-site Coulombic repulsion establishes a correlation between the first electron exiting the local level and another electron occupying the vacancy. Of importance to the current problem is the existence of a localized level, arising from the coupling of the impurity to the chain. Impurity levels have been proven to exist in PA. The starting point for such calculations has been the SSH Hamiltonian [27] and its continuum version, the TLM Hamiltonian [28]. These calculations were carried out in the absence of an on-site interaction term [23] and with the on-site U plus a soliton [29]. In all cases the localized level persists for all values of the relevant parameter space reinforcing the assertion that our starting point should contain an Anderson-type of interaction.

In order then to asses the nature of the log$T$ behavior, we consider the TLM Hamiltonian supplemented with an Anderson-type Hamiltonian that will take into account the presence of disorder as a single impurity in the chain. Because PA retains a bond-charge alternating pattern even at high doping, we will take into account a gap $2\Delta_o$ ($\Delta_o = .7$eV for undoped PA) in the density of states of the chain. Notice that by treating Δ_o as a constant rather than the usual global order parameter $\Delta(x)$, we are assuming a uniform bond-charge alternating pattern. The fact that Δ_o will be smaller than the value for pristine PA determines both the remaining alternation and the smallness of the gap. The main objective will be to explore to what extent the Kondo resonance is affected by the presence of a gap that contains the Fermi level. The path that we will follow in order to establish this objective will be to calculate the density of states at the impurity site. Then we will explore to what extent this density of states changes as a function of the size of the gap and other parameters like the hybridization energy between the conduction electrons and a localized electron. We anticipate the appearance of a Kondo resonance for a range of values of the gap in the system. We note that work on systems with magnetic impurities in non-magnetic hosts with a pseudogap [30] and with actual gaps in heavy fermion systems [31,32] have obtained a transition from a magnetic multiplet to a Kondo singlet state using renormalization, $1/N$, and Monte Carlo methods. Experiments on fluctuating-valence materials confirm existence of a gap in these types of systems [33].

3.2. Equations of Motion for the Green functions.

We start from the continuum Hamiltonian for Polyacetylene (PA) [28]

$$\mathcal{H}_{TLM} = \frac{1}{2\pi v_f \lambda}\int dx\Delta(x)^2 + \sum_s \int dx\psi_s^\dagger(x)[-iv_f\sigma_3\partial_x + \Delta(x)\sigma_1]\psi_s(x) \qquad (3.1)$$

where $\psi_s(x)$ is the two-component spinor for the π-electrons with spin s, $\Delta(x)$ the

order parameter, v_f the fermi velocity, σ_i the Pauli matrices, and λ the elastic coupling constant. The units are taken such that $\hbar = 1$. We consider impurities in the chain to be of an Anderson type in the form [34]

$$\mathcal{H}_A = E_d \sum_s d_s^\dagger d_s + V' \sum_s (d_s^\dagger c_{l,s} + c.c.) + U d_\uparrow^\dagger d_\uparrow d_\downarrow^\dagger d_\downarrow \tag{3.2}$$

where d_s is the annihilation operator of a localized electron at the impurity site l, E_d is the atomic level, V' is the mixing matrix element between the localized level and the π-electron orbital at the lth site, and U is the on-site Coulomb interaction at the atom at l. This type of Hamiltonian has been used previously proposed in ref. 35 (with no U interaction) to describe carbonyl (>C=O) defects in PA. Carbonyl defects that are naturally present in PA exposed to air, as well as atomic side groups that strongly interact with the chain are examples of cases where the Anderson model would be useful. The $\mathcal{H}_A$ will be incorporated with $\mathcal{H}_{TLM}$ by considering its continuum version (see for example ref. 23) given by

$$\mathcal{H}_A^c = E_d \sum_s n_{ds} + \sqrt{a} V' \sum_s [d_s^\dagger \chi_l^\dagger \psi_s(x_l) + \psi_s^\dagger(x_l) \chi_l d_s] + U n_{d\uparrow} n_{d\downarrow} \tag{3.3}$$

where $n_{ds} = d_s^\dagger d_s$, $x_l = la$ where a is the lattice constant of the undimerized system, and

$$\chi_l = \begin{pmatrix} e^{-il\pi/2} \\ e^{i(l+1)\pi/2} \end{pmatrix}. \tag{3.4}$$

There are two main assumptions in our considerations that we will explain and justify in what follows. First, we take as a starting point that the total Hamiltonian is $\mathcal{H} = \mathcal{H}_{TLM} + \mathcal{H}_A^c$ which is expected to exhibit the log$T$ behavior of the conductivity, as is the case of normal metals. When PA is in its highly doped region (HDR), $p > 10\%$, the conductivity is metal-like, as well as the T-behavior of the magnetic susceptibility. There have been many arguments why this is so [36]. It is believed, however, that even in the HDR there exists a small gap [8], which at first sight might rule out any log$T$ arising from a kondo-like mechanism. Thus, the second assumption is that we consider a small gap containing the Fermi level. We intend to show that even with this small gap, there is a strong modification in the

impurity density of states close to the fermi level (taken to be at the middle of the gap). The size of this small gap is taken in this work to be in the neighborhood of 0.04eV. As we have shown in the previous chapter along with other calculations concerning the magnetic susceptibility, the sudden rise in $\chi(T)$ as a function of doping can be shown to exist with gaps of this size [37, 38]. Related work has been performed using a pseudogap [30] and on materials with a BCS-type of gap [32] in a Kondo Hamiltonian. Also, other calculations have been carried out on an Anderson Hamiltonian using a $1/N$ expansion exploring the magnetic transition [31].

Having proposed the existence of this small gap, $2\Delta_o$, and positioning the Fermi level right at the center, we picture the density of states (DOS) for PA in the form depicted in figure 3.1 where (a) and (c) are the valence and conduction bands, respectively. Band (b) can be taken to belong either to polarons or solitons that form during doping, and that at this HDR its exact nature do not concern us. We will take those excitations as modifying the π-electon wavefunction uniformly throughout the chain, thus just adding another periodic modulation. This periodic modulation is the one giving rise to the actual (b) band. We have reasons to believe that this middle band corresponds to soliton-like excitations [39]. Because our main interest is on transport properties, we will consider a simplified DOS as depicted in figure 3.2 where we keep the relevant parameters around the Fermi level. Thus, the DOS to be considered is

$$\rho(\epsilon) = \begin{cases} \frac{L}{v_f \pi} \frac{|\epsilon|}{\sqrt{\epsilon^2 - \Delta_o^2}} & |\epsilon| > \Delta_o \\ 0 & |\epsilon| \leq \Delta_o \end{cases} \tag{3.5}$$

where L is the length of an unbroken chain, usually taken to be of a few thousand sites. To get equation (3.5) we have used $\epsilon_k = \sqrt{k^2 v_f^2 + \Delta_o^2}$ for the electron dispersion relation, the boundary condition $kL = 2n\pi$ [40], and the simplification $\Delta(x) = \Delta_o$ justified in the HDR from the arguments of the preceding paragraph. A factor of 2 for spin degeneracy has been taken into account. Equation (3.5) might be compared with the one in ref. 27, where we have taken the large bandwidth limit.

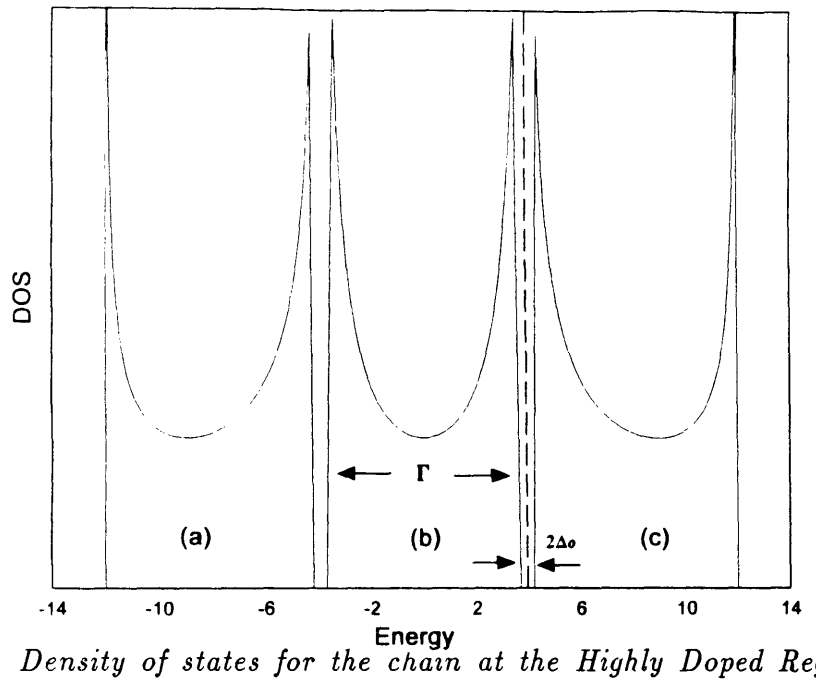

Figure 3.1. Density of states for the chain at the Highly Doped Regime (HDR). Bands (a) and (c) are the valence and conduction bands, respectively. Band (b) forms in the gap of the undoped polymer and as doping progresses diminishes the effective gap. Γ denotes the with of band (b), $2\Delta_o$ the size of the remnant gap, and the dashed line indicates the position of the Fermi level.

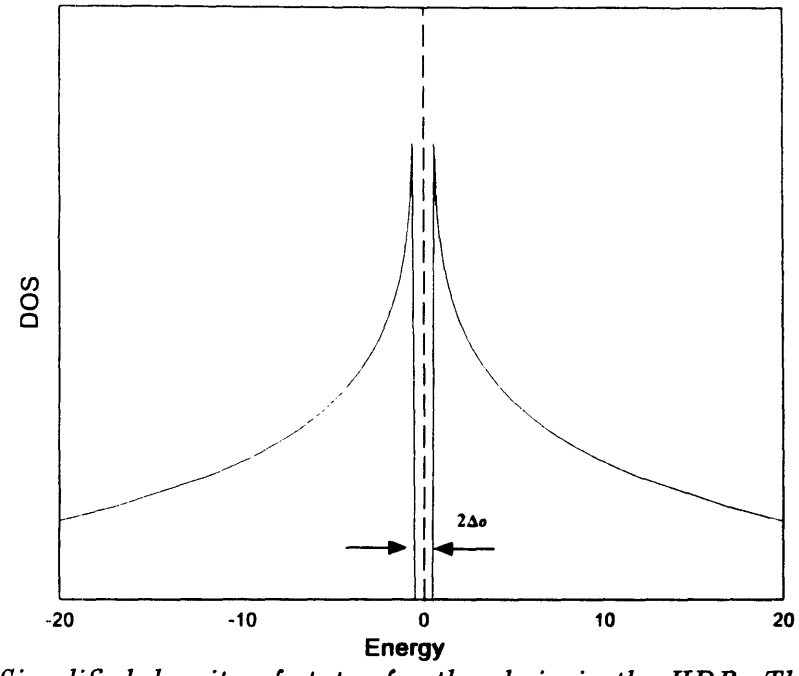

Figure 3.2. Simplified density of states for the chain in the HDR. The width of the remnant gap is parametrized by $2\Delta_o$. The dashed line indicates the position of the Fermi level.

The density of states at the impurity $-\mathrm{Im}G_d(\omega)/\pi$ will indicate, as a function of temperature and E_d, to what extent a Kondo resonance is realized close to the Fermi level. Here $G_d(\omega)$ is the Fourier transform of the temperature Green function for the d electrons defined by

$$G(d_s, d_s^\dagger; \tau) = - <T d_s(\tau) d_s(0)^\dagger> \tag{3.6}$$

where $d_s(\tau) = \exp(\mathcal{H}\tau) d_s \exp(-\mathcal{H}\tau)$, and τ is the "temperature" variable. $\mathcal{H}$ is given in k-space by

$$\begin{aligned} \mathcal{H} =& \frac{L\Delta_o^2}{2\pi v_f \lambda} + \sum_{s,k} \psi_{ks}^\dagger [v_f k \sigma_3 + \Delta_o \sigma_1] \psi_{ks} \\ &+ E_d \sum_s n_{ds} + \sqrt{\frac{a}{L}} V' \sum_{sk} [d_s^\dagger A_{ks} + A_{ks}^\dagger d_s] + U n_{d\uparrow} n_{d\downarrow} \end{aligned} \tag{3.7}$$

where

$$A_{ks} \equiv \chi_l^\dagger \psi_{ks} e^{ikx_l}. \tag{3.8}$$

In order to get (3.7) we have used

$$\psi_s(x) = \frac{1}{\sqrt{L}} \sum_k e^{ikx} \psi_{ks} \tag{3.9}$$

and

$$\int dx e^{i(k'-k)x} = L\delta_{k,k'}. \tag{3.10}$$

To simplify the notation we define $V \equiv \sqrt{\frac{a}{L}} V'$ and $\psi_{ks}^\dagger \tilde{B}_k \psi_{ks} \equiv D_{ks}$, where $\tilde{B}_k = v_f k \sigma_3 + \Delta_o \sigma_1$. Then (3.7) becomes

$$\mathcal{H} = \sum_{sk} D_{ks} + \frac{L\Delta_o^2}{2\pi v_f \lambda} + E_d \sum_s n_{ds} + V \sum_{sk} [d_s^\dagger A_{ks} + A_{ks}^\dagger d_s] + U n_{d\uparrow} n_{d\downarrow}. \tag{3.11}$$

For simplicity of expressions from now on we will omit the labels τ and ω in all of the arguments of the relevant quantities. The context of the expression will dictate if we are dealing with either the temperature or energy variable. Therefore, when we refer to $G(d_s, d_s^\dagger; \omega)$ or to $G(d_s, d_s^\dagger; \tau)$ both will be denoted by simply $G(d_s)$. Only for ambiguous cases we will specify the complete set of arguments.

Our goal will be to find $G(d_s)$ using the equations of motion (EOM) formalism for Green functions [41,42]. In the EOM, derivatives of the Green function are obtained with respect to temperature thereby generating higher order Green functions. These higher order functions are then approximated in order to close the system of equations. We will use the same decouplings as those presented in ref. 42. These decouplings prove to yield all the features at low and intermediate T for the kondo case in metals [43]. The kondo temperature obtained through this method, though, is only approximate, relative to the exact one in metals [44]. Therefore, results on that respect will only be considered qualitatively.

In the following derivations only the necessary equations of motion will be stated. A complete list of all the commutators and equations of motion used is given in Appendix I. The equation of motion for the impurity Green function in equation (3.7) is

$$\frac{d}{d\tau}G(d_s) = -\delta(\tau) - E_d G(d_s) - V\sum_k G(A_{ks}) - UG(n_{d\bar{s}}d_s) \tag{3.12}$$

which on Fourier transforming yields

$$\boxed{(i\omega - E_d)G(d_s) = 1 + V\sum_k G(A_{ks}) + UG(n_{d\bar{s}}d_s)} \tag{3.13}$$

where $i\omega$ stands for $\omega + i\alpha$. On getting (3.13) we used $G(\tau) = \sum_n e^{-i\overline{\omega}_n\tau}G(\overline{\omega}_n)$, $\delta(\tau) = \sum_n e^{-i\overline{\omega}_n\tau}$, and $\overline{\omega}_n$ stands for Matsubara's frequency. Also, we used

$$\frac{d}{d\tau}d_s = -E_d d_s - V\sum_k A_{ks} - Un_{d\bar{s}}d_s. \tag{3.14}$$

To find $G(A_{ks})$ we calculate its respective equation of motion

$$\frac{d}{d\tau}G(A_{ks}) = -G(P_{ks}) - VG(d_s) \tag{3.15}$$

where $P_{ks} \equiv \chi_l^\dagger \tilde{B}_k \psi_{ks} e^{ikx_l}$, and further

$$\frac{d}{d\tau}G(P_{ks}) = -\epsilon_k^2 G(A_{ks}) \tag{3.16}$$

in (3.15) yields

$$\boxed{[(i\omega)^2 - \epsilon_k^2]G(A_{ks}) = i\omega V G(d_s)} \tag{3.17}$$

where we have used

$$\frac{d}{d\tau}A_{ks} = -P_{ks} - Vd_s \tag{3.18}$$

and

$$\frac{d}{d\tau}P_{ks} = -\epsilon_k^2 A_{ks}. \tag{3.19}$$

Upon taking the derivative of the last term of (3.13) we obtain

$$\begin{aligned}\frac{d}{d\tau}G(n_{d\bar{s}}d_s) = &- \delta(\tau) <n_{d\bar{s}}> + V\sum_{k'} G(A^\dagger_{k'\bar{s}}d_{\bar{s}}d_s) - V\sum_{k'} G(d^\dagger_{\bar{s}}A_{k'\bar{s}}d_s) \\ &- E_d G(n_{d\bar{s}}d_s) - V\sum_{k'} G(n_{d\bar{s}}A_{k's}) - UG(n_{d\bar{s}}d_s)\end{aligned} \tag{3.20}$$

where

$$\frac{d}{d\tau}n_{d\bar{s}} = V\sum_k [A^\dagger_{k\bar{s}}d_{\bar{s}} - d^\dagger_{\bar{s}}A_{k\bar{s}}]. \tag{3.21}$$

On Fourier transforming of equation (3.20) we get

$$\boxed{\begin{aligned}(i\omega - E_d - U)G(n_{d\bar{s}}d_s) = &<n_{d\bar{s}}> + V\sum_{k'} G(n_{d\bar{s}}A_{k's}) \\ &+ V\sum_{k'} G(d^\dagger_{\bar{s}}A_{k'\bar{s}}d_s) - V\sum_{k'} G(A^\dagger_{k'\bar{s}}d_{\bar{s}}d_s).\end{aligned}} \tag{3.22}$$

Now we proceed to set up the equations of motion for the Green functions appearing in the r.h.s. of (3.22) and apply the decoupling scheme so as to close the set of equations. On the second term of the r.h.s. of (3.22) we get

$$\begin{aligned}\frac{d}{d\tau}G(n_{d\bar{s}}A_{k's}) = &V\sum_k G(A^\dagger_{k\bar{s}}d_{\bar{s}}A_{k's}) - V\sum_k G(d^\dagger_{\bar{s}}A_{k\bar{s}}A_{k's}) \\ &- G(n_{d\bar{s}}P_{k's}) - VG(n_{d\bar{s}}d_s)\end{aligned} \tag{3.23}$$

and

$$\frac{d}{d\tau}G(n_{d\bar{s}}P_{k's}) = V\sum_k G(A^\dagger_{k\bar{s}}d_{\bar{s}}P_{k's}) - V\sum_k G(d^\dagger_{\bar{s}}A_{k\bar{s}}P_{k's}) - \epsilon^2_{k'}G(n_{d\bar{s}}A_{k's}) \tag{3.24}$$

where we have used (3.16), (3.18), and (3.21). Upon transforming again and substituting (3.24) in (3.23) we get

$$\begin{aligned}[(i\omega)^2 - \epsilon_{k'}^2]G(n_{d\bar{s}}A_{k's}) =& V\sum_k \left[G(d_{\bar{s}}^\dagger A_{k\bar{s}}P_{k's}) - G(A_{k\bar{s}}^\dagger d_{\bar{s}}P_{k's})\right] \\ &+ i\omega V\sum_k \left[G(d_{\bar{s}}^\dagger A_{k\bar{s}}A_{k's}) - G(A_{k\bar{s}}^\dagger d_{\bar{s}}A_{k's})\right] \\ &+ i\omega V G(n_{d\bar{s}}d_s).\end{aligned} \tag{3.25}$$

It can be shown that this reduces to

$$\boxed{[(i\omega)^2 - \epsilon_{k'}^2]G(n_{d\bar{s}}A_{k's}) = i\omega V G(n_{d\bar{s}}d_s)} \tag{3.26}$$

For the third term in (3.22) we have

$$\begin{aligned}\frac{d}{d\tau}G(d_{\bar{s}}^\dagger A_{k'\bar{s}}d_s) =& -\delta(\tau) <d_{\bar{s}}^\dagger A_{k'\bar{s}}> + V\sum_k G(A_{k\bar{s}}^\dagger A_{k'\bar{s}}d_s) - G(d_{\bar{s}}^\dagger P_{k'\bar{s}}d_s) \\ &- VG(d_{\bar{s}}^\dagger d_{\bar{s}}d_s) - V\sum_k G(d_{\bar{s}}^\dagger A_{k'\bar{s}}A_{ks})\end{aligned} \tag{3.27}$$

and

$$\begin{aligned}\frac{d}{d\tau}G(d_{\bar{s}}^\dagger P_{k'\bar{s}}d_s) =& -\delta(\tau) <d_{\bar{s}}^\dagger P_{k'\bar{s}}> + V\sum_k G(A_{k\bar{s}}^\dagger P_{k'\bar{s}}d_s) - \epsilon_{k'}^2 G(d_{\bar{s}}^\dagger A_{k'\bar{s}}d_s) \\ &- V\sum_k G(d_{\bar{s}}^\dagger P_{k'\bar{s}}A_{ks})\end{aligned} \tag{3.28}$$

Again, combining (3.27) and (3.28) we get

$$\begin{aligned}-[(i\omega)^2 - \epsilon_{k'}^2]G(d_{\bar{s}}^\dagger A_{k'\bar{s}}d_s) =& -i\omega <d_{\bar{s}}^\dagger A_{k'\bar{s}}> - <d_{\bar{s}}^\dagger P_{k'\bar{s}}> - VG(n_{d\bar{s}}d_s)i\omega \\ &+ V\sum_k \left[G(A_{k\bar{s}}^\dagger P_{k'\bar{s}}d_s) + i\omega G(A_{k\bar{s}}^\dagger A_{k'\bar{s}}d_s)\right. \\ &\left. - G(d_{\bar{s}}^\dagger P_{k'\bar{s}}A_{ks}) - i\omega G(d_{\bar{s}}^\dagger A_{k'\bar{s}}A_{ks})\right]\end{aligned} \tag{3.29}$$

The set of decouplings to be used are

$$\begin{aligned}G(A_{k\bar{s}}^\dagger P_{k'\bar{s}}d_s) &\simeq <A_{k\bar{s}}^\dagger P_{k'\bar{s}}>\, G(d_s) \\ G(A_{k\bar{s}}^\dagger A_{k'\bar{s}}d_s) &\simeq <A_{k\bar{s}}^\dagger A_{k'\bar{s}}>\, G(d_s) \\ G(d_{\bar{s}}^\dagger P_{k'\bar{s}}A_{ks}) &\simeq <d_{\bar{s}}^\dagger P_{k'\bar{s}}>\, G(A_{ks}) \\ G(d_{\bar{s}}^\dagger A_{k'\bar{s}}A_{ks}) &\simeq <d_{\bar{s}}^\dagger A_{k'\bar{s}}>\, G(A_{ks})\end{aligned} \tag{3.30}$$

so that (3.29) reduces to

$$\boxed{\begin{aligned}[(i\omega)^2 - \epsilon_k^2]G(d_{\bar{s}}^\dagger A_{k'\bar{s}} d_s) = &<d_{\bar{s}}^\dagger F_{k\bar{s}}> + i\omega V G(n_{d\bar{s}} d_s) \\ &- V\sum_k \Big[<A_{k'\bar{s}}^\dagger F_{k\bar{s}}> G(d_s) \\ &- <d_{\bar{s}}^\dagger F_{k\bar{s}}> G(A_{k's})\Big]\end{aligned}} \tag{3.31}$$

where $F_{ks} \equiv P_{ks} + i\omega A_{ks}$.

Finally, for the last term in (3.22) we get

$$\begin{aligned}\frac{d}{d\tau}G(A_{k\bar{s}}^\dagger d_{\bar{s}} d_s) \cong &-\delta(\tau) <A_{k\bar{s}}^\dagger d_{\bar{s}}> + G(P_{k\bar{s}}^\dagger d_{\bar{s}} d_s) + VG(n_{d\bar{s}} d_s) \\ &- 2E_d G(A_{k\bar{s}}^\dagger d_{\bar{s}} d_s) - V\sum_k \Big[G(A_{k\bar{s}}^\dagger A_{k'\bar{s}} d_s) + G(A_{k\bar{s}}^\dagger d_{\bar{s}} A_{k's})\Big] \\ &- UG(A_{k\bar{s}}^\dagger d_{\bar{s}} d_s)\end{aligned} \tag{3.32}$$

where $<n_{d\bar{s}}> + <n_{ds}> = 1$, and

$$\begin{aligned}\frac{d}{d\tau}G(P_{k\bar{s}}^\dagger d_{\bar{s}} d_s) \cong &-\delta(\tau) <P_{k\bar{s}}^\dagger d_{\bar{s}}> + \epsilon_k^2 G(A_{k\bar{s}}^\dagger d_{\bar{s}} d_s) - 2E_d G(P_{k\bar{s}}^\dagger d_{\bar{s}} d_s) \\ &- V\sum_k \Big[G(P_{k\bar{s}}^\dagger A_{k'\bar{s}} d_s) + G(P_{k\bar{s}}^\dagger d_{\bar{s}} A_{k's})\Big] - UG(P_{k\bar{s}}^\dagger d_{\bar{s}} d_s).\end{aligned} \tag{3.33}$$

Combining (3.32) and (3.33), and after considerable algebraic manipulations, we obtain

$$\boxed{\begin{aligned}[(i\Omega)^2 - \epsilon_k^2]G(A_{k\bar{s}}^\dagger d_{\bar{s}} d_s) = &Vi\Omega G(n_{d\bar{s}} d_s) - <J_{k\bar{s}}^\dagger d_{\bar{s}}> \\ &- V\sum_k \Big[G(d_s) <J_{k\bar{s}}^\dagger A_{k'\bar{s}}> \\ &+ G(A_{k's}) <J_{k\bar{s}}^\dagger d_{\bar{s}}> \Big]\end{aligned}} \tag{3.34}$$

where $J_{ks} \equiv F_{ks} + (2E_d + U)A_{ks}$ and the parameter $i\Omega \equiv -i\omega + 2E_d + U$.

Solving the system of equations given by (3.13), (3.17), (3.22), (3.26), (3.31), and (3.34) we obtain for the impurity Green function,

$$G(d_s) = \frac{1 + UN(\omega)[<n_{d\bar{s}}> + V\sum_k \beta_k(\omega)]}{a(\omega) - V^2\sum_k \alpha_k(\omega) + UN(\omega)V^2\sum_{k,k'}[\eta_k^{k'}(\omega) - V\alpha_{k'}(\omega)\beta_k(\omega)]} \tag{3.35}$$

where

$$N(\omega) = \frac{1}{i\omega - E_d - U - V^2 \sum_k (\alpha_k(\omega) + \gamma_k(\omega))}$$

$$\beta_k(\omega) = \frac{<d_{\bar{s}}^\dagger F_{k\bar{s}}>}{[(i\omega)^2 - \epsilon_k^2]} + \frac{<J_{k\bar{s}}^\dagger d_{\bar{s}}>}{[(i\Omega)^2 - \epsilon_k^2]}$$

$$a(\omega) = i\omega - E_d$$

$$\alpha_k(\omega) = \frac{i\omega}{[(i\omega)^2 - \epsilon_k^2]}$$

$$\eta_k^{k'}(\omega) = \frac{<A_{k'\bar{s}}^\dagger F_{k\bar{s}}>}{[(i\omega)^2 - \epsilon_k^2]} - \frac{<J_{k\bar{s}}^\dagger A_{k'\bar{s}}>}{[(i\Omega)^2 - \epsilon_k^2]}$$

$$\gamma_k(\omega) = \frac{i\omega}{[(i\omega)^2 - \epsilon_k^2]} - \frac{i\Omega}{[(i\Omega)^2 - \epsilon_k^2]}.$$

In the limit of very large U, equation (3.35) reduces to

$$G(d_s) = \frac{1 - <n_{d\bar{s}}> - V \sum_k \frac{<d_{\bar{s}}^\dagger F_{k\bar{s}}>}{[(i\omega)^2 - \epsilon_k^2]}}{i\omega - E_d - V^2 \sum_k \frac{1}{[(i\omega)^2 - \epsilon_k^2]} \left(i\omega + \sum_{k'} <A_{k'\bar{s}}^\dagger F_{k\bar{s}}> - V \sum_{k'} \frac{<d_{\bar{s}}^\dagger F_{k\bar{s}}> i\omega}{[(i\omega)^2 - \epsilon_{k'}^2]} \right)} \tag{3.36}$$

where the expectation values above are given by

$$<A_{k'\bar{s}}^\dagger F_{k\bar{s}}> = <A_{k'\bar{s}}^\dagger P_{k\bar{s}}> + i\omega <A_{k'\bar{s}}^\dagger A_{k\bar{s}}> \tag{3.37}$$

and

$$<d_{\bar{s}}^\dagger F_{k\bar{s}}> = <d_{\bar{s}}^\dagger P_{k\bar{s}}> + i\omega <d_{\bar{s}}^\dagger A_{k\bar{s}}> \tag{3.38}$$

and subsequently

$$<A_{k'\bar{s}}^\dagger P_{k\bar{s}}> = -\frac{1}{\pi} \int f(\omega) \mathrm{Im} G(P_{k\bar{s}}, A_{k'\bar{s}}^\dagger; \omega) d\omega \tag{3.39}$$

$$<A_{k'\bar{s}}^\dagger A_{k\bar{s}}> = -\frac{1}{\pi} \int f(\omega) \mathrm{Im} G(A_{k\bar{s}}, A_{k'\bar{s}}^\dagger; \omega) d\omega \tag{3.40}$$

$$<d_{\bar{s}}^\dagger P_{k\bar{s}}> = -\frac{1}{\pi} \int f(\omega) \mathrm{Im} G(P_{k\bar{s}}, d_{\bar{s}}^\dagger; \omega) d\omega \tag{3.41}$$

$$<d_{\bar{s}}^\dagger A_{k\bar{s}}> = -\frac{1}{\pi} \int f(\omega) \mathrm{Im} G(A_{k\bar{s}}, d_{\bar{s}}^\dagger; \omega) d\omega. \tag{3.42}$$

The two Green functions appearing in (3.41) and (3.42) are defined by equations (3.16) and (3.17). The other two new Green functions introduced in equations (3.39) and (3.40) are solved in the following. We establish the equations of motion to be

$$\frac{d}{d\tau}G(P_{k\bar{s}}, A^{\dagger}_{k'\bar{s}}) = -\epsilon_k^2 G(A_{k\bar{s}}, A^{\dagger}_{k'\bar{s}}) \tag{3.43}$$

and

$$\frac{d}{d\tau}G(A_{k\bar{s}}, A^{\dagger}_{k'\bar{s}}) = -\delta(\tau)\delta_{k,k'} - G(P_{k\bar{s}}, A^{\dagger}_{k'\bar{s}}) - VG(d_{\bar{s}}, A^{\dagger}_{k'\bar{s}}) \tag{3.44}$$

Using the identity $G(d_{\bar{s}}, A^{\dagger}_{k'\bar{s}}) = G(A_{k'\bar{s}}, d^{\dagger}_{\bar{s}}) \equiv G(A_{k'\bar{s}})$ and equation (3.17) as $G(A_{k'\bar{s}}) = i\omega VG(d_{\bar{s}})/[(i\omega)^2 - \epsilon^2_{k'}]$ we obtain for the last one

$$-i\omega G(A_{k\bar{s}}, A^{\dagger}_{k'\bar{s}}) = -\delta_{k,k'} - G(P_{k\bar{s}}, A^{\dagger}_{k'\bar{s}}) - V^2 G(d_{\bar{s}})\frac{i\omega}{[(i\omega)^2 - \epsilon^2_{k'}]}. \tag{3.45}$$

Solving (3.43) and (3.45) we get

$$G(A_{k\bar{s}}, A^{\dagger}_{k'\bar{s}}) = \delta_{k,k'}\frac{i\omega}{[(i\omega)^2 - \epsilon_k^2]} + V^2\frac{(i\omega)^2}{[(i\omega)^2 - \epsilon_k^2][(i\omega)^2 - \epsilon^2_{k'}]}G(d_{\bar{s}}) \tag{3.46}$$

and

$$G(P_{k\bar{s}}, A^{\dagger}_{k'\bar{s}}) = \delta_{k,k'}\frac{\epsilon_k^2}{[(i\omega)^2 - \epsilon_k^2]} + V^2\frac{i\omega\epsilon_k^2}{[(i\omega)^2 - \epsilon_k^2][(i\omega)^2 - \epsilon^2_{k'}]}G(d_{\bar{s}}). \tag{3.47}$$

Therefore, using equations (3.16), (3.17), (3.41), and (3.42) the expectation values in equations (3.39) through (3.42) are determined.

The plan now is to use the previous results to further simplify equation (3.36). As the first step we substitute equations (3.39), (3.40), (3.46), and (3.47) into (3.37) and change from k-space to energy space via $\sum_k \rightarrow \int d\epsilon\rho(\epsilon)$, where $\rho(\epsilon)$ is the density of states, to obtain

$$\begin{aligned}\sum_{k,k'}\frac{<A^{\dagger}_{k'\bar{s}}F_{k\bar{s}}>}{[(i\omega')^2 - \epsilon_k^2]} = &-\frac{1}{2i\pi}\int f(\omega)d\omega\int d\epsilon\rho(\epsilon)\left[\frac{\epsilon^2 + i\omega' i\omega}{[(i\omega')^2 - \epsilon^2][(i\omega)^2 - \epsilon^2]}\right.\\ &\left. - \frac{\epsilon^2 + i\omega' i\omega^*}{[(i\omega')^2 - \epsilon^2][(i\omega^*)^2 - \epsilon^2]}\right]\\ &- \frac{V^2}{2i\pi}\int f(\omega)\int d\epsilon d\epsilon'\rho(\epsilon)\rho(\epsilon')\\ &\times\left[\frac{[\epsilon^2 i\omega + i\omega' i\omega^2]G(d_{\bar{s}})}{[(i\omega')^2 - \epsilon^2][(i\omega)^2 - \epsilon^2][(i\omega)^2 - \epsilon'^2]}\right.\\ &\left. - \frac{[\epsilon^2 i\omega^* + i\omega'(i\omega^*)^2]G(d_{\bar{s}})^*}{[(i\omega')^2 - \epsilon^2][(i\omega^*)^2 - \epsilon^2][(i\omega^*)^2 - \epsilon'^2]}\right]\end{aligned} \tag{3.48}$$

where $i\omega^* = \omega - i\alpha$. As the second step we do the same with equations (3.16), (3.17), (3.41), and (3.42) in equation (3.38) to get

$$\sum_k \frac{<d_{\bar{s}}^\dagger F_{k\bar{s}}>}{[(i\omega')^2 - \epsilon_k^2]} = -\frac{V}{2i\pi}\int f(\omega)d\omega \int d\epsilon\rho(\epsilon)\frac{1}{[(i\omega')^2 - \epsilon^2]}$$
$$\times \left[\frac{\epsilon^2 + i\omega' i\omega}{[(i\omega)^2 - \epsilon^2]}G(d_{\bar{s}}) - \frac{\epsilon^2 + i\omega' i\omega^*}{[(i\omega^*)^2 - \epsilon^2]}G(d_{\bar{s}})^*\right] \quad (3.49)$$

and as the final step,

$$\sum_k \frac{i\omega'}{[(i\omega')^2 - \epsilon_k^2]} = \int d\epsilon\rho(\epsilon)\frac{i\omega'}{[(i\omega')^2 - \epsilon^2]}. \quad (3.50)$$

With equations (3.48) through (3.50), the impurity Green function is determined by equation (3.36) in a self-consistent way. The only input now is the form of the density of states for $\rho(\epsilon)$. Then, the density of states of the impurity is obtained by $-\mathrm{Im}G(d_{\bar{s}})/\pi$.

Incorporating the results presented for the system with a gap in Appendix K into equations (3.48), (3.49), and (3.50) we obtain, after recombining and simplifying,

$$\sum_{k,k'} \frac{<A_{k'\bar{s}}^\dagger F_{k\bar{s}}>}{[(i\omega')^2 - \epsilon_k^2]} = \frac{\pi V^2}{\epsilon_o^2}\left\{\int_{-D}^{-\Delta_o} + \int_{\Delta_o}^{D} d\omega f(\omega)\mathcal{P}\frac{1}{\omega' - \omega}M[XJ' + YM]\right.$$
$$+ \int_{-\Delta_o}^{\Delta_o} d\omega f(\omega)\mathcal{P}\frac{1}{\omega' - \omega}NY[J' - N]$$
$$\left. + \pi M'^2 f' G'^* \theta(|\,\omega'\,| - \Delta_o) + Z' f' N' Y' \theta(\Delta_o - |\,\omega'\,|)\right\} \quad (3.51)$$
$$+ \frac{1}{\epsilon_o}\left\{\int_{-D}^{-\Delta_o} + \int_{\Delta_o}^{D} d\omega f(\omega)\mathcal{P}\frac{1}{\omega' - \omega}M\right.$$
$$\left. - i\pi M' f' \theta(|\,\omega'\,| - \Delta_o)\right\}$$

for the other,

$$\sum_k \frac{<d_{\bar{s}}^{\dagger} F_{k\bar{s}}>}{[(i\omega')^2 - \epsilon_k^2]} = -\frac{V}{\epsilon_o}\Bigg\{ \int_{-D}^{-\Delta_o} + \int_{\Delta_o}^{D} d\omega f(\omega)\mathcal{P}\frac{1}{\omega' - \omega}[YJ' - MX] + \int_{-\Delta_o}^{\Delta_o} d\omega f(\omega)\mathcal{P}\frac{1}{\omega' - \omega}Y[J' - N] + i\pi M' f' G'^{*}\theta(|\omega'| - \Delta_o) + Z' f' Y' \theta(\Delta_o - |\omega'|)\Bigg\} \tag{3.52}$$

and for the last,

$$\sum_k \frac{i\omega'}{[(i\omega')^2 - \epsilon_k^2]} = -\frac{\pi}{\epsilon_o}J' \tag{3.53}$$

where $\epsilon_o = \pi v_f/L$, $N(\omega) \equiv \omega g(\omega)$, $M(\omega) \equiv |\omega| g(\omega)$, $g(\omega) \equiv 1/\sqrt{|{\Delta_o}^2 - \omega^2|}$. We have used the shorthand notation $M = M(\omega)$, $M' = M(\omega')$, $N = N(\omega)$, $N' = N(\omega')$, $f' = f(\omega')$, and $G' = G(\omega')$. The parameter Z is defined by

$$Z(\omega') \equiv \frac{{\Delta_o}^2 \epsilon_o}{({\Delta_o}^2 - {\omega'}^2)^{3/2}}.$$

Also, wherever convenient we have separated G into its real and imaginary parts as $G(\omega) = X(\omega) + iY(\omega)$. We have also used the notation $J' = J(\omega') \equiv iM'\theta(|\omega'| - \Delta_o) + N'\theta(\Delta_o - |\omega'|)$.

Finally, putting equations (3.51), (3.52), and (3.53) into (3.36) we obtain for the Green function of the impurity in a one dimensional finite chain,

$$\boxed{G(\omega') = \frac{1 - \frac{1}{2}<n_d> - A(\omega')}{\omega' - E_d + i\Delta I' + \frac{\Delta}{\pi}C(\omega') - i\Delta[I'A(\omega') + B(\omega')]}} \tag{3.54}$$

where

$$A(\omega') = -\frac{\Delta}{\pi}\Bigg\{ \int_{-D}^{-\Delta_o} + \int_{\Delta_o}^{D} d\omega f(\omega)\mathcal{P}\frac{1}{\omega' - \omega}[YJ' - MX] + \int_{-\Delta_o}^{\Delta_o} d\omega f(\omega)\mathcal{P}\frac{1}{\omega' - \omega}Y[J' - N] + i\pi M' f' G'^{*}\theta(|\omega'| - \Delta_o) + Z' f' Y' \theta(\Delta_o - |\omega'|)\Bigg\} \tag{3.55}$$

$$B(\omega') = -i\frac{\Delta}{\pi}\Bigg\{\int_{-D}^{-\Delta_o} + \int_{\Delta_o}^{D} d\omega f(\omega)\mathcal{P}\frac{1}{\omega' - \omega}M[XJ' + YM] + \int_{-\Delta_o}^{\Delta_o} d\omega f(\omega)\mathcal{P}\frac{1}{\omega' - \omega}NY[J' - N] + \pi M'^2 f' G'^* \theta(\mid \omega' \mid - \Delta_o) + Z' f' N' Y' \theta(\Delta_o - \mid \omega' \mid)\Bigg\} \tag{3.56}$$

$$C(\omega') = -\left\{\int_{-D}^{-\Delta_o} + \int_{\Delta_o}^{D} d\omega f(\omega)\mathcal{P}\frac{1}{\omega' - \omega}M - i\pi M' f' \theta(\mid \omega' \mid - \Delta_o)\right\} \tag{3.57}$$

and

$$<n_d> = -\frac{2}{\pi}\int f(\omega')\mathrm{Im}G(d_s, d_s^\dagger; \omega')d\omega'.$$

We define also $I' \equiv -iJ'$ and $\Delta \equiv \pi V^2/\epsilon_o$.

3.3. Consequences.

In the previous section we developed expression (3.54) for the Green function of the impurity starting from the $\mathcal{H}_{TLM}$ Hamiltonian supplemented by an Anderson-type Hamiltonian. The final expression (3.54) is dependent on the size of the gap, Δ_o, the off-diagonal matrix element connecting the chain with the impurity site, V, the impurity level, E_d, the on-site repulsive energy, U, and the bare effective energy per site, ϵ_o. The bandwidth, D, has no significant impact on $G(d_s)$ as long as it is taken much larger than the other quantities with units of energy that enter into the problem (e.g. Δ_o, V, etc.).

The motivation for this type of Hamiltonian and formalism is to realistically account for the log$T$ behavior in the transport properties of PA [18]. Before we apply the results to PA, we analyze first the $\Delta_o = 0$ limit. In this limit the DOS is a constant. Therefore, all the features encountered in metals regarding the Kondo effect should be exhibited. Because the DOS is given by the imaginary part of the Green function, the resonances in the DOS will be dictated by the zeroes of the real

part of the denominator of the Green function. If we denote by $\mathcal{D}$ the denominator of equation (3.54), its real part is

$$\begin{aligned}\mathrm{Re}\mathcal{D}(\Delta_o = 0) =& \omega' - E_d - \frac{\Delta}{\pi}\int_{-D}^{D} d\omega f(\omega)\mathcal{P}\frac{1}{\omega' - \omega} \\ & - \frac{2\Delta^2}{\pi}\int_{-D}^{D} d\omega f(\omega)\mathcal{P}\frac{1}{\omega' - \omega}\mathrm{Y}(\omega) - 2\Delta^2 f(\omega')G(\omega')^*\end{aligned} \tag{3.58}$$

that to order $\mathcal{O}(\Delta)$ is

$$\mathrm{Re}\mathcal{D} = \omega' - E_d - \frac{\Delta}{\pi}\int_{-D}^{D} d\omega f(\omega)\mathcal{P}\frac{1}{\omega' - \omega}. \tag{3.59}$$

We can show that the main conclusions to be drawn at this order of approximation are also true even for Δ not small. We take the $\mathcal{O}(\Delta)$ approximation only for simplicity of calculation.

The resonances are given by $\mathrm{Re}\mathcal{D} = 0$, or that

$$\omega' - E_d - \frac{\Delta}{\pi}\int_{-D}^{D} d\omega f(\omega)\mathcal{P}\frac{1}{\omega' - \omega} = 0 \tag{3.60}$$

which at $T = 0$ yields

$$\boxed{\frac{\pi}{\Delta}(\omega' - E_d) = \ln\left|\frac{D + \omega'}{\omega'}\right|.} \tag{3.61}$$

We can get a feeling for the resonant solutions, ω', by analyzing (3.61) graphically, as shown in figure 3.3. Curve I refers to the l.h.s. and curve II to the r.h.s. of equation (3.61), respectively. The intersection points give on the horizontal axis the position of the resonant energies. For a given value of D and Δ, the value of E_d can make (3.61) possess one or three solutions. That is, as E_d increases, the curve denoted by I shifts downward, thus going from three energy solutions (a) to one (b). Note that the specific solution in (a) marked by E_d' corresponds to the resonance close to the impurity level. The prime indicates the possibility for this resonance to be shifted. That is, if $\omega' \sim E_d$, then

$$\frac{\pi}{\Delta}(E_d' - E_d) \cong \ln\left|\frac{D}{E_d}\right|$$

or that

$$\boxed{E_d' \cong E_d - \frac{\Delta}{\pi} \ln \left| \frac{E_d}{D} \right|.} \tag{3.62}$$

The other two solutions, when they exist, are close to zero, corresponding to the Kondo resonance. Although there are two of them, their proximity yields a single Kondo peak. By equation (3.62) the effect that Δ has is also apparent. As Δ increases, the level E_d' is pushed further away from $\omega' = 0$. Smaller values of Δ bring E_d' closer to the Kondo peak, and at a certain value, there is only one solution to (3.61) and it is positive. This is seen by the fact that smaller Δ increases the slope of curve I in figure 3.3

For non-zero (but small) temperatures, curve II shifts downward and becomes finite at $\omega' = 0$. This is shown by examining equation (3.59) in the following. We approximate the integral in (3.59) by

$$\begin{aligned} \int_{-D}^{D} d\omega f(\omega) \mathcal{P} \frac{1}{\omega' - \omega} \cong & \int_{-D}^{0} d\omega (1 - e^{\beta\omega}) \mathcal{P} \frac{1}{\omega' - \omega} \\ & + \int_{0}^{D} d\omega e^{-\beta\omega} (1 - e^{-\beta\omega}) \mathcal{P} \frac{1}{\omega' - \omega} \end{aligned} \tag{3.63}$$

and plot the resultant integral in figure 3.4. The situation now arises that as T increases, curve II keeps diminishing, thus creating the possibility that we cease to see a Kondo resonance. We define the Kondo temperature as that highest temperature at which the peak at $\omega' = 0$ of curve II just touches the line $\pi(\omega' - E_d)/\Delta$ (curve I). In order to find a quantitative expression for T_k we proceed as follows. Equation (3.63) can be rewritten as

$$\begin{aligned} \int_{-D}^{D} d\omega f(\omega) \mathcal{P} \frac{1}{\omega' - \omega} \cong & 2 \cosh(\beta\omega') [1 - e^{-\beta\omega'}] \ln \left| \frac{\omega'}{D} \right| \\ & + 2 \sum_{n=1} \frac{(-\beta D)^n}{nn!} \left[2^{n-1} e^{-2\beta\omega'} - \cosh(\beta\omega') \right]. \end{aligned}$$

Using this result in equation (3.60) and putting $\omega' = 0$ we get

$$-\frac{\pi}{\Delta} E_d = 2 \sum_{n=1} \frac{(-\beta D)^n}{nn!} \left[2^{n-1} - 1 \right].$$

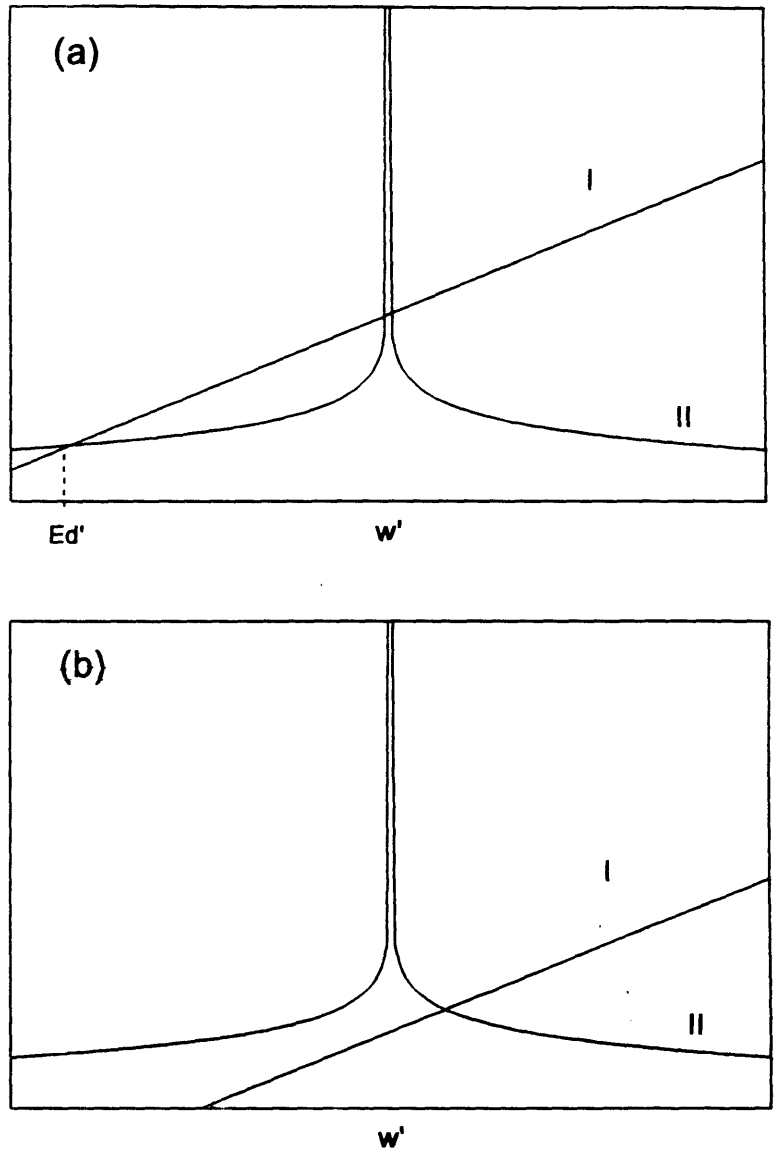

Figure 3.3. Graphs of the l.h.s. (I) and r.h.s. (II) of equation (3.61). (a) has three solutions for the resonances, indicated by the intersections of the two curves, where E'_d indicates the renormalized impurity level. (b) is for a greater value for E_d.

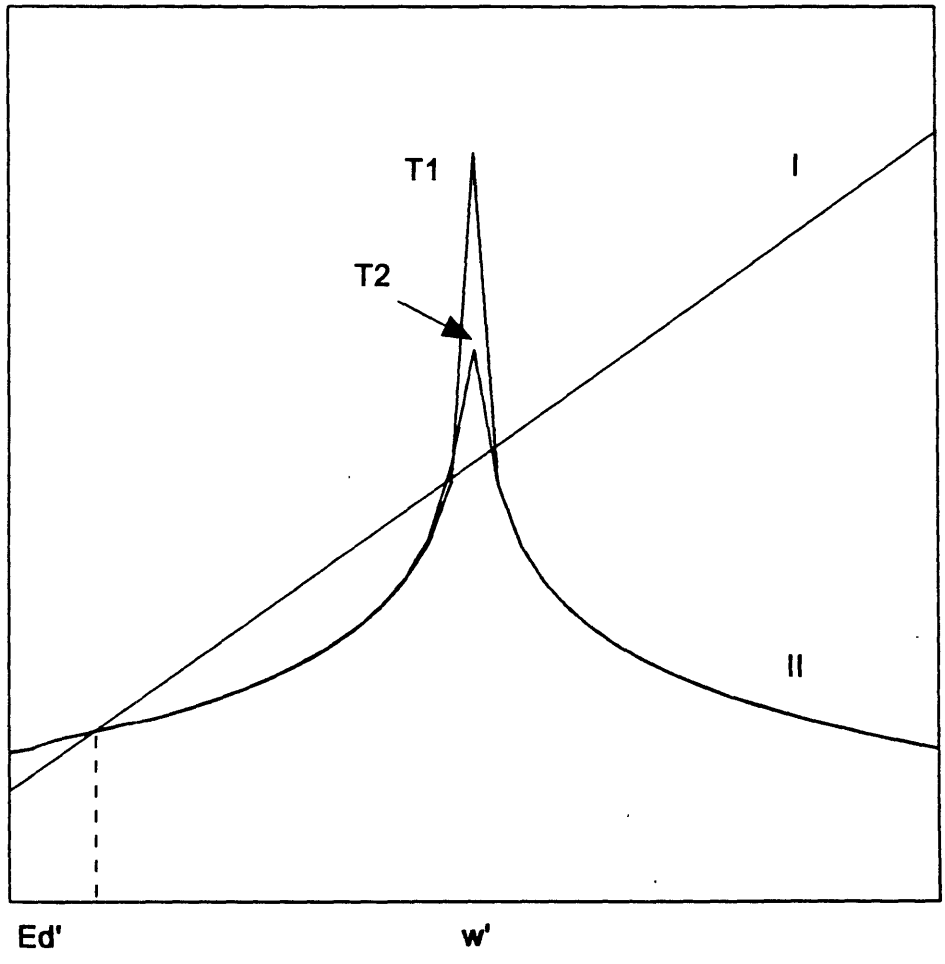

Figure 3.4. Same as figure 3.3 but for $T \neq 0$. T_1 *and* T_2 *denote the temperatures used to calculate each respective curve.* $T_1 < T_2$.

Using the fact that

$$\ln(\beta D) \approx -\sum_{n=1} \frac{(-\beta D)^n}{nn!}\left[2 - 2^n\right] \tag{3.64}$$

for large βD, then we get in (3.60)

$$-\frac{\pi}{\Delta} E_d \cong \ln(\beta D)$$

or that

$$\boxed{T_k = D e^{\pi E_d/\Delta}} \tag{3.65}$$

in accord with reference [42]. Note that the exact result for the Kondo temperature given in reference [44] contains a factor of a 1/2 in the argument of the exponent. Also, the result for the impurity Green function lacks symmetry around the Fermi level when the Kondo state is realized, as will be shown later. Nonetheless, the principal characteristics of the presence of a Kondo peak is displayed as well as its temperature dependence.

Now we proceed to analyze the system of concern in this work for which $\Delta_o \neq 0$. First, we investigate to what extend there are resonances in the Green function at $T = 0$. Equating the real part of the denominator of equation (3.54) to zero we have to calculate ω' such that

$$\frac{\pi}{\Delta}(\omega' - E_d) = \int_{-D}^{-\Delta_o} d\omega \mathcal{P} \frac{1}{\omega' - \omega} \frac{|\omega|}{\sqrt{\omega^2 - {\Delta_o}^2}}. \tag{3.66}$$

Performing the integral and taking into account that $D >> \Delta_o$ we get

$$\boxed{\frac{\pi}{\Delta}(\omega' - E_d) = \left\{ \ln(\frac{2D}{\Delta_o}) - \frac{|\omega'|}{\sqrt{\omega'^2 - {\Delta_o}^2}} \ln\left|\frac{1 + g(\omega', \Delta_o)}{1 - g(\omega', \Delta_o)}\right| \right\}.} \tag{3.67}$$

where $g(\omega', \Delta_o) \equiv \sqrt{(\omega' + \Delta_o)/(\omega' - \Delta_o)}$. The energy solutions, ω', to equation (3.67) correspond to the resonances in the impurity DOS at $T = 0$. A graphical analysis of both sides of equation (3.67) is shown in figure 3.5. Again, as the parameter E_d increases, curve I shifts downward, and as Δ increases the slope of

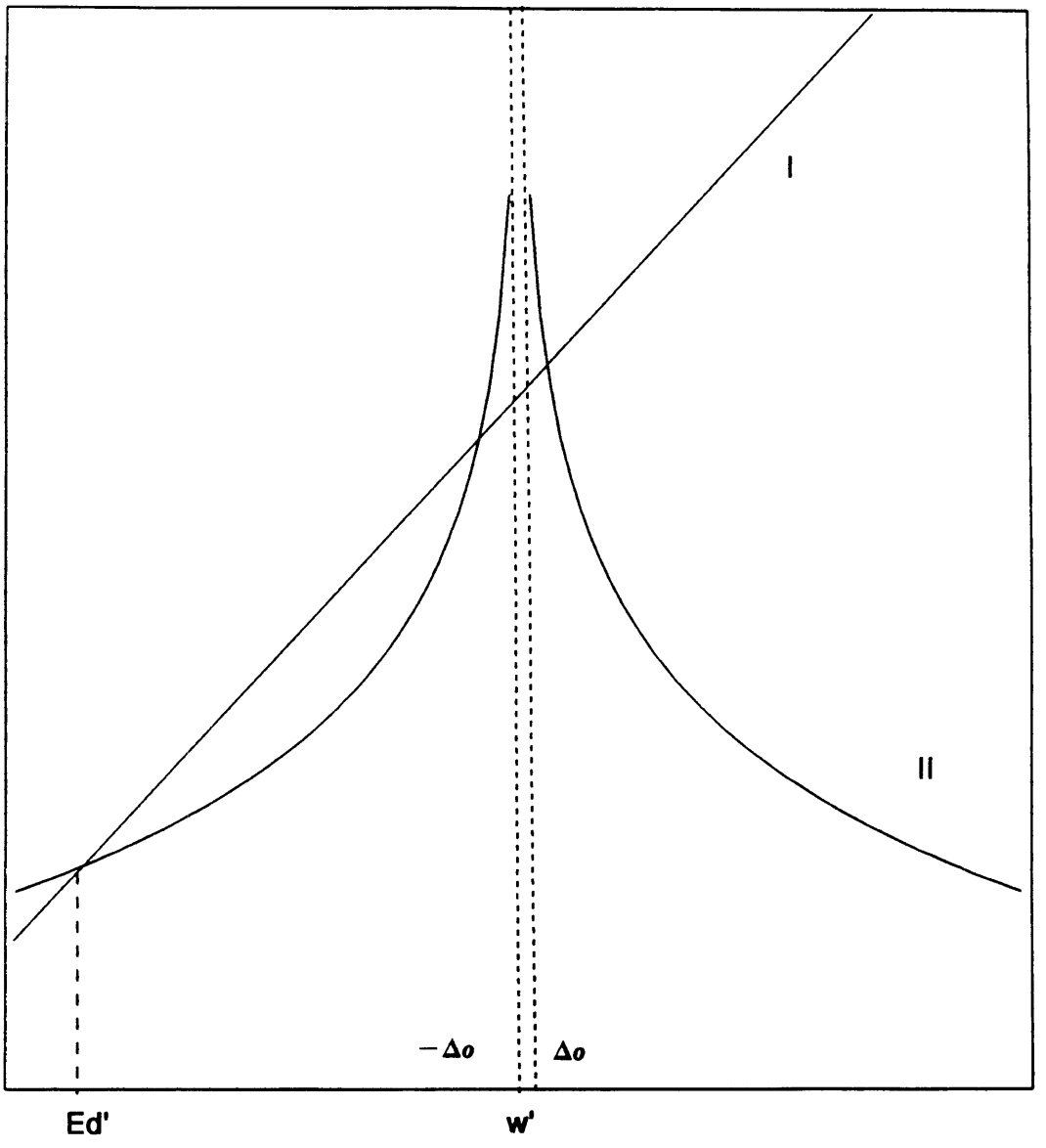

Figure 3.5. Graphical analysis of both sides of equation (3.67). The three intersections correspond to values of w' that yield a resonance in the impurity density of states. The value of E'_d indicates the position of the renormalized impurity resonant level.

I diminishes leading to the same arguments as in the $\rho(\epsilon) = c$ case. In this case, however, there is a gap of width $2\Delta_o$ that even at $T = 0$ may impede resonances close to the Fermi level. This means that unlike the normal system without the gap, where a Kondo resonance is always realized at $T = 0$, in the present case given an appropriately chosen set of Δ, E_d, and Δ_o we could preclude a Kondo resonance in the impurity density of states even at $T = 0$. Figure 3.6 illustrates this point. The value of E_d used to obtain figure 3.6(a) is greater than the one used in figure 3.6(b). This means that we could define a E_d^{crit} below which there are no resonances close to the Fermi level. To obtain this E_d^{crit} we proceed to examine equation (3.67) at $\omega' = \Delta_o + \xi$, where ξ is a small number. After some approximations we get

$$\boxed{E_d^{crit} = \Delta_o - \frac{\Delta}{\pi}\left[\ln(\frac{2D}{\Delta_o}) - 1\right].} \tag{3.68}$$

Again, values smaller than this E_d^{crit} will impede the resonance at $\omega' \sim \Delta_o$. To parallel the development done above for the DOS constant, we calculate now E_d', the renormalized impurity level. This is accomplished by considering $\omega' \sim E_d$ and also $\omega' >> \Delta_o$, that yield in equation (3.67) the result

$$\boxed{E_d' \cong E_d - \frac{\Delta}{\pi}\ln\left|\frac{E_d}{D}\right| - \frac{\Delta\Delta_o}{2\pi E_d}} \tag{3.69}$$

which differs from the normal metal result (see (3.62)) by the linear gap factor. The first two terms in equation (3.69) have been obtained in the normal $\Delta_o = 0$ problem [42,45].

Now we investigate the effect that the size of the gap has on the temperature dependence of the resonance. At the beginning of this section, for the case of $\Delta_o = 0$, we found T_k by finding T for which equation (3.60) is true (using $\omega' = 0$). By doing the same analysis in the $\Delta_o \neq 0$ case we will find a temperature T_1. This temperature T_1 is smaller than T_k and gives the temperature at which the

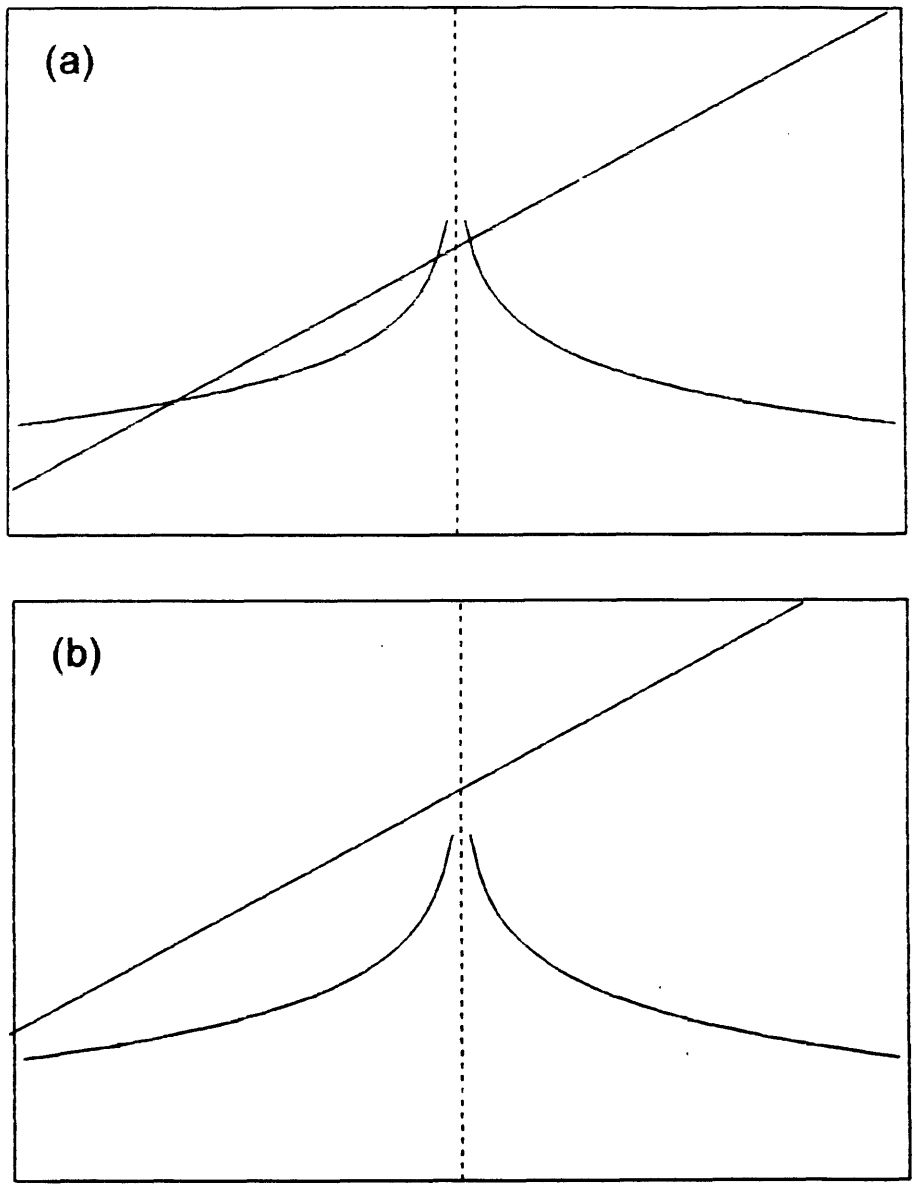

Figure 3.6. (a) shows the possibility of there being the three resonances, the one at E'_d and the two close to the Fermi level. (b) shows a possibility in which there are no resonances close to the Fermi level.

resonances dissapear. Carrying out the analysis with equation (3.66) we obtain the result shown in figure 3.7. The two top figures in figure 3.7 indicate how T_k was obtained by increasing T until the two graphs barely touched. The two bottom figures now show how this looks in the present case for $\Delta_o \neq 0$. The procedure is as follows: start with a set of E_d, Δ, and Δ_o that shows a Kondo resonance at $T = 0$, increase T, T_1 will be given when the two graphs barely touch at $\omega' = \Delta_o$. Because the effective "height" by which the graph has to shift down is smaller in the case of $\Delta_o \neq 0$ than in the case of $\Delta_o = 0$, it is expected that T_1 for the system with the gap will be less than T_k.

Now we proceed to carry out the procedure described in the previous paragraph in a formal way. The equation we have to solve in order to find T_1 is given by

$$\frac{\pi}{\Delta}(\omega' - E_d) = \int_{-D}^{-\Delta_o} + \int_{\Delta_o}^{D} d\omega f(\omega)\mathcal{P}\frac{1}{\omega' - \omega}\frac{|\omega|}{\sqrt{\omega^2 - {\Delta_o}^2}}. \tag{3.70}$$

where we will set $\omega' = \Delta_o$. Rearranging terms this means that the equation leading to T_1 is

$$\boxed{\begin{aligned}\frac{\pi}{\Delta}(\Delta_o - E_d) = &\int_{\Delta_o}^{D} d\omega \frac{1}{1 + e^{\beta\omega}}\frac{1}{\Delta_o + \omega}\frac{\omega}{\sqrt{\omega^2 - {\Delta_o}^2}} \\ &+ \int_{\Delta_o + \xi}^{D} d\omega \frac{1}{1 + e^{\beta\omega}}\frac{1}{\Delta_o - \omega}\frac{\omega}{\sqrt{\omega^2 - {\Delta_o}^2}}\end{aligned}} \tag{3.71}$$

The parameter ξ is a small number introduced to assure convergence. This parameter will not affect the results at the small temperatures that we will be looking at. In figure 3.8 we graph both sides of equation (3.71) (solid lines) and both sides of equation (3.61) (dashed lines). The four cases shown are meant to illustrate under what conditions we get and do not get a resonant temperature. For the case of the system without the gap (dashed lines) there will always be a T_k given by the intersection of the two lines. Figure 3.8(a) shows T_1 for the system with the gap as the intersection between the two solid lines. This intersection yields a T_1 that is more than an order of magnitude smaller than that for the system without the gap.

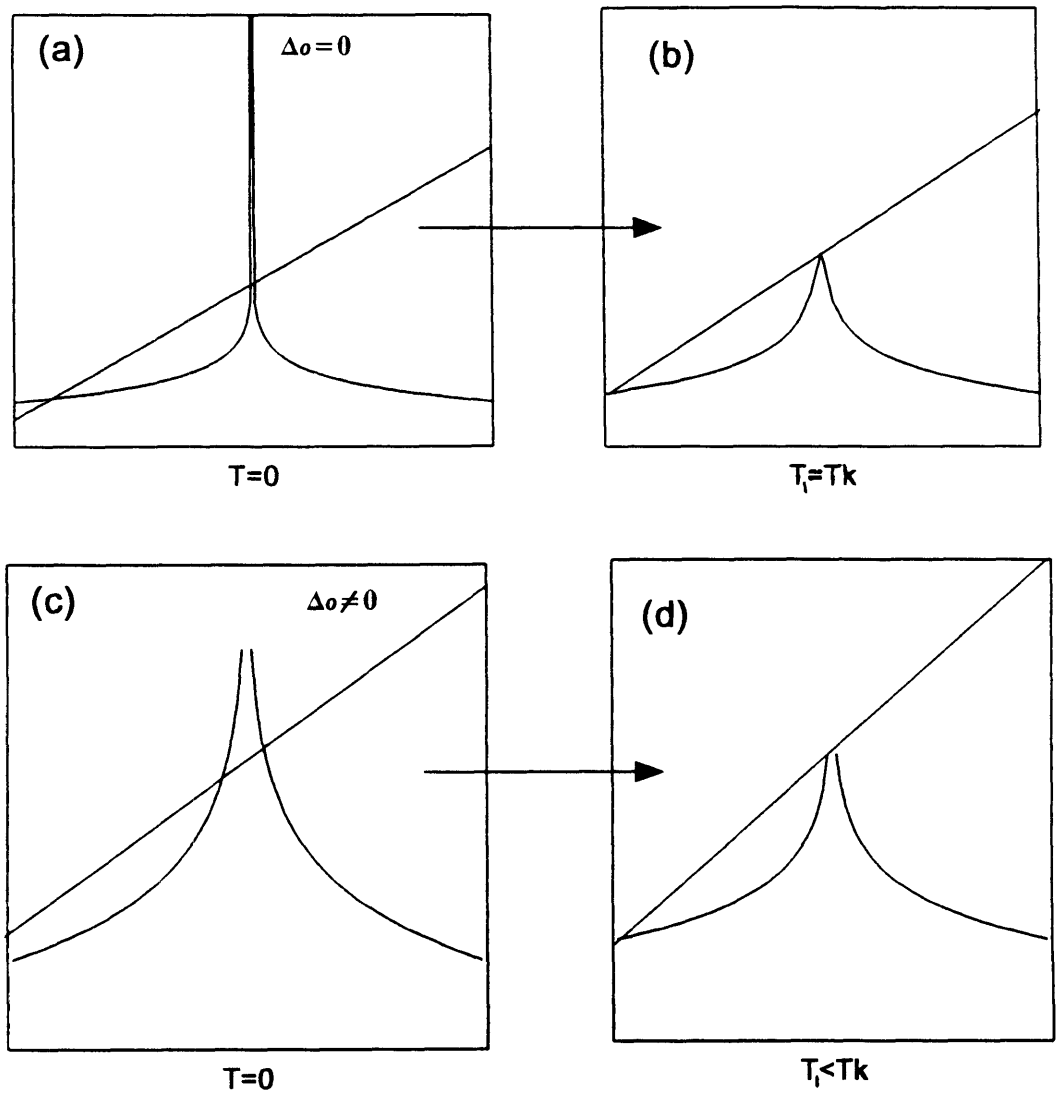

Figure 3.7. (a) and (b) present the analysis to extract the Kondo temperature for the system without the gap. (c) and (d) illustrate the same analysis from $T = 0$ to $T = T_1$.

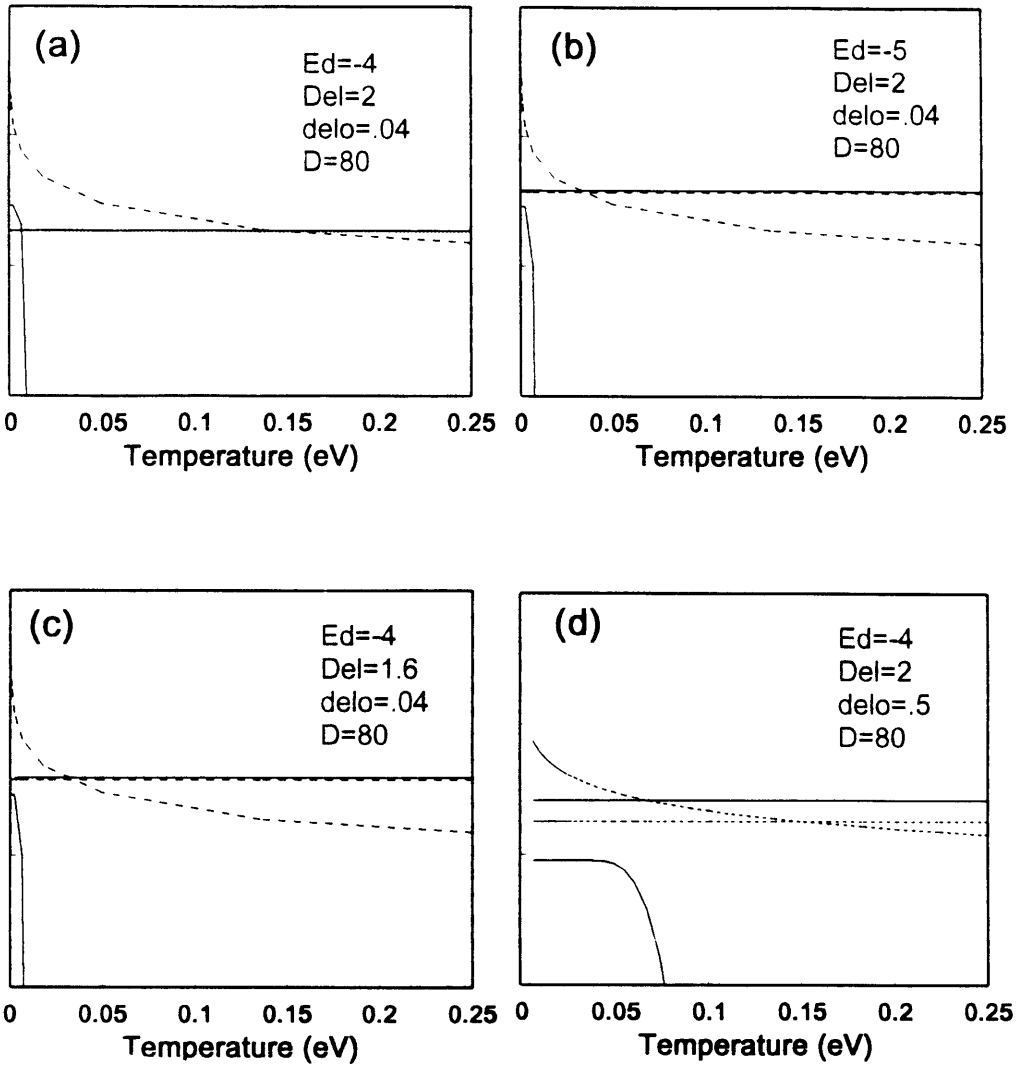

Figure 3.8. Graphs of both sides of equations (3.61) (dashed) and (3.71) (solid). Dashed lines indicate the results for the normal system without gap. Solid lines are for the system with the gap. The different sets of parameters are indicated for each figure. (b), (c), and (d) are shown in order to demonstrate that for other choices of parameters there is no intersection, therefore no resonance.

Because as Δ_o goes to 0 equation (3.71) leads smoothly to the system without the gap, we conclude that $T_1(\Delta_o \neq 0) < T_k(\Delta_o = 0)$ for the entire parameter space, as we expected. Note that none of the other three (figures 3.8(b), (c), nor (d)) were chosen to exhibit a resonance. This illustrates how sensitive the existence of the resonance is to the other parameters of the problem. In figure 3.8(b) the impurity level was diminished from $-4eV$ to $-5eV$ making T_k for the gapless system smaller, but also elliminating T_1 for the system with the gap. In figure 3.8(c) the value of Δ was diminished from $2eV$ to $1.6eV$ also causing the same effect. Figure 3.8(d) shows the effect of increasing the size of the gap from $.04eV$ to $.5eV$. The dependence of the existence of T_1 for the system with the gap on the size of the gap has been analyzed also in other systems in the cited references (e.g. ref.[32]).

3.4. Results.

Having done the $T = 0$ analysis in the previous section, we now present the results for $T \neq 0$. Note that using this $T = 0$ analysis we can now choose beforehand a given set of parameters that either will or will not yield resonances. In the present section we solve numerically equation (3.54). First, we present the results for $\Delta_o = 0$. Figure 3.9 shows the DOS by taking the imaginary part of (3.54) as a function of energy. The parameters used are $\Delta = 3$eV, $D = 80$eV, $E_d = -10$eV, and $\Delta_o = 0$. Calculations for two temperatures, $T = .0025$ and $T = .036$eV, are presented. Figure 3.9(a) shows the range of the spectrum where there are resonances. The peak at $\omega = E_d$ can clearly be seen. Also, the peak at $E_f = 0$ is very much apparent. The height of the peak at E_f is 1.7 times the height of the peak at E_d. In figure 3.9(b) we have blown up the range from $-.75eV$ to $.75eV$ to show detail. The dashed line corresponds to $T = .036eV$ and the solid line to $T = .0025eV$. The Kondo temperature for this model is given by equation (3.65) and is for this parameter set $T_k = .0023eV$. This puts the dashed line above T_k and

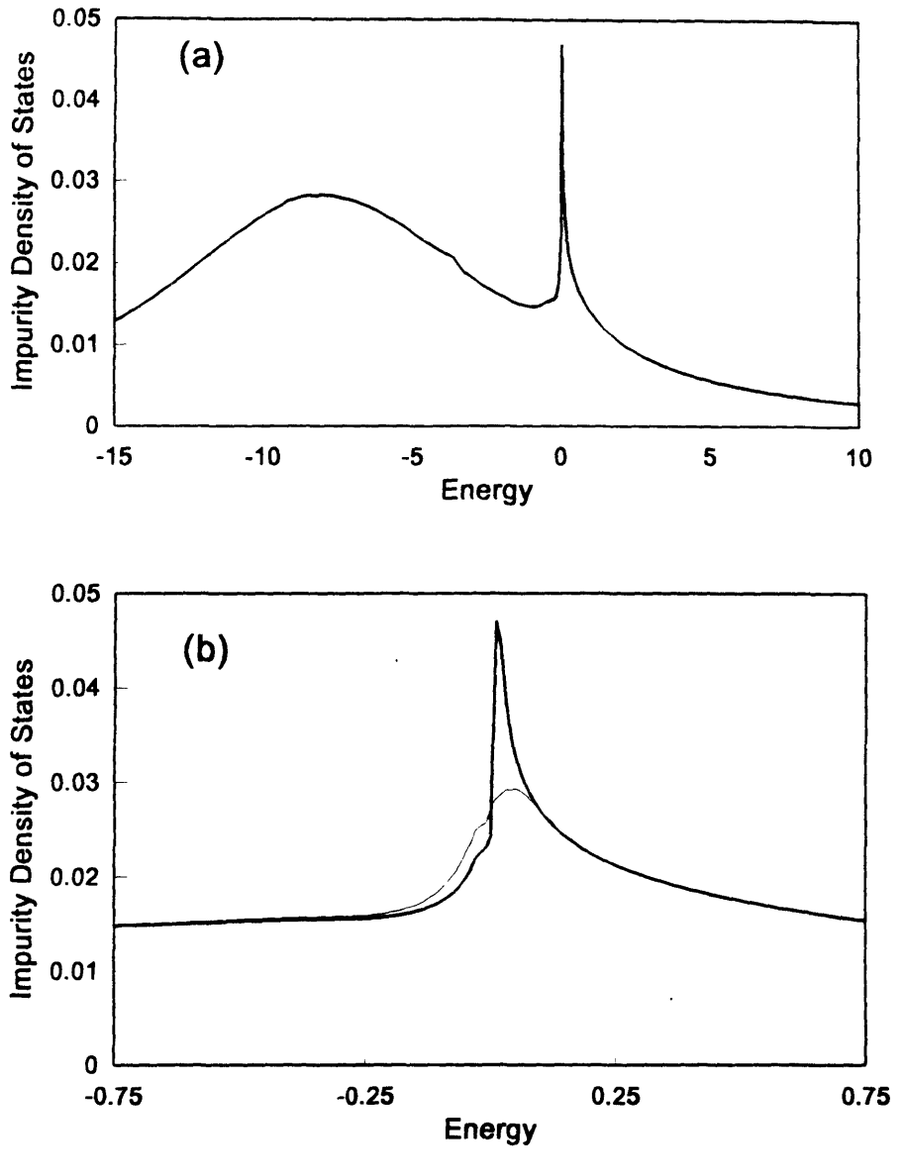

Figure 3.9. Impurity density of states for the normal system with $\Delta_o = 0$. *The resonance at* $\epsilon = 0$ *can clearly be seen being the Kondo resonance. The light and dark line correspond to* $T = .036$ *and* $.0025eV$, *respectively. (b) is the same graph blowing up the region around* ϵ_F. *The parameters used are* $\Delta = 3eV$, $D = 80eV$, *and* $E_d = -10eV$.

the solid line very close to T_k. The model then shows all the features of the Kondo effect regarding the density of states at the impurity including the resonance at E_d and E_f, and the relative widths and heights of each one. The peak at E_f can be shown to decrease as a function of T as log$T$ (ref. 43). Then, the conductivity, which is directly related to the imaginary part of the Green function, is also going to reflect the log$T$ behavior.

In figure 3.10 we present our first $\Delta_o \neq 0$ result. It is for the same parameters as in figure 3.9 but now with $\Delta_o = 0.04eV$. In figure 3.10(b) we show the detail around the gap. The solid line is again for T close to T_k, and the dashed line is for T just above it. The most apparent feature, as compared to figure 3.9, is the lack of T-dependence of the peaks around E_f. This fact alone is sufficient to indicate that these parameters are not in "tune" with a Kondo resonance. In fact, an analysis similar to the one carried out in the previous section shows that the denominator of the Green function behaves as in figure 3.6(b). There are no "hard" resonances in the Green function, although a little T-independent enhancement is observed at $\omega = \Delta_o$. The conclusion at this point is that a small gap can suppress the Kondo resonance (figure 3.9). Graphically this can be thought of as a truncation of the resonance at E_f by the gap.

Knowing, then, that we can tune the resonances, we graph the DOS in figure 3.11 with a new set of parameters. Now $\Delta = .5$eV, $D = 80$eV, $E_d = -1$eV, and $\Delta_o = .04$eV. An analysis of the same kind as that done in the previous section yields figure 3.6(a), showing that there are resonances near $\omega = \Delta_o$. This is precisely what is shown in figure 3.11. We have carried out the calculation and plotted a series of temperatures. They are $T = .001, .1, 1, 10$, and $100eV$. The Kondo temperature of this set of parameters is $T_k = .15eV$. This means that there should be at least two temperatures whose graphs show a resonance at $\omega = \Delta_o$. In figure 3.11, as the temperature decreases, the resonance at $\omega = E_d$ shifts to the right. In figure 3.11(b) the "growth" of the resonance at $\omega = \Delta_o$ is shown as a function of temperature. The lowest peak corresponds to $T = 100$, and the highest to $T = .001eV$, well below

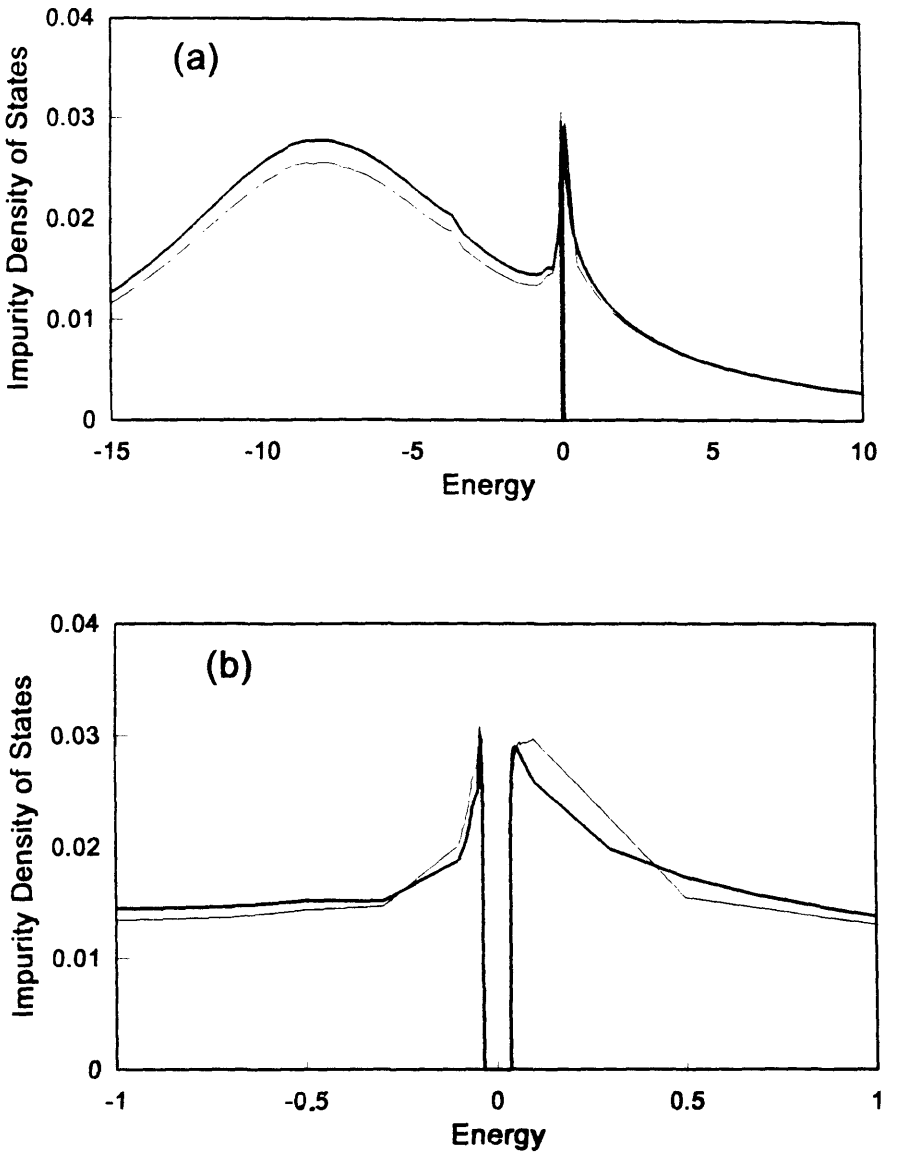

Figure 3.10. Impurity density of states for the system with a gap of $\Delta_o = .0355eV$. *Again, the light and dark lines correspond to* $T = .0025$ *and* $T = .036eV$. *The other parameters are as in figure 3.9.*

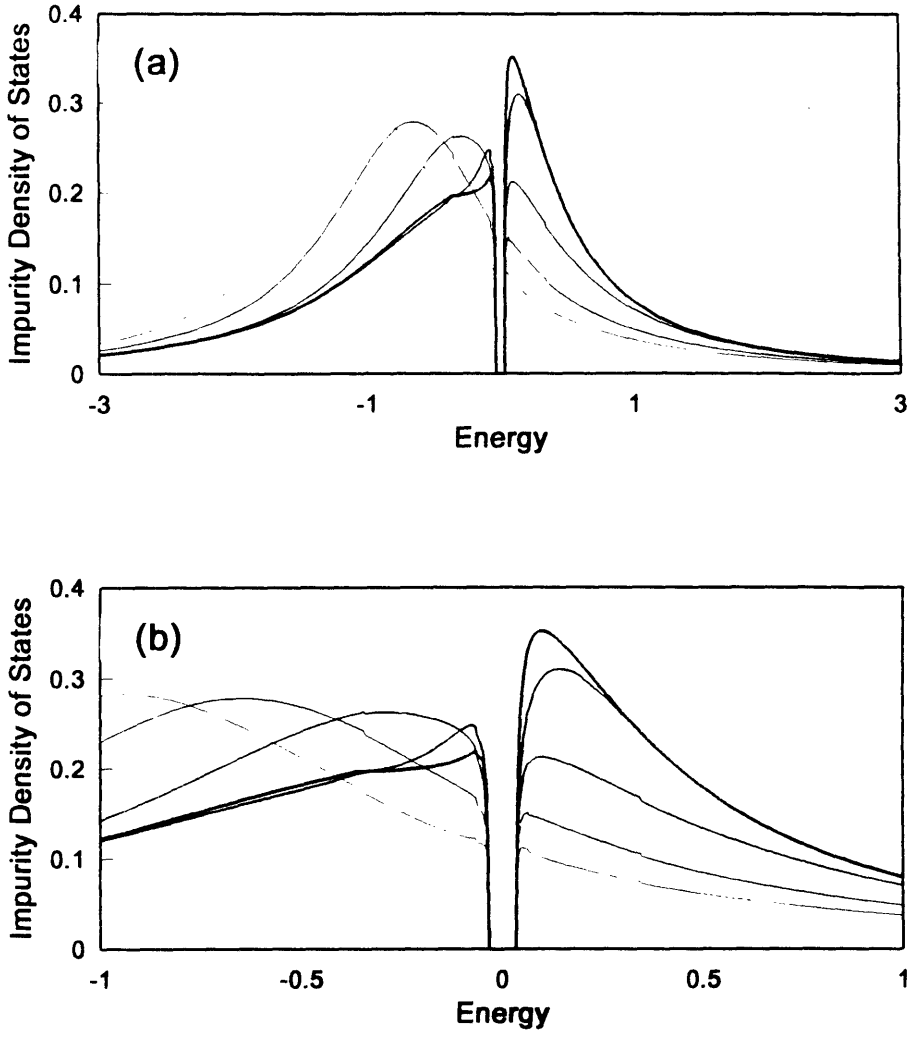

Figure 3.11. Impurity density of states for the system with $\Delta = .0355eV$. *Shown for various temperatures, the movement of the* E_d' *peak is illustrated. Darkest lines correspond to lower temperatures. The growth of the peak at* $\omega' = \Delta_o$ *is also shown. The other parameters are* $D = 80eV$, $E_d = -1eV$, *and* $\Delta = .5eV$.

the T_k. At this $T = .001$, the resonances are at $E_d' = -.21$ (as given by equation 3.69) and at $\omega = \Delta_o$. Their relative magnitudes are .2 and .35, respectively, showing a predominance of the Kondo peak over the impurity peak. The T-dependence of the peaks is apparent, thus showing a contrasting behavior to that of the system depicted in figure 3.10. The appearance of the resonance above the gap indicates the strong coupling that is developed between the impurity level and the conduction electrons in the conduction band.

A point that could be raised against figure 3.11 is that the resonance at $\omega = \Delta_o$ looks as if the resonance from $\omega = E_d$ shifted all the way up to Δ_o. Thus, making the whole picture as if there is only one resonance that simply shifted in energy. One might say then that there is no legitimate resonance close to E_f. In order to clear this point out we plot in figure 3.12 the DOS for the set $\Delta = 5$eV, $D = 80$eV, $E_d = -10$eV, at $T = .1$eV ($T_k = .15$eV). There are two graphs, as shown in figure 3.12(b), with $\Delta_o = 0$ and $\Delta_o = 0.04eV$. This comparison shows both resonances at E_d and at E_f separately and discernibly different. Both show the resonance at $\omega = -6.7eV$ (given by (3.69)) and at $\omega \sim 0$ and $\omega = \Delta_o$ for each case. From this figure we can conclude then, that the resonance at $\omega = \Delta_o$ is separate from the one at $\omega = E_d$, and Kondo-like.

In order to establish the T-dependence of the resonant peak at $\omega = \Delta_o$, we show in figure 3.13 a series of curves for different temperatures. The set of parameters is $\Delta = 2$, $D = 80$, $E_d = -4$, and $\Delta_o = 0.04eV$. In figure 3.14 we plot the height of the peak close to $\omega = \Delta_o$ versus the logarithm of the temperature. Three regions are clearly discernible. The region for low T (figure 3.14) shows the points corresponding to a saturation in the DOS. The region at high T well above T_k, shows the height of the DOS, but there is no apparent resonance (refer to figure 3.13) associated with them. The intermediate region ($.1 < T < .2$eV) very close to $T_k = .15$ shows a linear $\log T$ behavior of the peaks. From figure 3.13 these temperatures are seen to correspond to the peaks at $\omega = \Delta_o$ whose heights are well above the heights of the peaks at E_d'.

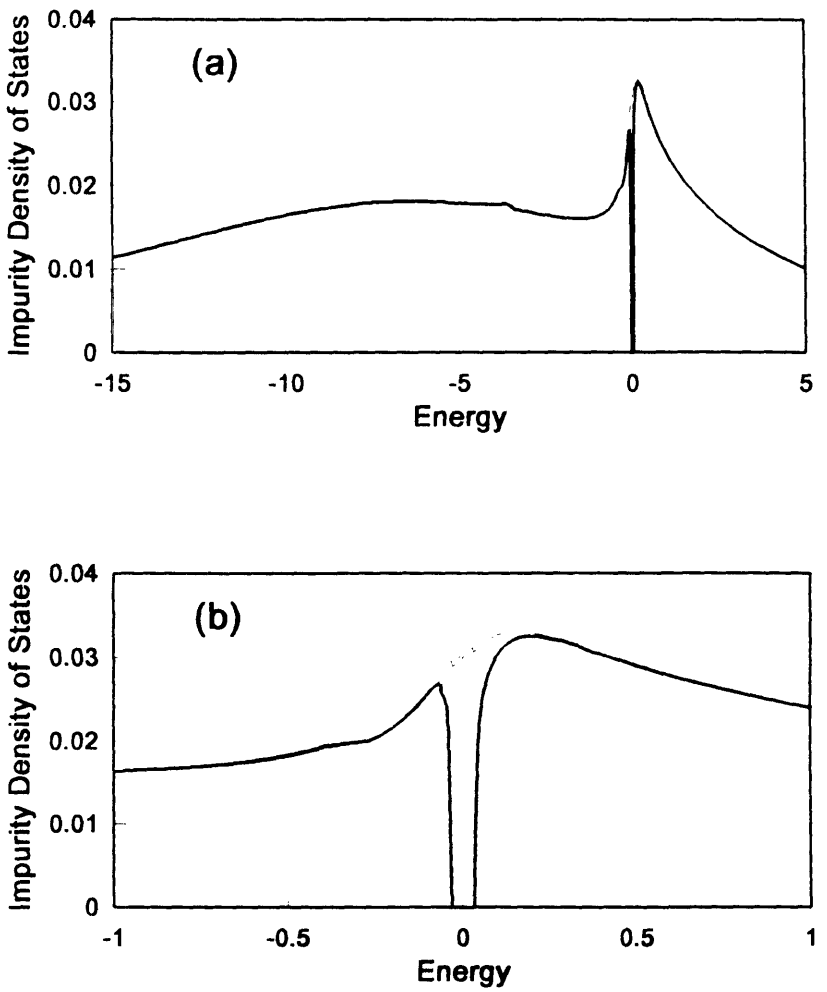

Figure 3.12. Comparison between the DOS of the system without the gap (light) and a system with $\Delta_o = .0355eV$ (dark). (b) shows the region around the Fermi level in more detail. Note that both resonances, at E_d' and at Δ_o, are distinct from one another.

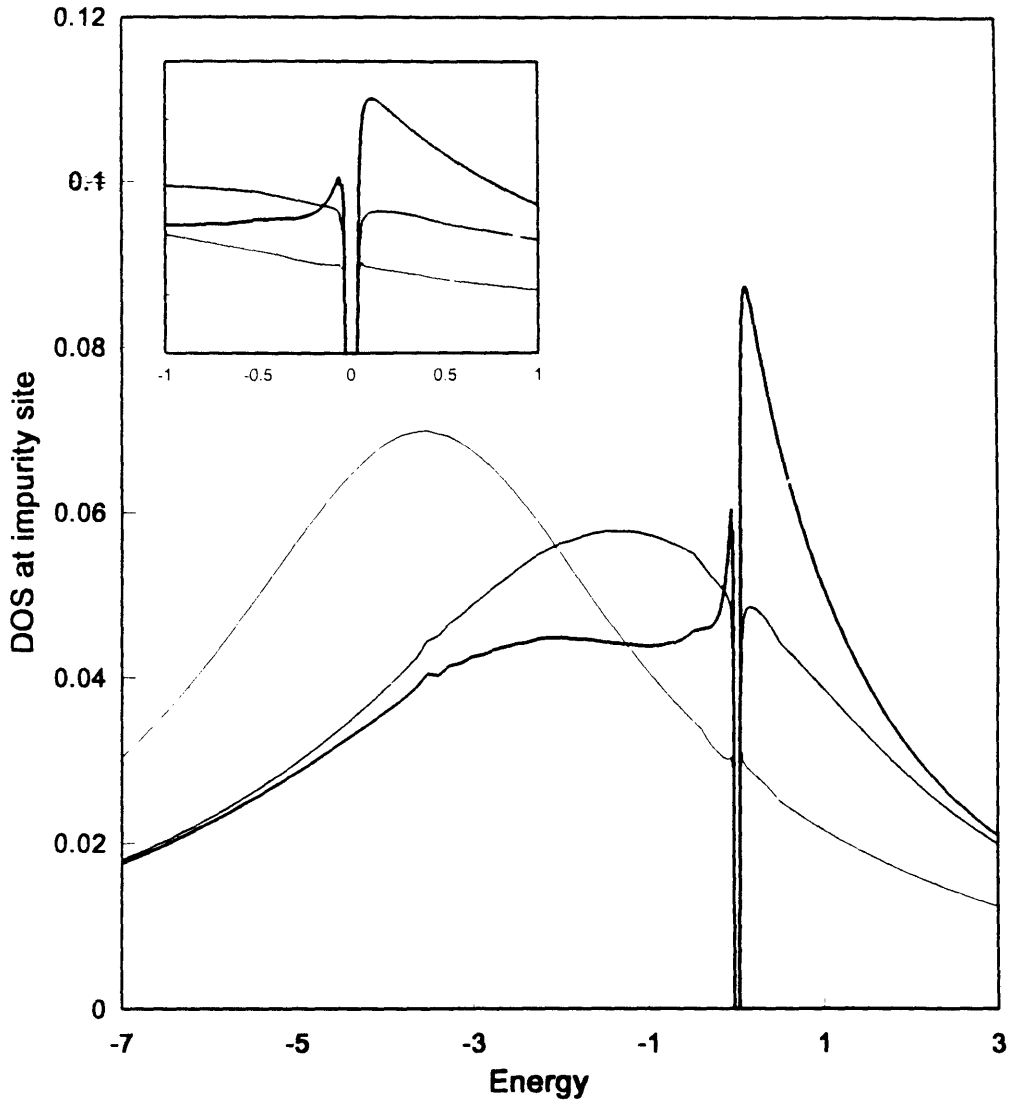

Figure 3.13. Impurity density of states for the parameters $D = 80eV$, $\Delta = 2eV$, $E_d = -4eV$, and a gap of $\Delta_o = .0355eV$. The inset shows detail. Temperature decreases for darker line types.

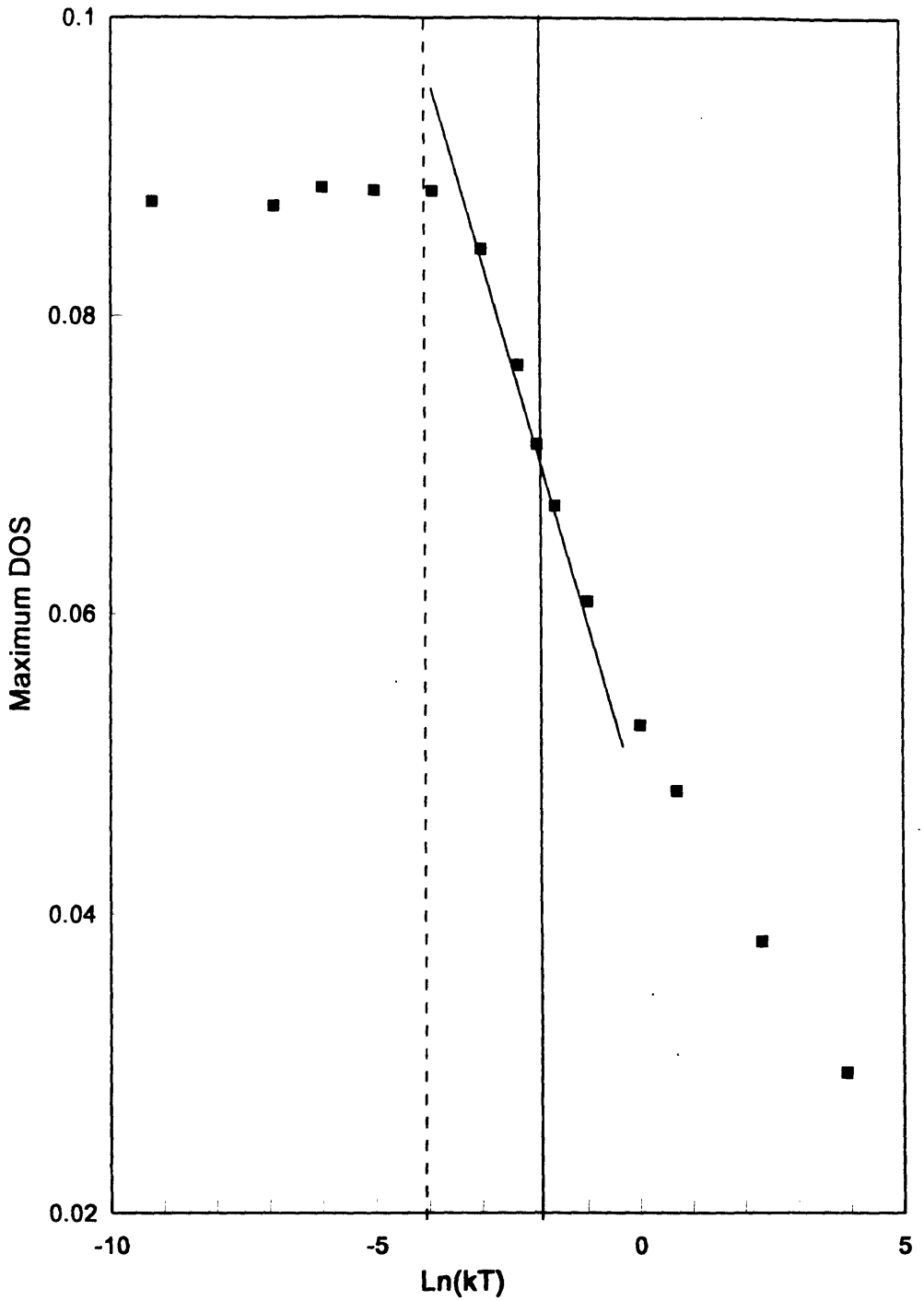

Figure 3.14. Maximum DOS (filled squares) at $\omega = \Delta_o$ taken from more curves of figure 3.13. The solid vertical line corresponds to the Kondo temperature of the system. The dashed line corresponds to T_1. The angled line is drawn to denote the linear logT behavior of the resonant peak.

Now we focus on the changes that other gap sizes might introduce in the results. Because the gap Δ_o enters in the expression of the DOS in a nontrivial way, we explore the dependence of the height of the DOS at $\omega \sim \Delta_o$ as a function of log$T$ and the size of the gap. We anticipate that increasing Δ_o from 0 to a critical value ${\Delta_o}^{crit}$, the value of the DOS will be affected. This fact comes because Δ_o introduces a cutoff below which a saturation is attained and no further growth is observed. Figure 3.15 shows for six gaps (Δ_o = 0, .04, .08, .1, .2, and .4eV) the advertised behavior. The parameters used are Δ = 2eV, E_d = −5.5eV, and D = 80eV. The solid vertical line indicates the position of the Kondo temperature for this parameter set. As the gap is increased, the point that separates the saturation region from the log$T$ region, T_1, shifts towards higher temperatures. In fact, it can be shown that as $\Delta_o \rightarrow {\Delta_o}^{crit}$, $T_1 \rightarrow T_k$, where T_k is the Kondo temperature of the normal system. Once $\Delta_o > {\Delta_o}^{crit}$, the maximum DOS at $\omega \sim \Delta_o$ does not increases beyond a marginal residual value as a function of decreasing temperature. Thus, there is a critical gap beyond which the resonance is not exhibited. Rewritting equation (3.68) we can show that ${\Delta_o}^{crit}$ satisfies

$$ {\Delta_o}^{crit} = E_d - \frac{\Delta}{\pi}\left[\ln \frac{{\Delta_o}^{crit}}{2D} + 1\right]. \tag{3.72} $$

It is interesting to notice that equation (3.72) can be rewritten in terms of the Kondo temperature as $\Delta_o e^{1+\frac{\pi\Delta_o}{\Delta}} < 2T_k$, where the inequality assures a resonance. This inequality shows that the value for Δ_o will always be less than the Kondo temperature of the normal system. Also, this inequality is very similar to other calculations with the same density of states (3.5) [32,31]. In figure 3.15 the solution to equation (3.72) yields ${\Delta_o}^{crit} \cong$ .157eV. Using typical parameters for PA, $v_f = 2t_o a$, t_o = 2.5eV, a = 1.22A, D = 7.89eV (using the linearized dispersion relation for the TLM model), we get for Δ_o = .01eV, the values of E_d = −.02eV and V' = .28eV for $T_k \sim$ .1eV. For a bigger gap of Δ_o = .1eV, solution to (3.72) again give E_d = −.21eV and V' = 1.1eV if $T_k \sim$ .5eV. Also, for Δ_o = .2eV we get E_d = −.9eV and V' = 2.27eV for $T_k \sim$ .5eV.

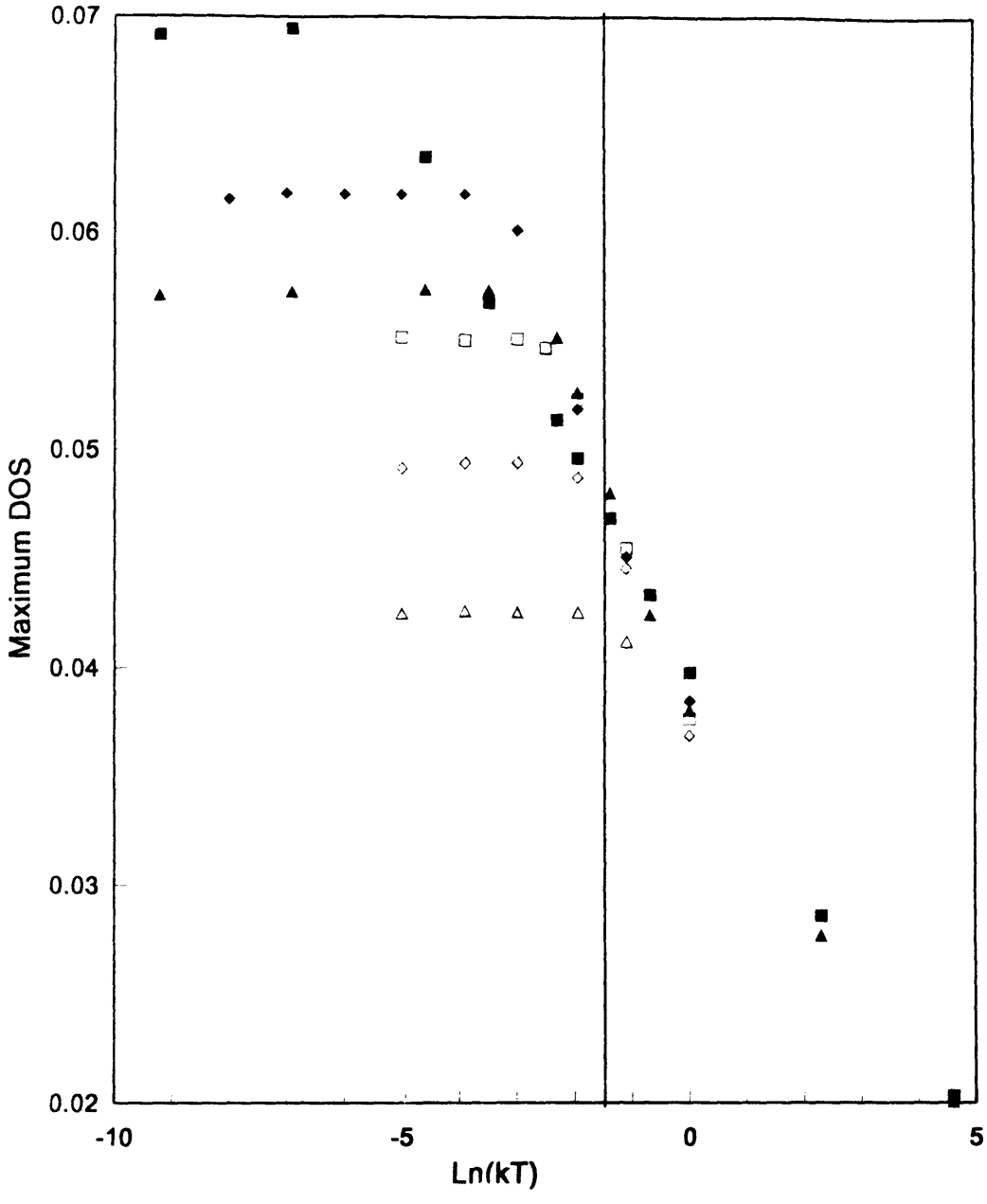

Figure 3.15. Plot of the maximum value of the DOS at $\omega = \Delta_o$ for several values of the gap. The solid vertical line indicates the position of the Kondo temperature. Other parameters are $\Delta = 3eV$, $D = 80eV$, and $E_d = -5.5eV$. The gaps are $\Delta = 0$, .0355, .0755, .101eV, .201eV, and .401eV for the solid squares, solid diamonds, solid triangles, open squares, open diamonds, and open triangles, respectively.

3.5. Conclusions.

Because of the close relationship between the DOS and the resistivity, we conclude that the experimentally observed log$T$ in PA could be explained in terms of the model considered here. The saturation of the DOS at very low T indicates that the occupancy of the impurity level is very close to one. From the point of view of the resistivity, a saturation marks the end of the spin-flip scattering and the beginning of the Kondo state. Therefore, we have shown how we can account for a Kondo-like behavior in the resistance of systems that possess a gap containing the Fermi level. Experimental results on the newly synthesized HCPA show a log$T$ behavior at low T. Taking into account then, that for heavily doped PA there are IRAV modes that suggest the existence of a gap, our model explains the log$T$ and further saturation of the resistance. A Hamiltonian that is composed of the usual non-interacting part of PA and complemented by an Anderson Hamiltonian is used in order to take into account impurities in the system. A relation that puts an upper bound on the size of the gap has been given in terms of other quantities such as the atomic level and the magnitude of hybridization.

References for Chapter 3.

1. A.J. Heeger, S. Kivelson, J.R. Schrieffer, W.-P. Su, *Rev. Mod. Phys.*, **60**, 781 (1988).
2. H. Naarmann, N. Theophilou, *Synth. Met.*, **22**, 1 (1987).
3. H. Naarmann, *Synth. Met.*, **17**, 223 (1987).
4. N. Basescu, Z.-X. Liu, D. Moses, A.J. Heeger, H. Naarmann, N. Theophilou, *Nature*, **327**, 403 (1987).
5. Th. Schimmel, W. Rieβ, J. Gmeiner, G. Denninger, M. Schwoerer, H. Naarmann, N. Theophilou, *Sol. State Commun.*, **65**, 1311 (1988).
6. Th. Schimmel, G. Denninger, W, Rieβ, J. Voit, M. Schwoerer, W. Schoepe, H. Naarmann, *Synth. Met.*, **28**, D11 (1989).
7. P. Sheng, *Phys. Rev. B*, **21**, 2180 (1980).
8. Y.H. Kim, A.J. Heeger, *Phys. Rev. B* **40**, 8393 (1989).
9. X.Q. Yang, D.B. Tanner, A. Feldblum, H.W. Gibson, M.J. Rice, A.J. Epstein, *Mol. Cryst. Liq. Cryst.*, **117**, 267 (1985).
10. X.Q. Yang, D.B. Tanner, M.J. Rice, H.W. Gibson, A. Feldblum, A.J. Epstein, *Sol. State Commun.*, **61**, 335 (1987).
11. J.F. Rabolt, T.C. Clarke, G.B. Street, *J. Chem. Phys.*, **71**, 4614 (1979).
12. C. Benoit, O. Berhard, M. Palpawer, M. Rolland, M.J.M. Abadie, *J. Phys.* (Paris), **44**, 1307 (1983).
13. D.B. Tanner, G.L. Doll, A.M. Rao, P.C. Eklund, G.A. Arbuckle, A.G. MacDiarmid, *Synth. Met.*, **28**, D141 (1989).
14. K. Tanaka, M. Okada, T. Koike, T. Yamabe, *Synth. Met.*, **31**, 181 (1989).
15. K. Tanaka, M. Okada, T. Tamabe, *Synth. Met.*, **38**, 395, (1990). Ibid, **43**, 3509 (1991).
16. J. Tsukamoto, A. Takahashi, K. Kawasaki, *J. Appl. Phys.*, **29**, 125 (1990).
17. Y. Nogami, H. Kaneko, H. Ito, T. Ishiguro, T. Sasaki, N. Toyota, A. Takahashi, J. Tsukamoto, *Phys. Rev. B*, **43**, 11829 (1991).

18. T.Ishiguro, H. Kaneko, Y. Nogami, H. Ishimoto, H. Nishiyama, J. Tsukamoto, A. Takahashi, M. Yamaura, T. Hagiwara, K. Sato, *Phys. Rev. Lett.* **69**, 660 (1992).

19. H. Kaneko, T, Ishiguro, J. Tsukamoto, A. Takahashi, *J. Phys. Soc. Jpn.*, **62**, 3621 (1993).

20. N.F. Mott, *Rev. Mod. Phys.*, **50**, 203 (1978).

21. Y. Nogami,M. Yamashita,H. Kaneko,T. Ishiguro,A. Takahashi, J. Tsukamoto, *J. Phys. Soc. Jpn.*, **62**, 664 (1993).

22. V.N. Prigodin, K.B. Efetov, *Phys. Rev. Lett.*, **70**, 2932 (1993).

23. K. Harigaya, *J. Phys.:Condens. Matter* **3**, 4841 (1991).

24. K. Ingersent, B.A. Jones, J.W. Wilkins, *Phys. Rev. Lett.*, **69**, 2594 (1992).

25. J. Kondo, *Prog. Theo. Phys.*, **32**, 37 (1964).

26. G.D. Mahan, *Many-Particle Physics*, Plenum Press, N.Y., 2nd edition, p. 977 (1990).

27. W.-P. Su, J.R. Schrieffer, A.J. Heeger, *Phys. Rev. B*, **22**, 2099 (1980).

28. H. Takayama, Y.R. Lin-Liu, K. Maki,*Phys. Rev. B* **21**, 2388 (1980).

29. K. Harigaya, *J. Phys.:Condens. Matter*, **3**, 4857 (1991).

30. D. Withoff, E. Fradkin, *Phys. Rev. Lett.* **64**, 1835 (1990).

31. T. Saso, *J. Phys. Soc. Jpn.* **61**, 3439 (1992).

32. T. Saso, J. Ogura, *Physica B* **186–188**, 372 (1993).

33. T. Nanba, H. Ohta, M. Motokawa, S. Kimura, S. Kunii, T. Kasuya, *Physica B*, **186-188**, 440 (1993).

34. P.W. Anderson, *Phys. Rev.* **124**, 41 (1961).

35. H.A. Mizes, E.M. Conwell, *1991 Proc. Int. Conf. on Science and Technology of Synthetic Metals* (1990).

36. S. Kivelson, A.J. Heeger, *Synth. Met.* **17**, 183 (1987).

37. P. Phillips, L. Cruz, *to be published.*

38. M. Dinter, *Phys. Rev. B*, **39**, 8423 (1989).

39. L. Cruz, P. Phillips, *Phys. Rev. B*, **49**, 5149 (1994).

40. S. Kivelson, T.-K. Lee, Y.R. Lin-Liu, I. Peschel, L. Yu, *Phys. Rev. B*, **25**, 4173 (1982).

41. J.A. Appelbaum, D.R. Penn, *Phys. Rev.*, **188**, 874 (1969).

42. C. Lacroix, *J. Phys. F:Metal Phys.* **11**, 2389 (1981).

43. C. Lacroix, *J. Appl. Phys.* **53**, 2131 (1982).

44. F.D.M. Haldane, *J. Phys. C:Solid State Phys.* **11**, 5015 (1978).

45. F.D.M. Haldane, *Phys. Rev. Lett.*, **40**, 416 (1978).

Appendix A

In the first part of this Appendix we present the transformation used to change the creation and annihilation operators from the real to the k-space representation. As an illustration, the actual transformation is carried out for the SSH Hamiltonian. The second part is concerned with the relationship between the wavefunctions used in this work and those conventionally used in the literature regarding the continuum representation of the SSH Hamiltonian. Also, in this second part the repercussion on the boundary conditions of the wavefunctions, brought about by this transformation, is derived.

A.1. Transformation of the Electron Operators.

In general, the first step in the calculations presented in this thesis has proceeded by transforming the site SSH Hamiltonian into its k-space representation. The procedure consists in decomposing the creation and destruction operators $c_{n,s}$ for the electrons at site n and spin s into operators that create and destroy electrons in the valence and conduction band $c^v_{k,s}$ and $c^c_{k,s}$, respectively. Using equations (3.5) in ref. 1 of chapter 2 as the starting point, we construct the following equality

$$c_{n,s} = \frac{1}{\sqrt{2N}} \sum_k e^{-ikan}[c^v_{k,s} + i(-1)^n c^c_{k,s}], \qquad (A.1)$$

where N is the number of carbon atoms in the chain. We prove this relation by

showing that it works in deriving the expression for the energy given in ref. 1 of chapter 2 for the non-interacting case.

First, we need the same relation but for the $n+1$ site

$$c_{n+1,s} = \frac{1}{\sqrt{2N}} \sum_k e^{-ikan} e^{-ika} [c^v_{k,s} - i(-1)^n c^c_{k,s}] \tag{A.2}$$

so that we can derive

$$\begin{aligned} \sum_n c^\dagger_{n+1,s} c_{n,s} =& \frac{1}{2} \sum_k e^{ika} [c^{v\dagger}_{k,s} c^v_{k,s} - c^{c\dagger}_{k,s} c^c_{k,s}] \\ &+ \frac{i}{2} \sum_k e^{ika} e^{-i\pi} [c^{c\dagger}_{k-\frac{\pi}{a},s} c^v_{k,s} + c^{v\dagger}_{k-\frac{\pi}{a},s} c^c_{k,s}]. \end{aligned} \tag{A.3}$$

Now, from the definition of the $c^v_{k,s}$ and $c^c_{k,s}$ operators

$$\begin{aligned} c^v_{k,s} =& \frac{1}{\sqrt{N}} \sum_n e^{ikan} c_{n,s} \\ c^c_{k,s} =& -\frac{i}{\sqrt{N}} \sum_n e^{ikan} (-1)^n c_{n,s} \end{aligned} \tag{A.4}$$

we can see that

$$\begin{aligned} c^c_{k-\frac{\pi}{a},s} =& -ic^v_{k,s} \\ c^v_{k-\frac{\pi}{a},s} =& ic^c_{k,s}. \end{aligned} \tag{A.5}$$

Substituting in (A.3), we have then that

$$\sum_n c^\dagger_{n+1,s} c_{n,s} = \sum_k e^{ika} [c^{v\dagger}_{k,s} c^v_{k,s} - c^{c\dagger}_{k,s} c^c_{k,s}]$$

so that

$$\sum_n [c^\dagger_{n+1,s} c_{n,s} + c^\dagger_{n,s} c_{n+1,s}] = 2 \sum_k \cos(ka) [c^{v\dagger}_{k,s} c^v_{k,s} - c^{c\dagger}_{k,s} c^c_{k,s}]. \tag{A.6}$$

Now, upon using the identity $(-1)^n = e^{i\pi n}$ we obtain that

$$\sum_n (-1)^n [c^\dagger_{n+1,s} c_{n,s}] = i \sum_k e^{ika} [c^{v\dagger}_{k,s} c^c_{k,s} + c^{c\dagger}_{k,s} c^v_{k,s}] \tag{A.7}$$

so that

$$\sum_n (-1)^n [c^\dagger_{n+1,s} c_{n,s} + c^\dagger_{n,s} c_{n+1,s}] = -\sum_k 2\sin(ka) [c^{v\dagger}_{k,s} c^c_{k,s} + c^{c\dagger}_{k,s} c^v_{k,s}]. \tag{A.8}$$

Now we are ready to substitute into the site-representation Hamiltonian. Substituting (A.6) and (A.8) into the SSH non-interacting Hamiltonian we get

$$\begin{aligned}\mathcal{H} &= -\sum_{n,s}[t_o + (-1)^n 2\alpha u][c^{\dagger}_{n+1,s}c_{n,s} + c^{\dagger}_{n,s}c^{\dagger}_{n+1,s}] \\ &= \sum_{k,s} 2t_o \cos(ka)[c^{c\dagger}_{k,s}c^{c}_{k,s} - c^{v\dagger}_{k,s}c^{v}_{k,s}] \\ &\qquad + 4\alpha u \sin(ka)[c^{v\dagger}_{k,s}c^{c}_{k,s} + c^{c\dagger}_{k,s}c^{v}_{k,s}]\end{aligned} \tag{A.9}$$

which yields finally

$$\boxed{\mathcal{H} = \textstyle\sum_{k,s}[\epsilon_k(c^{c\dagger}_{k,s}c^{c}_{k,s} - c^{v\dagger}_{k,s}c^{v}_{k,s}) + 4\alpha u \sin(ka)(c^{v\dagger}_{k,s}c^{c}_{k,s} + c^{c\dagger}_{k,s}c^{v}_{k,s})]} \tag{A.10}$$

where $\epsilon_k = 2t_o \cos(ka)$. This is equation (3.6) in ref. 1 of chapter 2.

A.2. Boundary Conditions.

The convention adopted in this work regarding the continuum version of the SSH Hamiltonian is the use of σ_2 instead of σ_3 (see equation (2.2)). This convention permits us to directly identify the wavefunctions with the electronic site amplitudes in the chain. We can relate these wavefunctions to the ones normally used by directly comparing the electronic parts of both the normal TLM Hamiltonian (ref. 28 of chapter 2) and the ones used here (ref. 31 of chapter 2). The following relationship between both electronic amplitudes is obtained,

$$\begin{aligned}u_{tlm}(x) &= u(x) - iv(x) \\ v_{tlm}(x) &= -iu(x) + v(x)\end{aligned} \tag{A.11}$$

up to a normalization constant. The transformation takes the amplitudes given by the subscript TLM relating to the left and right-moving electrons to a representation where they stand for the amplitudes at odd and even sites. The boundary

conditions that these new amplitudes have to satisfy are easily derived using the same formalism as outlined in reference 36 of chapter 2. Using the periodicity in the charge density,

$$\Psi^{\dagger}(x+L)\Psi(x+L) = \Psi^{\dagger}(x)\Psi(x) \tag{A.12}$$

and the periodicity in the current density,

$$\Psi^{\dagger}(x+L)\sigma_2\Psi(x+L) = \Psi^{\dagger}(x)\sigma_2\Psi(x) \tag{A.13}$$

and defining $\Psi(x+L) = B\Psi(x)$ we get that

$$B = \begin{cases} e^{i\alpha_1} I & \text{even number of excitations} \\ \\ e^{i\alpha_2}\sigma_3 & \text{odd number of excitations} \end{cases} \tag{A.14}$$

for the case of reference 36. For the case of reference 31 the same periodicity conditions lead to

$$B = \begin{cases} e^{i\alpha_1} I & \text{even number of excitations} \\ \\ e^{i\alpha_2}\sigma_2 & \text{odd number of excitations.} \end{cases} \tag{A.15}$$

The periodicity conditions given by equations (A.15) are the ones used throughout this work which lead directly to the density of states.

Appendix B

This appendix is designed as an outline of how the Inverse Scattering Formalism works. In the first part, the Inverse Scattering Formalism is used to obtain the order parameter correponding to a single soliton and polaron, separately. The only input parameters in the results are shown to be the energy of the bound state level and the occupation number for that same level. In the second part of this appendix, explicit formulas are derived for the case of two bound states and the boundary condition for two and three levels is derived. The generalization to the n-level system follows in a straightforward way from this presentation.

B.1. Order parameter for single excitations.

Starting from the eigenvalue equation of the TLM Hamiltonian we obtain the two coupled equations

$$\begin{aligned} [-v_f\partial_x + \Delta(x)]v(x) &= \epsilon u(x) \\ [v_f\partial_x + \Delta(x)]u(x) &= \epsilon v(x) \end{aligned} \tag{B.1}$$

which on decoupling yield

$$\begin{aligned} -\partial_x^2 v(x) + U_o(x)v(x) &= \lambda v(x) \\ -\partial_x^2 u(x) + U_e(x)u(x) &= \lambda u(x) \end{aligned} \tag{B.2}$$

where

$$\begin{aligned} U_o(x) =& \frac{1}{v_f}\partial_x\Delta(x) + \frac{1}{v_f^2}[\Delta(x)^2 - \Delta_o^2] \\ U_e(x) =& -\frac{1}{v_f}\partial_x\Delta(x) + \frac{1}{v_f^2}[\Delta(x)^2 - \Delta_o^2] \end{aligned} \tag{B.3}$$

and $\lambda = [\epsilon^2 - \Delta_o^2]/v_f^2$.

Inverse Scattering Theory gives the solution of the potentials as

$$U(x) = -2\frac{d^2}{dx^2}\ln\det(\hat{A} + \hat{I}) \tag{B.4}$$

where

$$\hat{A}_{nm} = a_n^{1/2}a_m^{1/2}\frac{e^{(k_n+k_m)x}}{(k_n + k_m).} \tag{B.5}$$

A. Single soliton on odd sites. The occupation number of a negative soliton is $N = 1$, and energy the level lies at $\epsilon = 0$. This means that $\lambda = -(\Delta_o/v_f)^2$ and also $k = \Delta_o/v_f$. From equation (B.5) we get

$$\hat{A} = a_1\frac{e^{2kx}}{2k}$$

putting this in (B.4) yields

$$\begin{aligned} U_o(x) =& -2\frac{d^2}{dx^2}\ln(1 + a_1\frac{e^{2kx}}{2k}) \\ =& -2k^2\mathrm{sech}^2(kx - \delta_1) \end{aligned} \tag{B.6}$$

where δ_1 is defined by $e_1^{\delta} \equiv \sqrt{2k/a_1}$. By inverting equations (B.3) and solving for $\Delta(x)$, and using $U_e = 0$ we get for the order parameter,

$$\Delta(x) = -\Delta_o\tanh(kx - \delta_1) + C.$$

Upon using the boundary condition that $\Delta(\infty) = -\Delta_o$ we obtain that $C = 0$. Also, because the order parameter is translationally invariant, we can freely choose δ_1 to be 0. Then the order parameter for the single soliton becomes,

$$\boxed{\Delta(x) = -\Delta_o\tanh(kx)} \tag{B.7}$$

B. Single soliton on even sites. Following the same reasoning and calculations as above for the case of even sites leads to $U_e(x) = -2k^2\,\mathrm{sech}^2(kx-\delta_2)$ and $U_o(x) = 0$. The order parameter turns out to be

$$\boxed{\Delta(x) = \Delta_o \tanh(kx).} \tag{B.8}$$

C. Single polaron. Because the polaron has equal charge distribution on even and odd sites, both cases are equal and the same. Then the occupation number is $N = 1$, the energy level lies at $\epsilon = -\omega_o$, and $\lambda = k^2$. The potentials are given by

$$\begin{aligned} U_i(x) &= -2k\frac{d}{dx}\tanh(kx-\delta_i) \\ &= -2k^2\mathrm{sech}^2(kx-\delta_i) \end{aligned} \tag{B.9}$$

thus $\Delta(x) = -v_f k[\tanh(kx-\delta_o) - \tanh(kx-\delta_e)] + C$ where e, o mean even and odd, respectively. Applying the boundary condition that $\Delta(\pm\infty) = \Delta_o$, and the translational symmetry $\delta_e = -\delta_o \equiv -\delta$ we get

$$\boxed{\Delta(x) = \Delta_o - v_f k[\tanh(kx-\delta) - \tanh(kx+\delta)]} \tag{B.10}$$

where $kv_f = \sqrt{\Delta_o^2 - \omega_o}$. For a chain of infinite length the value of ω_o is given by $\omega_o = \Delta_o/\sqrt{2}$.

B.2. Two level wavefunctions and treatment of boundary conditions.

From the system of equations given by equation (2.19) consider two levels denoted by k_1 and k_2, where $k_i v_f = \sqrt{\Delta_o^2 - \omega_i^2}$. Then the system to solve is given by

$$\begin{aligned} u_1^r(x)e^{k_1 x} &= 1 - \frac{c_{1e}^2 u_1^r(x)e^{-k_1 x}}{2k_1} - \frac{c_{2e}^2 u_2^r(x)e^{-k_2 x}}{k_1+k_2} \\ u_2^r(x)e^{k_2 x} &= 1 - \frac{c_{1e}^2 u_1^r(x)e^{-k_1 x}}{k_1+k_2} - \frac{c_{2e}^2 u_2^r(x)e^{-k_2 x}}{2k_2} \end{aligned} \tag{B.11}$$

where $u_1^r(x)$ and $u_2^r(x)$ are the unnormalized electron amplitudes for even sites. The first solution to (B.11) is given by

$$\boxed{u_1^r(x) = \frac{\sigma}{2W_e(x)}(e^{k_2 x - \delta_{1e}} + e^{-k_2 x - \delta_{2e}})} \qquad (B.12)$$

where

$$\frac{c_{2e}}{c_{1e}}\sqrt{\frac{k_1}{k_2}} \equiv e^{-\delta_{2e}} \quad \text{and} \quad \frac{2\sqrt{k_1 k_2}}{c_{1e}c_{2e}}\frac{\rho}{\sigma} \equiv e^{-\delta_{1e}}.$$

Also, the definitions $\rho \equiv k_1 + k_2$ and $\sigma \equiv k_1 - k_2$ have been made. The term in the denominator is defined as

$$W_e(x) \equiv \rho\cosh(\sigma x - \delta_{2e}) + \sigma\cosh(\rho x - \delta_{1e}).$$

The other solution to (B.11) is

$$\boxed{u_2^r(x) = \frac{\sigma}{2W_e(x)}(e^{k_1 x - \delta_{1e}} - e^{-k_1 x + \delta_{2e}}).} \qquad (B.13)$$

The electron amplitude for the odd sites are

$$\boxed{\begin{aligned} v_1^r(x) &= \frac{\sigma}{2W_o(x)}(e^{k_2 x - \delta_{1o}} + e^{-k_2 x - \delta_{2o}}) \\ v_2^r(x) &= \frac{\sigma}{2W_o(x)}(e^{k_1 x - \delta_{1o}} - e^{-k_1 x + \delta_{2o}}) \end{aligned}} \qquad (B.14)$$

where

$$W_o(x) = \rho\cosh(\sigma x - \delta_{2o}) + \sigma\cosh(\rho x - \delta_{1o}).$$

From the boundary conditions on the electronic amplitudes it can be shown that $\delta_o = -\delta_e$. From this fact we can easily see that $u(-x) = v(x)$ and that $W_e(x) = W_o(-x)$ for the present case of two levels. In Appendix D a more general relation between the odd and even site amplitudes will be presented.

Using expressions (B.12), (B.13), and (B.14) into the expressions for the continuum electronic amplitudes, as given in equation (2.20), we can show that for the system of two levels, the amplitudes in the continuum are,

$$\begin{aligned} u_k^r(x) =& e^{ikx}\Big\{1 - \frac{\rho}{W_e(x)}\Big[\frac{k_1}{k_1 - ik}\big(e^{-\sigma x+\delta_2} + e^{-\rho x+\delta_1}\big) \\ &+ \frac{k_2}{k_2 - ik}\big(e^{\sigma x-\delta_2} - e^{-\rho x+\delta_1}\big)\Big]\Big\} \\ v_k^r(x) =& e^{ikx}\Big\{1 - \frac{\rho}{W_o(x)}\Big[\frac{k_1}{k_1 - ik}\big(e^{-\sigma x-\delta_2} + e^{-\rho x-\delta_1}\big) \\ &+ \frac{k_2}{k_2 - ik}\big(e^{\sigma x+\delta_2} - e^{-\rho x-\delta_1}\big)\Big]\Big\}. \end{aligned} \tag{B.15}$$

The boundary condition to be verified is the one given by the equation in the paragraph just before equation (2.13). Namely,

$$\begin{pmatrix} u(x+L) \\ v(x+L) \end{pmatrix} = e^{i\theta}\begin{pmatrix} u(x) \\ v(x) \end{pmatrix} \tag{B.16}$$

as given in appendix A for an even number of excitations. The phase θ is a multiple of π, (see ref. 36 of chapter 2). Now, on taking the length of the chain L large, or by taking $k_1 L >> \delta_2, \delta_1$, we approximate the following quantities. The first one

$$W_e(x+L) \cong \frac{\rho}{2}e^{\sigma(x+L)-\delta_2} + \frac{\sigma}{2}e^{\rho(x+L)-\delta_1} \tag{B.17}$$

and the wavefunctions

$$u_k^r(x+L) \cong e^{ik(x+L)}\Big\{1 - \frac{\rho}{W_e}\frac{k_2}{k_2 - ik}e^{\sigma(x+L)-\delta_2}\Big\}. \tag{B.18}$$

Because $\rho > \sigma$ we finally get

$$\begin{aligned} u_k^r(x+L) \cong& e^{ik(x+L)} \\ v_k^r(x+L) \cong& e^{ik(x+L)}. \end{aligned} \tag{B.19}$$

For the electronic amplitudes at x, after approximating, we get

$$\begin{aligned} u_k^r(x) \cong& e^{ikx}\Big\{1 + \frac{2ik\rho}{(k_1 - ik)(k_2 - ik)}\Big\} \\ v_k^r(x) \cong& e^{ikx}\Big\{1 + \frac{2ik\rho}{(k_1 - ik)(k_2 - ik)}\Big\} \end{aligned} \tag{B.20}$$

where we have taken x big, but kept it such that $|x| < L$, and used the fact that $W_e(x) \cong \frac{\sigma}{2} e^{-\rho x + \delta_1}$ and $W_o(x) \cong \frac{\sigma}{2} e^{-\rho x - \delta_1}$. After inserting the previous approximations into equation (B.16) the condition now stands as

$$e^{ikL} = e^{i\theta}\left\{1 + \frac{2ik\rho}{(k_1 - ik)(k_2 - ik)}\right\}$$

or that

$$\begin{aligned} e^{i(kL-\theta)} =& \frac{(k_1 + ik)(k_2 + ik)}{(k_1 - ik)(k_2 - ik)} \\ =& e^{2i\tan^{-1} k/k_1} e^{2i\tan^{-1} k/k_2}. \end{aligned}$$

Therefore,

$$\boxed{kL - \theta = 2\tan^{-1}\frac{k}{k_1} + 2\tan^{-1}\frac{k}{k_2}.} \qquad (B.21)$$

A shortcut to get to the same result, that will be used to verify the boundary condition for three levels, is to note that conditon (B.16) is true for any x, so we take x to be a big negative number, but less than L. Then the system given by equation (2.19)

$$\begin{pmatrix} e^{k_1 x} + \frac{c_{1e}^2 e^{-k_1 \infty}}{2k_1} & \frac{c_{2e}^2 e^{-k_2 \infty}}{k_1 + k_2} \\ \frac{c_{1e}^2 e^{-k_1 \infty}}{k_1 + k_2} & e^{k_2 x} + \frac{c_{2e}^2 e^{-k_2 \infty}}{2k_2} \end{pmatrix} \begin{pmatrix} u_1^r(x) \\ u_2^r(x) \end{pmatrix} = \begin{pmatrix} 1 \\ 1 \end{pmatrix} \qquad (B.22)$$

for x a large negative number yields

$$\begin{aligned} u_1^r(x) \cong& \frac{2k_1\rho}{c_{1e}^2\sigma} e^{k_1 x} \\ u_2^r(x) \cong& -\frac{2k_2\rho}{c_{2e}^2\sigma} e^{k_2 x} \end{aligned} \qquad (B.23)$$

so that

$$u_k(x) \cong e^{ikx}\left\{1 + i\frac{2\rho k}{(k_1 - ik)(k_2 - ik)}\right\}$$

as in equation (B.20).

The same system for $x \to x + L$ and $L \to \infty$ yields

$$\begin{pmatrix} e^{k_1(x+L)} & 0 \\ 0 & e^{k_2(x+L)} \end{pmatrix} \begin{pmatrix} u_1^r(x+L) \\ u_2^r(x+L) \end{pmatrix} = \begin{pmatrix} 1 \\ 1 \end{pmatrix}$$

that results in $u_1^r(x+L) \cong e^{-k_1(x+L)}$ and $u_2^r(x+L) \cong e^{-k_2(x+L)}$, as obtained in (B.19).

Now we can use the same trick for three levels. The system is now given by

$$\begin{pmatrix} e^{k_1 x} + \frac{c_{1e}^2 e^{-k_1 \infty}}{2k_1} & \frac{c_{2e}^2 e^{-k_2 \infty}}{k_1+k_2} & \frac{c_{3e}^2 e^{-k_3 \infty}}{k_1+k_3} \\ \frac{c_{1e}^2 e^{-k_1 \infty}}{k_1+k_2} & e^{k_2 x} + \frac{c_{2e}^2 e^{-k_2 \infty}}{2k_2} & \frac{c_{3e}^2 e^{-k_3 \infty}}{k_2+k_3} \\ \frac{c_{1e}^2 e^{-k_1 \infty}}{k_1+k_3} & \frac{c_{2e}^2 e^{-k_2 \infty}}{k_2+k_3} & e^{k_3 x} + \frac{c_{3e}^2 e^{-k_3 \infty}}{2k_3} \end{pmatrix} \begin{pmatrix} u_1^r(x) \\ u_2^r(x) \\ u_3^r(x) \end{pmatrix} = \begin{pmatrix} 1 \\ 1 \\ 1 \end{pmatrix}. \tag{B.24}$$

First we consider the system for x large and negative. This results in

$$\begin{aligned} u_1^r(x) &= \frac{2k_1\rho_{12}\rho_{13}}{c_{1e}^2\sigma_{12}\sigma_{13}} e^{k_1 x} \\ u_2^r(x) &= -\frac{2k_2\rho_{12}\rho_{23}}{c_{2e}^2\sigma_{23}\sigma_{12}} e^{k_2 x} \\ u_3^r(x) &= \frac{2k_3\rho_{13}\rho_{23}}{c_{3e}^2\sigma_{23}\sigma_{13}} e^{k_3 x} \end{aligned} \tag{B.25}$$

where $\rho_{ij} \equiv k_i + k_j$ and $\sigma_{ij} \equiv k_i - k_j$. The continuum wavefunction is given, on using (B.25),

$$\begin{aligned} u_k^r(x) &= -e^{ikx} \frac{(k_1+ik)(k_2+ik)(k_3+ik)}{(k_1-ik)(k_2-ik)(k_3-ik)} \\ &= -e^{ikx} \exp\Big(\sum_1^3 2i \tan^{-1} \frac{k}{k_i} \Big) \end{aligned} \tag{B.26}$$

Now putting $x \to x+L$ and taking $L \to \infty$ in system (B.24), get that

$$u_k^r(x+L) \cong e^{ik(x+L)}. \tag{B.27}$$

Equations (B.26) and (B.27) in the boundary condition (B.16) yield

$$e^{ikL} = e^{i\theta} - i\frac{\pi}{2} + 2i \sum_1^3 \tan^{-1} \frac{k}{k_i}$$

or that

$$\boxed{kL - \theta + \frac{\pi}{2} = \sum_1^3 2 \tan^{-1} \Big(\frac{k}{k_i} \Big).} \tag{B.28}$$

Following the same arguments, it is easy to generalize the previous result for the case of n levels in the system. Taking into account the phase of $e^{i2m\pi}$, we get for the n level case (up to a constant) the boundary condition $kL = 2m\pi + \sum_i^n 2tan^{-1}(k/k_i)$. This is the condition used throughout chapters 2 and 3.

Appendix C

Before deriving the exact expression for the wavefunctions, we define some of the notation to be used in this appendix. We will define objects with an arrow overhead to indicate the vector form of that set, e.g. $\vec{k} = (k_1, k_2, \ldots)$ and $\vec{\delta} = (\delta_1, \delta_2, \ldots)$ whose dimension (number of elements) is given by the number s of levels (electrons) introduced into the gap. Subscripts on these objects indicate the same vector but with the subscript element omited. For example, $\vec{k}_1 = (k_2, k_3, \ldots)$, so that this new vector has dimension $s-1$. A matrix L of dimension $2^{s-1} \times s$ whose elements are either 1 or -1 will be used. Its row-vectors L_{nm} will be denoted for convenience by two indices. The first index n denotes how many -1 elements it has and the second m denotes which row-vector it is. The definition of this L matrix is given below. By the dot product $L_{nm} \cdot \vec{k}$ for example, we denote the dot product of the specified L_{nm} row-vector with $\vec{k}$. If a superscript is included such as $L^1_{nm} \cdot \vec{\delta}_s$ the dot product is carried between the $\vec{\delta}$ vector, whose s element has been omited, with the L_{nm} row-vector, whose element number 1 has been omited also. A matrix P will be used and it is constructed in the same way as the L matrix, but with dimension $2^{s-2} \times (s-1)$ instead. In both cases $P_{nm}(j)$ or $L_{nm}(j)$ refer to the element j of the row-vector of the respective matrix. The rules for the construction of the L matrix, and so for the P matrix, are given below.

The wavefunctions that solve the system (2.19) were derived by induction and

are given for any number s of levels ($s > 1$) by

$$u_q = \frac{1}{W_e} \prod_{j>q}^{s} \sigma_{qj} e^{-\frac{1}{2}\left[\sum_{i=1}^{s} \delta_i - (s-2)\delta_s\right]} \times \sum_{n=0}^{s-2} \sum_{m=1}^{\binom{s-2}{n}} a_{nm}^{q-1} C_{nm}^{q} F_q\left[\beta_{nm}^{q} x - \frac{1}{2}(\vec{\delta}_s \cdot P_{nm} + [2n+1-s]\delta_s)\right] \qquad (C.1)$$

for $q = 1$, and

$$u_q = \frac{1}{W_e} \prod_{j<q}^{q-1} \sigma_{jq} \prod_{j>q}^{s} \sigma_{qj} e^{-\frac{1}{2}(\delta_{q-1} - \delta_s)} \sum_{n=0}^{s-2} \sum_{m=1}^{\binom{s-2}{n}} a_{nm}^{q-1} C_{nm}^{q} F_q\left[\beta_{nm}^{q} x - \frac{1}{2}\gamma_{nm}^{sq}\right] \qquad (C.2)$$

for $q > 1$, where $F_q[\ ] \equiv \sinh[\ ], \cosh[\ ]$ for q even or odd respectively. Also $\beta_{nm}^{q} \equiv \vec{k}_q \cdot P_{nm}$, $\sigma_{ij} = k_i - k_j$ and

$$\gamma_{nm}^{sq} \equiv \alpha_{nm}^{s} + \sum_{j=2}^{q-1} a_{nm}^{j} a_{nm}^{j-1} (\delta_{j-1} - \delta_j) \qquad (C.3)$$

$$\alpha_{nm}^{s} \equiv \vec{\delta}_s \cdot P_{nm} + \sum_{i=2}^{s-1} \delta_i + [2(n-s)+5]\delta_s. \qquad (C.4)$$

Other symbols used above are defined as follows;

$$C_{nm}^{q} \equiv \prod_{\eta<\nu\neq q}^{s} (k_\eta - k_\nu [P_{nm}(\eta - \delta_{\eta>s}) P_{nm}(\nu - \delta_{\nu>s})]) \qquad (C.5)$$

and

$$a_{nm}^{q} = \prod_{j=1}^{q} P_{nm}(j) \qquad (C.6)$$

where $a_{nm}^{0} = a_{nm}^{-1} = 1$ and $\delta_{i>j} \equiv \theta(i-j)$ is the normal step function. Note that the wavefunctions (C.1) and (C.2) are given in terms of a set $\{\delta\}$ instead of the set $\{\alpha\}$ introduced in equation (2.19). The transformation was done for convenience and is given by

$$e^{2\alpha_e^1} = \prod_{j=2}^{s} \frac{\rho_{1j}}{\sigma_{1j}} e^{\left[\sum_{i=1}^{s} \delta_i - (s-2)\delta_s\right]} \qquad (C.7)$$

for $q = 1$, and

$$e^{2\alpha_e^q} = \prod_{j=2}^{q-1} \frac{\rho_{jq}}{\sigma_{jq}} \prod_{j=q+1}^{s} \frac{\rho_{qj}}{\sigma_{qj}} e^{(\delta_{q-1} - \delta_s)} \qquad (C.8)$$

for $q > 1$, where $\rho_{i,j} = k_i + k_j$. The term W_e in the denominator of the u_q, which is the determinant of the matrix $(A + I)$, as defined in the paragraph containing equation (2.17), is given by

$$W_e(x) = \sum_{n=0}^{s-1} \sum_{m=1}^{\binom{s-1}{n}} D^s_{nm} \cosh\left[(L_{nm}\cdot\vec{k})x - \frac{1}{2}L^1_{nm}\cdot\vec{\delta}_s - \frac{1}{2}\sum_{i=1}^{s-1}\delta_i - (n+2-s)\delta_s\right] \quad (C.9)$$

where we have used the short-hand notation

$$D^s_{nm} \equiv \prod_{i<j}^{s}(k_i - k_j[L_{nm}(i)L_{nm}(j)]). \quad (C.10)$$

Note that for $s = 1$ the only wavefunction is just $u_1 = e^{-\delta_1}/2W_e$. The amplitude for the odd sites v_q can be obtained from the relation $v_q(x) = \text{sign}(\omega_q)(-1)^{q+1}$ $u_q(-x)$, and since it also satisfies a relation similar to equation (2.19)

$$v_q(x) = e^{-k_q x}\left[1 - \sum_n \frac{2k_n e^{2\alpha^n_o} v_n(x)e^{-k_n x}}{k_n + k_q}\right] \quad (C.11)$$

it can be shown that $W_e(x) = W_o(-x)$.

The L matrix is defined as follows. The first column of this matrix is composed of +1 elements only, and the rest of the matrix follows an ordering that exhausts all the combinations of +1 and -1. The form used in this article for a given s, n, and m is as follows. Let the indices $i, j, k, \ldots, l$ denote the individual L row-vector element positions whose values are equal to -1, where $i < j < k < \ldots < t < l$ and

there are n of them. Then

$$L_{nm}(i) = -1, \text{ if } \binom{s-i}{n} < m \leq \binom{s+1-i}{n}$$

$$L_{nm}(j) = -1, \text{ if } \binom{s-i}{n-1} < m - \binom{s-i}{n} \leq \binom{s+1-j}{n-1}$$

$$L_{nm}(k) = -1, \text{ if } \binom{s-k}{n-2} < m - \binom{s-i}{n} - \binom{s-j}{n-1} \leq \binom{s+1-k}{n-2} \qquad (C.12)$$

$$\vdots$$

$$L_{nm}(l) = -1, \text{ if } \binom{s-l}{n-2} < m - \binom{s-i}{n} - \binom{s-j}{n-1} - \binom{s-k}{n-2} - \cdots$$

$$- \binom{s-t}{2} \leq \binom{s+1-l}{1}$$

All other elements that do not satisfy these conditions are equal to $+1$. Note that for a given m and n the first line of equation (C.12) completely determines the position of the first -1 in the row-vector, i. Once this position is determined, it is used in the second line to determine the next position j, and so on. The matrix P is constructed in exactly the same way as the L matrix but using $s-1$, instead of s.

From equations (C.7) and (C.8) we have a relation between the set of $\{\alpha_e^n\}$ and a set of $\{\delta_i\}$, which turn out to be convenient in our case. Now we present the relation between the $\{\delta_i\}$ and the $\{\omega_i\}$, therefore establishing the dependence of the u_q on the energy levels. Let us define the quantity $Q_i \equiv \frac{k_i v_f}{C(L)}$ where $C(L) = \Delta_o - f(\frac{L}{2})$, as defined in the text following equation (2.23). Also defining the vector $\vec{R} = (R_1, R_2, \ldots, R_s)$ where its individual elements are further defined by $R_i \equiv \tanh Q_i$, we have

$$\delta_s = \frac{1}{2} L_{(s-1),1} \cdot \vec{R} \qquad (C.13)$$

for $q = s$, and

$$\delta_q = \frac{1}{2} L_{(s-2),q} \cdot \vec{R} \qquad (C.14)$$

for $q < s$. Thus, starting from a given set of $\{\omega_i\}$, by equations (C.13) and (C.14) we obtain the corresponding $\{\delta_i\}$. The $\{k_i\}$ are determined by $k_i v_f = \sqrt{\Delta_o^2 - \omega_i^2}$ so that all the σ_{ij} and ρ_{ij} are determined. In conclusion, by the above developments the wavefunctions (C.1) and (C.2) depend solely on the parameters $\{\omega_i\}$, the energy levels of the bound states.

Now we proceed to show how equation (2.18) can be obtained from equation (2.24). The sufficient relation comes from examining equation (C.9) in the limit of $L \rightarrow \pm\infty$. Note that for x very big we obtain $W_e(x) \cong D_{01}^s \cosh[(L_{01} \cdot \vec{k})x]$ since the biggest term in the sum is the one in which all the $\{k_i\}$ are summed. For its derivative we obtain then $\dot{W}_e(x) \cong (L_{01} \cdot \vec{k}) D_{01}^s \cosh[(L_{01} \cdot \vec{k})x]$. Then the condition follows that $\lim_{L \rightarrow \pm\infty} \left[\frac{\dot{W}_e(x)}{W_e(x)}\right] = \sum_i k_i$. Thus equation (2.18) is obtained by considering also that in this limit the quantity $C(L) - \Delta_o$ vanishes.

Appendix D

In this appendix several relations and results regarding the wavefunctions from the Inverse Scattering Formalism will be given. Approximations usefull in calculating the expectation values of the interacting Hamiltonian will also be given.

The relation between the odd and even bound state wavefunctions is given by

$$v_n^r(x,\delta) = (-1)^{n+1} u_n^r(-x,\delta)\mathrm{sgn}(\epsilon_n) \qquad (D.1)$$

where v_n^r and u_n^r refer to the unnormalized odd and even-site wavefunctions belonging to level n. Depending upon the sign of the energy of the level, if it lies above or below $\epsilon = 0$, there will be an extra negative sign given by the $\mathrm{sgn}\epsilon_n$. The relation between the continuum odd and even wavefunctions is given by

$$\begin{aligned}\mathrm{sgn}(\epsilon_k) v_k^r(x,\delta) =& \frac{ikv_f + \Delta(x)}{|\epsilon_k|} u_k^r(x,\delta) \\ &+ \frac{e^{ikx}}{|\epsilon_k|} \sum_n \frac{2k_n e^{2\alpha_e^n} e^{-k_n x}}{k_n - ik} \Big\{ (k_n v_f + \Delta(x)) u_n^r(x,\delta) - v_n^r(x,\delta)\epsilon_n \Big\} \\ \cong& \frac{ikv_f + \Delta(x)}{|\epsilon_k|} u_k^r(x,\delta) \qquad (D.2)\end{aligned}$$

Equation (D.2) can be derived in a straightforward way using equations (2.10). The last step in equation (D.2) is taken for simplicity and was verified for several explicit wavefunctions. For future use we state the relation

$$u_k^r(x,\delta) v_k^r(x,\delta)^* \mathrm{sgn}(\epsilon_k) \cong \frac{\Delta(x) - ikv_f}{|\epsilon_k|} |u_k^r(x,\delta)|^2. \qquad (D.3)$$

Another set of expressions that are useful are given starting from equation (2.20) and taking the square,

$$\begin{aligned}|u_k^r(x)|^2 =& 1 - \sum_i \left\{ c_i^2 u_i^r(x) e^{-k_i x} \frac{2k_i}{(k_i^2 + k^2)} - c_i^4 u_i^r(x)^2 e^{-2k_i x} \frac{1}{(k_i^2 + k^2)} \right\} \\ &+ 2 \sum_{i>j} c_i^2 c_j^2 u_i^r(x) u_j^r(x) e^{-(k_i + k_j)x} \left[\frac{k_i k_j + k^2}{(k_i^2 + k^2)(k_j^2 + k^2)} \right].\end{aligned} \tag{D.4}$$

Upon defining $c_i/\sqrt{2k_i} \equiv e^{\alpha_i}$ we get

$$\boxed{|u_k^r(x)|^2 = 1 - \sum_i f_i(k_i, x) \frac{1}{(k_i^2 + k^2)} + \sum_{i>j} g_{ij}(k_i, k_j, x) \frac{k_i k_j + k^2}{(k_i^2 + k^2)(k_j^2 + k^2)}} \tag{D.5}$$

where the following has been defined,

$$f_i(k_i, x) \equiv 4k_i^2 u_i^r(x) e^{-k_i x + 2\alpha_i} \left[1 - u_i^r(x) e^{-k_i x + 2\alpha_i} \right] \tag{D.6}$$

and

$$g_{ij}(k_i, k_j, x) \equiv 8k_i k_j u_i^r(x) u_j^r(x) e^{-(k_i + k_j)x + 2(\alpha_i + \alpha_j)} \tag{D.7}$$

The normalization of the continuum wavefunctions is taken to be $A_k \cong 1/\sqrt{2L}$. This approximation is derived starting from equation (2.11).

Appendix E

Here we present the derivation of equation (2.24) for the creation energy of the non-interacting system for finite chain lengths. Lets calculate first the electronic contribution to the energy. From equation (2.12) the electronic part is given by

$$E = \sum_k n_{k,s}\epsilon_k + \sum_{i=1}^{n_b}(n_{i+} - n_{i-})\omega_i \qquad (E.1)$$

where $n_{k,s}$ is the occupation number of state k with spin s, $n_{i\pm}$ is the occupation number of the bound state level i that is above $(+)$ or below $(-)$ the energy $\epsilon = 0$. The ω_i is the corresponding energy of the bound state, and $\epsilon_k = \sqrt{\Delta_o^2 + k^2 v_f^2}$. Note that we have explicitly taken out of the sum the bound states. Now, considering the boundary condition $kL = n\pi + \phi_k$ we get,

$$E = E_o + \frac{2}{\pi}\int dk \epsilon_k \frac{d\phi_k}{dk} + \sum_{i=1}^{n_b}(n_{i+} - n_{i-})\omega_i \qquad (E.2)$$

where E_o is the energy of the undoped system. The electronic contribution to the creation energy of the excitations is then defined as $E_e \equiv E - E_o$ and given by

$$\begin{aligned} E_e =& \frac{4}{\pi}\sqrt{\Delta_o^2 + k_f^2 v_f^2}\sum_{i=1}^{n_b}\tan^{-1}\left(\frac{k_f}{k_i}\right) - \frac{4}{\pi}\sum_{i=1}^{n_b}\int_{-k_f}^{0}\frac{d\epsilon_k}{dk}\tan^{-1}\left(\frac{k}{k_i}\right)dk \\ &+ \sum_{i=1}^{n_b}(n_{i+} - n_{i-})\omega_i \end{aligned} \qquad (E.3)$$

On taking the approximation $k_f >> k_i$ we use then that $\tan^{-1}\frac{k_f}{k_i} \cong \frac{\pi}{2}$. Also,

$$\int_0^{k_f}\frac{d\epsilon_k}{dk}\tan^{-1}\left(\frac{k}{k_i}\right)dk = \sqrt{\Delta_o^2 + k_f^2 v_f^2}\tan^{-1}\frac{k_f}{k_i} - \omega_i \tan^{-1}\left[\frac{k_f\omega_i}{k_i\sqrt{\Delta_o^2 + k_f^2 v_f^2}}\right]$$

$$
\begin{aligned}
&- v_f k_i \ln\left[k_f + \frac{\sqrt{\Delta_o^2 + k_f^2 v_f^2}}{v_f}\right] + v_f k_i \ln \frac{\Delta_o}{v_f} \\
&\cong \sqrt{\Delta_o^2 + k_f^2 v_f^2}\tan^{-1}\left(\frac{k_f}{k_i}\right) - \omega_i \tan^{-1}\left(\frac{\omega_i}{k_i v_f}\right) \\
&- \frac{v_f k_i}{2\lambda}
\end{aligned}
\tag{E.4}
$$

and using

$$
\sqrt{\Delta_o^2 + k_f^2 v_f^2}\tan^{-1}\frac{k_f}{k_i} \cong \frac{v_f k_f \pi}{2} + \frac{\pi \Delta_o^2}{4 k_f v_f} - v_f k_i \tag{E.5}
$$

and $\sqrt{\Delta_o^2 + k_f^2 v_f^2}/v_f \cong k_f + \Delta_o^2/2k_f v_f^2$ we get for the electronic contribution to the creation energy

$$
\boxed{
\begin{aligned}
E_e =& \frac{2v_f}{\pi}(2 + \frac{1}{\lambda})\sum_{i=1}^{n_b} k_i + \frac{4}{\pi}\sum_{i=1}^{n_b} \omega_i \tan^{-1}\left(\frac{\omega_i}{k_i v_f}\right) \\
&+ \sum_{i=1}^{n_b}(n_{i+} - n_{i-})\omega_i .
\end{aligned}
}
\tag{E.6}
$$

The elastic contribution to the creation energy is given by integrating over equation (2.22) with finite limits. This can be shown to give

$$
\boxed{
E_{el} = -\frac{v_f}{\pi\lambda}\left\{\frac{\dot{W}_o(\frac{L}{2})}{W_o(\frac{L}{2})} + \frac{\dot{W}_e(\frac{L}{2})}{W_e(\frac{L}{2})}\right\} + \frac{L}{2\pi\lambda v_f}(C^2 - \Delta_o^2)
}
\tag{E.7}
$$

where the prime indicates the derivative with respect to x evaluated at $\frac{L}{2}$. The creation energy for the excitations in the chain is given by $E = E_e + E_{el}$.

Appendix F

In this appendix we present the calculations leading to the results given in equations (2.7) through (2.9). In the first part the general outline of the procedure is presented. In the second part the on-site interaction term is treated, and in the third and fourth the nearest-neighbor and Bond-Charge repulsion terms are derived, respectively.

F.1. General Scheme.

The interaction terms will be transformed from a site to an energy representation. Once on the energy representation the expectation values are carried out using the generalized Hartree-Fock wavefunctions, as described in chapter 2. The destruction operators on site j and spin s are related to the operators for the valence and conduction band as follows (see appendix A),

$$c_{n,s} = \frac{1}{\sqrt{2N}} \sum_k e^{-ikan} [c^v_{k,s} + i(-1)^n c^c_{k,s}]. \qquad (F.1)$$

Once equation (F.1) is incorporated in the Hamiltonian, the valence and conduction band operators will be expressed in terms of the particle fields using,

$$\begin{aligned} c^v_{k,s} &= \frac{1}{\sqrt{N}} \sum_n e^{ikan} \psi^2_{n,s} \\ c^c_{k,s} &= \frac{1}{\sqrt{N}} \sum_n e^{ikan} \psi^1_{n,s}. \end{aligned} \qquad (F.2)$$

Finally, the particle fields will be elliminated in favor of the electronic amplitudes at the even and odd sites using the relations,

$$\begin{aligned}\psi^1_{n,s}(R_n) =&(-1)^n\sqrt{a}\sum_k c_{k,s}f_k(R_n)\\ \psi^2_{n,s}(R_n) =&-i(-1)^n\sqrt{a}\sum_k c_{k,s}g_k(R_n)\end{aligned} \tag{F.3}$$

where $f_k(x) \equiv u_k(x) - iv_k(x)$ and $g_k(x) \equiv u_k(x) + iv_k(x)$. At this point all quatities can be evaluated using the expression for the electronic amplitudes given in Appendix C.

F.2. On-Site Interaction.

Starting from the on-site interaction term given by

$$\mathcal{H}_U = U\sum_j n_{j,s}n_{j,s'} \tag{F.4}$$

we substitute in equations (F.1) and (A.5) to get the expression

$$\mathcal{H}_U = U\frac{1}{2N}\sum_{k,l,l'} A_{l,l',k,l+l'-k,s',s} \tag{F.5}$$

where

$$A_{l,l',k,k',s',s} \equiv a^\dagger_{ll'ss'}a_{kk'ss'} + b^\dagger_{ll'ss'}b_{kk'ss'}$$

and

$$\begin{aligned}a_{kk'ss'} \equiv& c^v_{k,s}c^v_{k',s'} - c^c_{k,s}c^c_{k',s'}\\ b_{kk'ss'} \equiv& c^c_{k,s}c^v_{k',s'} + c^v_{k,s}c^c_{k',s'}.\end{aligned}$$

Using now equation (F.2) we get for equation (F.5)

$$\mathcal{H}_U = \frac{U}{2}\sum_n \left[C^\dagger_{nnss'}C_{nnss'} + D^\dagger_{nnss'}D_{nnss'}\right] \tag{F.6}$$

where

$$\begin{aligned}C_{nn'ss'} \equiv& \psi^2_{n,s}\psi^2_{n',s'} - \psi^1_{n,s}\psi^2_{n',s'}\\ D_{nn'ss'} \equiv& \psi^1_{n,s}\psi^2_{n',s'} + \psi^2_{n,s}\psi^1_{n',s'}.\end{aligned} \tag{F.7}$$

Finally, using equation (F.3) in equation (F.6) we get

$$\mathcal{H}_U = \frac{U}{2}\sum_n a^2 \sum_{kk'll'} c^\dagger_{l',s'} c^\dagger_{l,s} c_{k,s} c_{k',s'} \left[(g^*_l g^*_{l'} + f^*_l f^*_{l'})(g_k g_{k'} + f_k f_{k'}) + (f^*_l g^*_{l'} + g^*_l f^*_{l'})(f_k g_{k'} + g_k f_{k'})\right] \tag{F.8}$$

where the $g_l(R_n)$ and the $f_l(R_n)$ have been defined in the previous section in terms of the electronic amplitudes in the odd and even sites. On taking the expectation value of equation (F.8) we obtain

$$\boxed{<\mathcal{H}_U> = 2aU \int dx \sum_{kl} n_{l\uparrow} n_{k\downarrow} \left[|u_k|^2 |u_l|^2 + |v_k|^2 |v_l|^2\right].} \tag{F.9}$$

This is equation (2.7) in a slightly different form. To explicitly account for this result in terms of the wavefunctions found in Appendix C we integrate first over k,

$$\sum_k n_{k,s} |u_k(x)|^2 = \int_{-k_f}^{0} dk \left[\frac{L}{\pi} - \frac{1}{\pi}\frac{d\phi_k}{dk}\right] |u_k(x)|^2 + \sum_i n_{i,s} |u_i(x)|^2 \tag{F.10}$$

where we separated the contribution due to the bound states from the continuum states, and used the boundary condition $kL = n\pi + \phi_k$. The wavefunctions $u_k(x)$ and $u_i(x)$ are the normalized wavefunctions. The second term in equation (F.10) is dropped because the normalized wavefunctions of the continuum are proportional to $1/\sqrt{L}$. Using the expression given in equation (D.5), we get,

$$\sum_k n_{k,s} |u_k(x)|^2 \cong \frac{k_f}{2\pi} - \frac{1}{2\pi}\sum_i f_i(k_i, x)\left[\frac{\pi}{2k_i} - \frac{1}{k_f}\right] + \frac{1}{2\pi}\sum_{i>j} g_{ij}(k_i, k_j, x)\left[\frac{\pi}{(k_i + k_j)} - \frac{1}{k_f}\right] + \sum_i n_{i,s} |u_i(x)|^2 \tag{F.11}$$

where the approximations

$$\int_{-k_f}^{0} dk \frac{1}{(k_i^2 + k^2)} \cong \frac{\pi}{2k_i} - \frac{1}{k_f}$$

and

$$\int_{-k_f}^{0} dk \frac{k_i k_j + k^2}{(k_i^2 + k^2)(k_j^2 + k^2)} \cong \frac{\pi}{(k_i + k_j)} - \frac{1}{k_f}$$

have been taken. Substituting equation (F.11) in equation (F.9) and subtracting the contribution from the undoped system

$$<\mathcal{H}_U>_o = Ua\frac{k_f^2 L}{\pi^2}$$

we get

$$\begin{aligned}<\mathcal{H}_U> - <\mathcal{H}_U>_o = 2Ua\Big\{ \int dx \sum_{ij} n_{i\uparrow} n_{j\downarrow} A_{k_i}^2 A_{k_j}^2 \big[u_i^r(x,\delta)^2 u_j^r(x,\delta)^2 \\ + u_i^r(-x,\delta)^2 u_j^r(-x,\delta)^2\big] \\ + \int dx\big[(G + \frac{k_f}{2\pi})P_e + (H + \frac{k_f}{2\pi})P_o + E\big]\Big\}\end{aligned} \tag{F.12}$$

where

$$\begin{aligned}G &= -\frac{1}{2\pi}\sum_i f_i(k_i,x)(\frac{\pi}{2k_i} - \frac{1}{k_f}) + \frac{1}{2\pi}\sum_{i>j} g_{ij}(k_i,k_j,x)\Big(\frac{\pi}{(k_i+k_j)} - \frac{1}{k_f}\Big) \\ P_e &= G + \sum_i A_{k_i}^2 |u_i^r(x,\delta)|^2 (n_{i\uparrow} + n_{i\downarrow}) \\ H &= -\frac{1}{2\pi}\sum_i M_i(k_i,x)(\frac{\pi}{2k_i} - \frac{1}{k_f}) + \frac{1}{2\pi}\sum_{i>j} N_{ij}(k_i,k_j,x)\Big(\frac{\pi}{(k_i+k_j)} - \frac{1}{k_f}\Big) \\ P_o &= H + \sum_i A_{k_i}^2 |u_i^r(-x,\delta)|^2 (n_{i\uparrow} + n_{i\downarrow}) \\ E &= \frac{k_f}{2\pi}[G+H]\end{aligned}$$

and

$$\begin{aligned}f_i(k_i,x) &= 4k_i^2 u_i^r(x,\delta) e^{-k_i x + 2\alpha_e^i}\big[1 - u_i^r(x,\delta)e^{-k_i x + 2\alpha_e^i}\big] \\ M_i(k_i,x) &= 4k_i^2 u_i^r(x,-\delta) e^{-k_i x + 2\alpha_o^i}\big[1 - u_i^r(x,-\delta)e^{-k_i x + 2\alpha_o^i}\big] \\ g_{ij}(k_i,k_j,x) &= 8k_i k_j u_i^r(x,\delta) u_j^r(x,\delta) e^{-(k_i+k_j)x + 2(\alpha_e^i + \alpha_e^j)} \\ N_{ij}(k_i,k_j,x) &= 8k_i k_j u_i^r(x,-\delta) u_j^r(x,-\delta) e^{-(k_i+k_j)x + 2(\alpha_o^i + \alpha_o^j)}.\end{aligned}$$

The normalization factors A_{k_i} for the bound states are determined using equation (2.11). For the actual calculations these normalization factors were found without approximations by numerically integrating each individual wavefunction in (2.11).

F.3. Nearest-Neighbor Interaction.

The nearest-neighbor repulsive interaction can similarly be expressed in terms of the electronic odd and even amplitudes. Thus,

$$\begin{aligned}\mathcal{H}_V =& V\sum_j n_j n_{j+1} \\ =& V\sum_j\sum_{s,s'} c^\dagger_{j+1,s'}c^\dagger_{j,s}c_{j,s}c_{j+1,s'}\end{aligned} \tag{F.13}$$

becomes upon using (F.1) and (A.5),

$$\mathcal{H}_V = V\sum_{s,s'}\frac{1}{2N}\sum_{kll'} e^{ia(k-l)}A_{l,l',k,l+l'-k,s,s'} \tag{F.14}$$

where

$$A_{ll'kk'ss'} \equiv a^\dagger_{ll'ss'}a_{kk'ss'} + b^\dagger_{ll'ss'}b_{kk'ss'}$$

and

$$\begin{aligned}a_{kk'ss'} \equiv& c^v_{k,s}c^v_{k',s'} + c^c_{k,s}c^c_{k',s'} \\ b_{kk'ss'} \equiv& c^c_{k,s}c^v_{k',s'} - c^v_{k,s}c^c_{k',s'}.\end{aligned}$$

Substituting (F.2) and (F.3) we get

$$\begin{aligned}\mathcal{H}_V =& \sum_{ss'}\frac{V}{2}\sum_n a^2\sum_{kk'll'} c^\dagger_{l',s'}c^\dagger_{l,s}c_{k,s}c_{k',s'}\left[(g^*_l g^*_{l'} - f^*_l f^*_{l'})(g_k g_{k'} - f_k f_{k'})\right. \\ &\left. + (f^*_l g^*_{l'} - g^*_l f^*_{l'})(f_k g_{k'} - g_k f_{k'})\right].\end{aligned} \tag{F.15}$$

Taking the expectation value yields

$$\begin{aligned}<\mathcal{H}_V>=& 4aV\int dx\sum_{kl}\left[|u_k(x)|^2|v_l(x)|^2(n_{l\uparrow}+n_{l\downarrow})(n_{k\uparrow}+n_{k\downarrow})\right. \\ &\left. - \Re(v_k(x)u^*_k(x)u_l(x)v^*_l(x))(n_{l\uparrow}n_{k\uparrow}+n_{l\downarrow}n_{k\downarrow})\right].\end{aligned} \tag{F.16}$$

Equation (F.16) is the same as equation (2.8). To put equation (F.16) in a form containing the explicit form of the wavefunctions we first calculate, using equation (D.3), the term given by $\sum_{kl} \Re(v_k u_k^* u_l v_l^*)(n_{l\uparrow} n_{k\uparrow} + n_{l\downarrow} n_{k\downarrow})$. But first we do

$$\sum_{kl} \Re(v_k u_k^* u_l v_l^*) n_{ls} n_{ks} = \sum_k v_k u_k^* n_{ks} \sum_l u_l v_l^* n_{ls}$$

and

$$\sum_k u_k v_k^* n_{ks} = \frac{1}{2\pi} \int_{-k_f}^{0} dk u_k v_k^* + \sum_i u_i v_i n_{i,s}$$

are considered. Using (D.3) it can be shown that

$$\begin{aligned} \int_0^{k_f} u_k(x,\delta) v_k^*(x,\delta) dk =& \frac{\Delta(x)}{v_f} \Big[\ln \frac{2k_f v_f}{\Delta_o} + \frac{\Delta_o^2}{4k_f^2 v_f^2} \Big] + \Delta(x) P_F \\ & - i \Big[k_f + \frac{\Delta_o^2}{2k_f v_f^2} - \frac{\Delta_o}{v_f} \Big] - i v_f P_G \end{aligned} \tag{F.17}$$

where

$$\begin{aligned} P_F \equiv& - \sum_i f_i(k_i, x) F_i + \sum_{i>j} \big[X_{ij} F_i + Y_{ij} F_j \big] \\ P_G \equiv& - \sum_i f_i(k_i, x) G_i + \sum_{i>j} \big[X_{ij} G_i + Y_{ij} G_j \big] \\ F_i \equiv& \frac{1}{k_i |\epsilon_i|} \cos^{-1} \frac{k_i v_f}{\Delta_o} \\ G_i \equiv& \frac{1}{|\epsilon_i|} \left\{ \tanh^{-1} \Big(\frac{|\epsilon_i|}{\Delta_o} \Big) - \tanh^{-1} \left[\frac{|\epsilon_i|}{\sqrt{\Delta_o^2 + k_f^2 v_f^2}} \right] \right\} \\ X_{ij} \equiv& \frac{g_{ij} k_i}{(k_i + k_j)} \\ Y_{ij} \equiv& \frac{g_{ij} k_j}{(k_i + k_j)}. \end{aligned}$$

The f_i and g_{ij} where defined in Appendix D. Now, putting together all the previous results we get

$$\begin{aligned} \sum_{kl} \Re(v_k u_k^* u_l v_l^*)(n_{l\uparrow} n_{k\uparrow} + n_{l\downarrow} n_{k\downarrow}) =& \frac{1}{2\pi^2} \big[A_1^2 + A_2^2 \big] \\ & - \frac{A_1}{\pi} \sum_i u_i v_i (n_{i\uparrow} + n_{i\downarrow}) + \sum_{ij} u_i v_i (n_{i\uparrow} n_{j\uparrow} + n_{i\downarrow} n_{j\downarrow}) \end{aligned} \tag{F.18}$$

where

$$\begin{aligned} A_1 =&\Delta(x)[C_1 + P_F] \\ A_2 =&C_2 + v_f p_G \\ C_1 =&k_f\Big[\ln\frac{2k_f v_f}{\Delta_o} + \frac{\Delta_o^2}{4k_f^2 v_f^2}\Big] \\ C_2 =&k_f + \frac{\Delta_o^2}{2k_f v_f^2} - \frac{\Delta_o}{v_f}. \end{aligned} \tag{F.19}$$

Subtracting from the total contribution the one coming from the undoped system

$$<\mathcal{H}_V>_o = 4aV\int dx\Big[\frac{k_f^2}{\pi^2} - \frac{1}{2\pi^2}(\Delta_o^2 C_1^2 + C_2^2)\Big]$$

we finally get for the contribution to the creation energy from the nearest-neighbor repulsive energy

$$\boxed{<\mathcal{H}_V> - <\mathcal{H}_V>_o = 4aV\int dx\big\{d_1(x,\delta) + d_2(x,\delta) + d_3(x,\delta)\big\}} \tag{F.20}$$

where

$$\begin{aligned} d_1(x,\delta) =&\frac{k_f}{\pi}\sum_s (T_s^e(x) + T_s^o(x)) + \sum_{ss'} T_s^e(x) T_{s'}^o(x) \\ d_2(x,\delta) =&-\frac{1}{2\pi^2}[B_1(x) + B_2(x)] + \frac{A_1}{\pi}\sum_i u_i(x)v_i(x)(n_{i\uparrow} + n_{i\downarrow}) \\ d_3(x,\delta) =&-\sum_{ij} u_i(x)v_i(x)u_j(x)v_j(x)\big[n_{i\uparrow}n_{j\uparrow} + n_{i\downarrow}n_{j\downarrow}\big] \end{aligned}$$

and subsequently

$$\begin{aligned} T_s^e(x) =&G + \sum_i n_{is} u_i^2(x,\delta) \\ T_s^o(x) =&H + \sum_i n_{is} v_i^2(x,\delta) \\ B_1 =&C_1^2[\Delta(x)^2 - \Delta_o^2] + \Delta(x)[\Delta(x)C_1 P_F + (C_1 + P_F)\Delta(x)P_F] \\ B_2 =&v_f P_G(2C_2 + v_f P_G). \end{aligned}$$

Further definitions are given in the previous section.

F.4. Bond-Charge Interaction.

The bond-charge repulsion term is given by

$$\mathcal{H}_W = W \sum_j (B_{j,j+1})^2 \qquad (F.21)$$

where $B_{j,j+1} = \sum_s (c^\dagger_{j,s} c_{j+1,s} + c^\dagger_{j+1,s} c_{j,s})$. Expanding the square we have,

$$\begin{aligned}\mathcal{H}_W =& W \sum_j \sum_{ss'} \left[c^\dagger_{j,s'} c^\dagger_{j,s} c_{j+1,s} c_{j+1,s'} + c^\dagger_{j+1,s'} c^\dagger_{j+1,s} c_{j,s} c_{j,s'} \right. \\ & \left. + c^\dagger_{j+1,s'} c^\dagger_{j,s} c_{j+1,s} c_{j,s'} + c^\dagger_{j,s'} c^\dagger_{j+1,s} c_{j,s} c_{j+1,s'} \right] \qquad (F.22) \\ & + W \sum_j \sum_s \left[c^\dagger_{j,s} c_{j,s} + c^\dagger_{j+1,s} c_{j+1,s} \right]\end{aligned}$$

Substituting from (F.1) through (F.3) for each one of the terms we have

$$\begin{aligned}\sum_j \left[c^\dagger_{j,s'} c^\dagger_{j,s} c_{j+1,s} c_{j+1,s'} + c^\dagger_{j+1,s'} c^\dagger_{j+1,s} c_{j,s} c_{j,s'} \right] =& a^2 \sum_n \sum_{kk'll'} c^\dagger_{k',s'} c^\dagger_{k,s} c_{l,s} c_{l',s'} \\ \times \left[(g^*_k g^*_{k'} + f^*_k f^*_{k'})(g_l g_{l'} + f_l f_{l'}) - (f^*_k g^*_{k'} + g^*_k f^*_{k'})(f_l g_{l'} + g_l f_{l'}) \right] & \qquad (F.23) \\ \sum_j \left[c^\dagger_{j+1,s'} c^\dagger_{j,s} c_{j+1,s} c_{j,s'} + c^\dagger_{j,s'} c^\dagger_{j+1,s} c_{j,s} c_{j+1,s'} \right] =& a^2 \sum_n \sum_{kk'll'} c^\dagger_{k',s'} c^\dagger_{k,s} c_{l,s} c_{l',s'} \\ \times \left[(g^*_k g^*_{k'} - f^*_k f^*_{k'})(g_l g_{l'} - f_l f_{l'}) - (f^*_k g^*_{k'} - g^*_k f^*_{k'})(f_l g_{l'} - g_l f_{l'}) \right] & \qquad (F.24) \\ \sum_j \left[c^\dagger_{j,s} c_{j,s} + c^\dagger_{j+1,s} c_{j+1,s} \right] = 2a \sum_n \sum_{k,k'} c^\dagger_{k,s} c_{k,s'} (g^*_k g_{k'} + f^*_k f_{k'}) & \qquad (F.25)\end{aligned}$$

Substituting equations (F.23) through (F.25) into equation (F.22) and upon taking expectation values we get

$$\boxed{\begin{aligned}<\mathcal{H}_W> = & 2W \int dx \sum_k (|u_k(x)|^2 + |v_k(x)|^2)(n_{k\uparrow} + n_{k\downarrow}) \\ & + 8aW \int dx \sum_{kl} \left[2\Im\left[v_k(x) u^*_k(x)\right] \Im\left[v_l(x) u^*_l(x)\right] (n_{k\uparrow} + n_{k\downarrow})(n_{l\uparrow} + n_{l\downarrow}) \right. \\ & \left. + \left\{ \Re\left[v_k(x) u^*_k(x) v_l(x) u^*_l(x)\right] - |u_k(x)|^2 |v_l(x)|^2 \right\} (n_{k\uparrow} n_{l\uparrow} + n_{k\downarrow} n_{l\downarrow}) \right]\end{aligned}}$$

$$(F.26)$$

In the same way as was done in the previous sections we can show that

$$\sum_{kl} \Re\big[v_k(x)u_k^*(x)v_l(x)u_l^*(x)\big](n_{k\uparrow}n_{l\uparrow}+n_{k\downarrow}n_{l\downarrow}) = \frac{1}{2\pi^2}(A_1^2 - A_2^2)$$
$$-\frac{A_1}{\pi}\sum_i u_i(x)v_i(x)(n_{i\uparrow}+n_{i\downarrow}) + \sum_{ij} u_i(x)v_i(x)u_j(x)v_j(x)(n_{i\uparrow}n_{j\uparrow}+n_{i\downarrow}n_{j\downarrow}) \tag{F.27}$$

and also

$$\sum_{kl} \Im\big[v_k(x)u_k^*(x)\big]\Im\big[v_l(x)u_l^*(x)\big]n_{ks}n_{ls'} = \frac{A_2^2}{4\pi^2}. \tag{F.28}$$

Subtracting the expectation value of equation (F.21) for the undoped system

$$<\mathcal{H}_W>_o = 2WN + 8aWL\Big[\frac{2C_2^2}{\pi^2} + \frac{1}{2\pi^2}(\Delta_o^2 C_1^2 - C_2^2) - \frac{k_f^2}{2\pi^2}\Big] \tag{F.29}$$

we get for the creation energy contribution from the bond-charge term

$$\boxed{\begin{aligned}<\mathcal{H}_W> - <\mathcal{H}_W>_o = 2W\Big[\sum_i (n_{i\uparrow}+n_{i\downarrow})\Big] \\ + 8aW\int dx\big[h_1(x)+h_2(x)-d_3(x)\big]\end{aligned}} \tag{F.30}$$

where

$$\begin{aligned} h_1(x) &= -\frac{k_f}{2\pi}\sum_s (T_s^e(x)+T_s^o(x)) - \sum_s T_s^e(x)T_s^o(x) \\ h_2(x) &= \frac{1}{2\pi^2}(B_1(x)+3B_2(x)) - \frac{A_1}{\pi}\sum_i u_i(x)v_i(x)(n_{i\uparrow}+n_{i\downarrow}) \end{aligned} \tag{F.31}$$

Appendix G

The calculation of the magnetic susceptibility starts assuming a shift in the density of states of $g(\epsilon) \rightarrow g(\epsilon \pm \mu_B B)$ in the presence of a magnetic field B. We can count then the number of electrons with spin up and down. This is simply given by

$$\begin{aligned} N_+ =& \frac{1}{2}\int_{-\epsilon_F+\mu_B}^{\infty} d\epsilon f(\epsilon) g(\epsilon - \mu_B B) \\ =& \frac{1}{2}\int_{-\epsilon_F}^{\infty} d\epsilon g(\epsilon) f(\epsilon + \mu_B B) \qquad (G.1) \\ N_- =& \frac{1}{2}\int_{-\epsilon_F-\mu_B}^{\infty} d\epsilon f(\epsilon) g(\epsilon + \mu_B B) \\ =& \frac{1}{2}\int_{-\epsilon_F}^{\infty} d\epsilon g(\epsilon) f(\epsilon - \mu_B B) \qquad (G.2) \end{aligned}$$

and the Magnetization is given by

$$\begin{aligned} M =& \mu_B (N_- - N_+) \\ =& \frac{\mu_B}{2}\int_{-\epsilon_F}^{\infty} d\epsilon g(\epsilon)[f(\epsilon - \mu_B B) - f(\epsilon + \mu_B B)]. \end{aligned} \qquad (G.3)$$

Taking the limit of $k_B T >> \mu_B B$ we approximate the magnetization as

$$M \cong \mu_B^2 B\beta \int_{-\epsilon_F}^{\epsilon_F} d\epsilon g(\epsilon) f(\epsilon)[1 - f(\epsilon)] \qquad (G.4)$$

and the magnetic susceptibility is given by $\chi = \partial M / \partial B$ as

$$\chi = \frac{\mu_B^2}{N k_B T}\int_{-\epsilon_F}^{\epsilon_F} d\epsilon g(\epsilon) f(\epsilon)[1 - f(\epsilon)] \qquad (G.5)$$

where $\mu_B^2 = 3.24 \times 10^{-5}$ in order to get χ in units of emu/mol. For the density of states we will use

$$g(\epsilon) = \frac{2}{\pi v_f}\Big[L - 2\sum_i \frac{v_f\sqrt{\Delta_o^2 - \omega_i^2}}{\epsilon^2 - \omega_i^2}\Big]\frac{|\epsilon|}{\sqrt{\epsilon^2 - \Delta_o^2}}\theta(|\epsilon| - \Delta_o) + 2\sum_i \delta(\epsilon - \omega_i) \qquad (G.6)$$

where the boundary condition $kL = n\pi + \phi_k$ and $\phi_k = 2\sum_i \tan^{-1}(k/k_i)$ were used. Substituting then equation (G.6) into equation (G.5) we get for the magnetic susceptibility

$$\boxed{\chi \cong \frac{\mu_B^2 \beta}{2N} \sum_i \left\{ \cosh^{-2}\left[\frac{\beta}{2}(\omega_i - \mu)\right] + \cosh^{-2}\left[\frac{\beta}{2}(\omega_i + \mu)\right] \right\}} \qquad (G.7)$$

where we have dropped the contribution coming from the continuum states for being too far from the Fermi level μ.

Appendix H

The results presented in chapter 2 regarding the on-set of the magnetic susceptibility are clearly dependent on the particular length of the chain used. This fact does not seem reasonable at first because all calculations are parametrized by the concentration and not by the length of the chain. However, the length of the chain L enters into the problem in a particular way and here we account for this dependence using a very simple description and qualitative arguments.

Suppose the solitons stay a distance d away from each other and the solitons closest to the extremes of the chain stay a distance ξ from each end of the chain. The purpose now is to calculated d as a function of the length of the chain. It is clear that if $\xi = d/2$, then for a given concentration p ($100 \times p =$ dopant percent) there is no dependence of d on L.

The following relation can be written down for N solitons (N even)

$$(N-1)d + 2\xi = L. \tag{H.1}$$

These solitons would be paired in soliton-antisoliton pairs to satisfy the topological constraints. If $\xi = d/2$ then $d = L/N \equiv 1/p$, therefore resulting in a constant d. However, from all the graphs of the order parameter presented in chapter 2 we can only conclude that ξ is independent of d. Therefore, now we take ξ as an independent parameter from d. Solving (H.1) we get

$$\begin{aligned} d =& \frac{L-2\xi}{N-1} \\ =& \frac{1}{p} + \frac{1/p - 2\xi}{pL-1}. \end{aligned} \tag{H.2}$$

As long as $1/p - 2\xi < 0$, then d is an increasing function of L, at fixed p. This means that for longer chains, d gets bigger. This in turn means that the interaction energy is lower (because the inter-soliton distance d is bigger) and the levels close more slowly. Remember that the more the solitons interact with each other, the farther the levels will be thus closing the gap more rapidly. The above condition, namely

$$\xi > \frac{1}{2p} \tag{H.3}$$

is easily met at $p = .06$ for the cases analyzed in chapter 2.

In conclusion, the rate of closure of the levels will be smaller for bigger lengths of chains. This result comes directly from the fact that the inter-solitonic distances are much more sensitive to L than the distances from the solitons to the ends of the chain.

Appendix I

In the present appendix a list of commutators and derivatives of the operators used in chapter 3 is given. For convenience we define the operator

$$A_{ks} = \chi_l^\dagger \psi_{ks} e^{ikx_l} \tag{I.1}$$

where $x_l = la$ and $\chi_l^\dagger$ is defined by equation (3.4). Also,

$$\tilde{B}_k = v_f k \sigma_3 + \Delta_o \sigma_1 \tag{I.2}$$

where $\tilde{B}_k^2 \equiv \epsilon_k^2 = v_f^2 k^2 + \Delta_o^2$ defines the energy dispersion relation. A useful relation that can easily be checked is

$$\chi_l^\dagger (v_f k \sigma_3 + \Delta_o \sigma_1) \chi_l = 0. \tag{I.3}$$

For the anticommutators we have

$$\{A_{ks}, d_s\} = 0 \tag{I.4}$$

and all combinations of them and their conjugates. Also,

$$\begin{aligned} \{d_s, \psi_k\} &= 0 \\ \{\psi_{ks}, \psi_{k's'}^\dagger\} &= \delta_{ss'}\delta_{kk'} \\ \{A_{ks}, A_{k's'}^\dagger\} &= \delta_{ss'}\delta_{kk'} \end{aligned} \tag{I.5}$$

and of course

$$\{d_s, d_{s'}^\dagger\} = \delta_{ss'} \tag{I.6}$$

with other combinations equal to zero. The following commutators are used,

$$
\begin{aligned}
[d_s, n_{ds'}] &= \delta_{ss'} d_s \\
[n_{d\uparrow} n_{d\downarrow}, d_s] &= [d_s^\dagger, n_{d\uparrow} n_{d\downarrow}] \\
&= -n_{d\bar{s}} d_s \\
[A_{ks}, n_{ds'}] &= 0 \\
[A_{ks'}^\dagger d_{s'}, d_s] &= 0 \\
[d_{s'}^\dagger A_{ks'}, d_s] &= -\delta_{ss'} A_{ks'} \\
[A_{k's'}^\dagger d_{s'}, d_{\bar{s}}^\dagger] &= \delta_{s'\bar{s}} A_{k's'}^\dagger \\
[d_{s'}^\dagger A_{ks'}, n_{d\bar{s}}] &= -\delta_{\bar{s}s'} d_{s'}^\dagger A_{ks'} \\
[A_{ks'}^\dagger d_{s'}, n_{d\bar{s}}] &= \delta_{\bar{s}s'} A_{ks'}^\dagger d_{s'} \\
[d_{s'}^\dagger A_{k's'}^\dagger, A_{ks}] &= 0 \\
[d_{s'} A_{k's'}^\dagger, A_{ks}] &= \delta_{ss'} \delta_{kk'} d_{s'}.
\end{aligned}
\tag{I.7}
$$

Between the A's and the individual spinors

$$
\begin{aligned}
\{A_{ks}, \psi_{k's'}^\dagger\} &= \delta_{ss'} \delta_{kk'} \chi_l^\dagger e^{ikx_l} \\
\{A_{ks}, \psi_{k's'}\} &= 0
\end{aligned}
\tag{I.8}
$$

and defining $D_{ks} \equiv \psi_{ks}^\dagger \tilde{B}_k \psi_{ks}$ and $P_{ks} \equiv \chi_l^\dagger \tilde{B}_k \psi_{ks} e^{ikx_l}$ we get the following

$$
\begin{aligned}
[D_{k's'}, A_{ks}] &= -\delta_{ss'} \delta_{kk'} P_{k's'} \\
[D_{k's'}, A_{ks}^\dagger] &= \delta_{ss'} \delta_{kk'} P_{k's'}^\dagger \\
\{P_{k'\bar{s}}, A_{ks}^\dagger\} &= 0.
\end{aligned}
\tag{I.9}
$$

Therefore, for the equations of motion of each individual operator we get

$$
\begin{aligned}
\frac{d}{d\tau}d_s &= -E_d d_s - V\sum_k A_{ks} - U n_{d\bar{s}} d_s \\
\frac{d}{d\tau}d_{\bar{s}}^\dagger &= E_d d_{\bar{s}}^\dagger + V\sum_k A_{k\bar{s}}^\dagger + U n_{ds} d_{\bar{s}}^\dagger \\
\frac{d}{d\tau}n_{d\bar{s}} &= V\sum_k [A_{k\bar{s}}^\dagger d_{\bar{s}} - d_{\bar{s}}^\dagger A_{k\bar{s}}] \\
\frac{d}{d\tau}\psi_{ks} &= -\tilde{B}_k \psi_{ks} - V d_s \chi_l e^{-ikx_l} \\
\frac{d}{d\tau}\psi_{k's'}^\dagger &= \psi_{k's'}^\dagger \tilde{B}_k + V d_{s'}^\dagger \chi_l^\dagger e^{ik'x_l} \\
\frac{d}{d\tau}A_{ks} &= -P_{ks} - V d_s \\
\frac{d}{d\tau}A_{ks}^\dagger &= P_{ks}^\dagger + V d_s^\dagger \\
\frac{d}{d\tau}P_{ks} &= -\epsilon_k^2 A_{ks} \\
\frac{d}{d\tau}P_{ks}^\dagger &= \epsilon_k^2 A_{ks}^\dagger .
\end{aligned}
\tag{I.10}
$$

Appendix J

In the following appendix we give a brief account of the Kondo Hamiltonian, the Kondo effect in normal metals, and the relation between the Kondo and Anderson Hamiltonian.

Formally, the Kondo effect is a consequence of the fact that at low temperatures ($T < T_k$, where T_k is the Kondo temperature), the local spin of a magnetic impurity dissolved in a non-magnetic matrix does not have the same energy when its spin is either in the up or down configuration (as it does at high temperatures). Physically, at this low temperature each local spin becomes "locked" into a collective state with the conduction band spins. This collective state has a binding energy which must be overcome during a spin-flip process. For lower temperatures this spin-flip becomes frozen out and the Kondo effect saturates. The collective state can be viewed as a screening effect not from a single electron in the conduction band, but from a linear combination of conduction states. It is a many particle entity. Its first formal description comes from ref. 1. The collective state can be written as either a linear combination of hole states or of electron states. It consists of putting one electron above the Fermi level and leaving behind a hole.

The Kondo temperature, T_k, defined by $k_B T_k = W e^{-1/2g(0)|J|}$ is similar to the change in energy in the ground state due to the presence of the collective state. A general definition is that the change in ground state energy defines an energy scale that also defines a characteristic temperature. T_k is also very close to the T at which the Kondo effect becomes important in the resistivity.

Exact solutions to the Kondo Hamiltonian have been given in references 2 and 3. In the following we give a brief and "dirty" account of the Kondo effect using the Kondo Hamltonian. First we consider that the interaction between the conduction electrons and the magnetic ion consists of a spin-dependent and a spin-independent part. The latter can be represented by $V(r)$ and may resemble a Coulomb potential. The spin-dependent part is due to an exchange interaction of the form

$$\mathcal{H} = -J(r)\vec{\sigma} \cdot \vec{S} \tag{J.1}$$

where $J(r)$ is the exchange parameter, $\vec{\sigma}$ is the conduction electron spin, and $\vec{S}$ the spin operator for the localized moment. $J(r)$ has a range similar to the radius of the ion and has an appreciable value only where the wavefunctions of the d- or f-electron that give rise to the magnetic properties of the ion have significant amplitudes. This exchange interaction between the electrons and ion is a consequence of the electrostatic Coulomb interaction between the appropriate electrons; it depends on the magnetic states of the electron and ion because these determine through their symmetry properties and the Pauli exclusion principle the allowed spatial configurations of the electrons. Typical values of the exchange coupling constant for metals are of the order of .2eV.

The scattering of the conduction electrons by the localized moment can be of an elastic or inelastic nature. Consider first the elastic collisions. Suppose the ion is in a spin state m_s and the electron has $\sigma = 1$, then the total potential is $V(r) - m_s J(r)$. The Scattering probability is proportional to

$$(\int \psi^*_{k'}[V(r) - m_s J(r)]\psi_k d\tau)^2 = \overline{V}^2 + m_s^2\overline{J}^2 - 2m_s\overline{JV} \tag{J.2}$$

with no spin flip. $\overline{V}$ and $\overline{J}$ are the corresponding Fourier transforms for the space-dependent counterparts. For $\sigma = -1$ equation (J.2) gives

$$(\int \psi^*_{k'}[V(r) - m_s J(r)]\psi_k d\tau)^2 = \overline{V}^2 + m_s^2\overline{J}^2 + 2m_s\overline{JV}. \tag{J.3}$$

Note that they depend on m_s and that they are different for each spin configuration.

Consider now inelastic scatterings between the conduction electrons and the localized moment. Spin-flips are now allowed and for each conduction electron spin flip there is a corresponding change in m_s in order to conserve total spin angular momentum in the z-axis. Then, for an electronic spin-flip of $\pm 1/2 \rightarrow \mp 1/2$ (with an incurring energy change of $\pm \mu_B g H_o$) there is a change in the localized moment given by $m_s \rightarrow m_s \pm 1$ (with an incurring energy change of $\mp \mu_B g H_o$). The field H_o is the field by which the ions interact with each other in a Weiss-like model. H_o does not affect the conduction electrons. Note that the spin-up electron always increases its energy and a spin-down electron always decreases it.

The matrix element of the transtion is

$$<S; m_s + 1; -\frac{1}{2}| - J\vec{\sigma} \cdot \vec{S}|S; m_s; \frac{1}{2}> = J[(S - m_s)(S + m_s + 1)]^{1/2} \qquad (J.4)$$

and the other transition is

$$= J[(S - m_s + 1)(S + m_s)]^{1/2} \qquad (J.5)$$

where again the different transitions have different probabilities.

In order to see the Kondo effect, it is enough to consider up to second order in the scattering. This second order consideration takes into account the process where the electron is scattered into an intermediate state by the localized moment which likewise makes a transition into its intermediate state. Then the impurity is restored to its original state and the conduction electron is scattered to its final state. Consider then the electronic wavefunction

$$\psi_k = \phi_k + \sum \frac{V_{nk}\phi_n}{\epsilon_k - \epsilon_n} \qquad (J.6)$$

where ϕ_k is the unperturbed wavefunction. We want the matrix element

$$| <\phi_{k'}|V|\psi_k> |^2 = |V_{kk'}|^2 + (V_{kk'} \sum_n \frac{V_{k'n}V_{nk}}{\epsilon_k - \epsilon_n} + c.c.) \qquad (J.7)$$

so that the probability of scattering from state a to state b is

$$P_{a \rightarrow b} \sim \frac{2\pi}{\hbar}[V_{ab}V_{ba} + \sum_{c \neq a} \frac{V_{ab}V_{bc}V_{ca}}{\epsilon_a - \epsilon_c} + c.c.]. \qquad (J.8)$$

This probability is composed of the probability to go directly from $a \rightarrow b$ plus the probability of going through all possible intermediate states c by $a \rightarrow c \rightarrow b$. It can be shown that the term $V_{ab}V_{ba}$ is temperature independent. The scattering to c may entail a spin flip of the conduction electron with the compensated spin change of the ion. In addition, only processes in which $a \rightarrow c \rightarrow a$ prove to give appreciable contribution.

For the spin-flip process there are two possibilities. The first is to have an electronic transition $k_\uparrow \rightarrow q_\downarrow$, $q_\downarrow \rightarrow k'_\uparrow$ with an accompanying ion transition of $m_s \rightarrow m_s+1$, $m_s+1 \rightarrow m_s$, where q_s is an intermediate electronic state. The second possibility is to have $q_\downarrow \rightarrow k'_\uparrow$, $k'_\uparrow \rightarrow q_\downarrow$ with the accompanying $m_s \rightarrow m_s - 1$, $m_s - 1 \rightarrow m_s$. In the first process an electron is scattered by the impurity to c and then back to a. In the second, an electron is scattered to its final state and then another electron is scattered into the vacant state so created. Because the probabilities

$$\begin{aligned} P_{m_s+1} &= J^2(S - m_s)(S + m_s + 1) \\ P_{m_s-1} &= J^2(S + m_s)(S - m_s + 1) \end{aligned} \tag{J.9}$$

are different, by using (J.4) and (J.5), the two processes will have different weights. The total probability is given by

$$\sum_q \frac{A(1 - f(q)}{\epsilon_k - \epsilon_q} P_{m_s+1} - \sum_q \frac{Af(q)}{\epsilon_q - \epsilon_{k'}} P_{m_s-1}$$

where the first process is weighed by $1 - f(q)$ because q must be empty, and the second process is weighed by $f(q)$ for it to be occupied. The constant A contains the coupling constant J, among other things. The minus sign comes from the interchange in the wavefunctions of the k' and q states. Using $k' = k$ we get

$$\sum_q \frac{AP_{m_s+1}}{\epsilon_k - \epsilon_q} - \sum_q Af(q) \frac{(P_{m_s+1} - P_{m_s-1})}{\epsilon_k - \epsilon_q}. \tag{J.10}$$

For simplicity we now take the $T = 0$ limit and the dispersion relation $\epsilon_k = \hbar^2 k'^2/2m$ to find

$$-\sum_q \frac{f(q)}{\epsilon_k - \epsilon_q} = -\frac{3zNm}{k_f^3 \hbar^2} \int_0^{k_f} \frac{q^2 dq}{k^2 - q^2} \tag{J.11}$$

where zN is the number of conduction electrons. Equation (J.11) yields

$$= \frac{3zN}{2\epsilon_f}\left(1 + \frac{k}{2k_f}\ln\left|\frac{k-k_f}{k+k_f}\right|\right). \qquad (J.12)$$

For $T \neq 0$ and $kT << kT_f$, we approximate $k - k_f \sim (\frac{kT}{\epsilon_f})k_f$ as the fraction of thermally excited electrons. Substituting, we get for the T-dependent part of the scattering

$$\frac{3NzA}{4\epsilon_f}(P_{m_s,+1} - P_{m_s,-1})\ln\frac{kT}{2\epsilon_f}$$

where $k \sim k_f$ so that $k + k_f \sim 2k_f$. Including transition from $k_\downarrow$ to $k'_\downarrow$, $k_\downarrow$ to $k'_\uparrow$, and $k_\uparrow$ to $k'_\downarrow$ (all involve $\ln T$) we get for the resistivity

$$\rho = \rho_o - \rho_K \ln T. \qquad (J.13)$$

The negative in front of the $\ln T$ term comes because we need $J < 0$ in order to have the collective state. For $J > 0$ the collective state is supressed because the conduction electrons and the localized moment form a singlet state in an antiferromagnetic spin configuration.

Another model used that yields equivalent results is the Anderson model (equation 3.2). The transformation given in reference 4 shows that the Anderson model has some terms that are similar to the Kondo model. The Kondo model treats the local spin as a separate entity while the Anderson model treats it as just another electron. It can undergo exchange and other processes with the conduction electrons. In the Anderson model, however, the spin localized in the impurity atom does not get flipped. Because of the hybridization term, a local spin that is down can become a conduction state with spin down, and wander away. Later, a different conduction electron with spin up can come and reside in the local orbital. This process appears as a local down to up spin flip, with a companion up to down spin flip in the conduction electrons. Now one can see the important role of the electron-electron interaction U. The spin-flip is carried out in two steps; the departure of the old spin and the arrival of the new local electron. If $U = 0$ these two steps are totally independent and can occur in any order. However, once $U > 0$ then the two steps become correlated because it is energetically unfavorable to have up and down spin electrons both on the local orbital. Then the two steps become sequential.

The Anderson Model is sufficiently similar to the Kondo model that it also has a characteristic energy which can be related to an effective temperature known as the Kondo temperature T_k. The Kondo resonance is believed to be a Lorentzian shape of width $T_k\pi/N_f$, where N_f is the number of f-orbitals in the impurity. The total area under the Kondo resonance is $T_k/N_f\Delta$. In the Anderson model $D(0) \sim \pi/\Delta N_f$, where D is the density of states.

References

1. K. Yosida, *Phys. Rev.*, **147**, 223 (1966).

2. N. Andrei, K. Furuya, J.H. Lowenstein, *Rev. Mod. Phys.*, **55**, 3 (1983).

3. P. Wiegmann, *J. Phys. C*, **14**, 1463 (1981).

4. J.R. Schrieffer, P.A. Wolff, *Phys. Rev.*, **149**, 491 (1966).

Appendix K

K.1. Constant Density of States.

In order to check equation (3.36) against the literature, we will take for illustration $\rho(\epsilon) = 1/2D$, i.e., a constant density of states, where D is the bandwidth. Using this $\rho(\epsilon)$ we get for equation (3.50), for large D

$$\sum_k \frac{i\omega'}{[(i\omega')^2 - \epsilon_k^2]} = -\frac{i\omega'}{2D}\int d\epsilon \frac{1}{(\epsilon - \omega' - i\alpha)(\epsilon + \omega' + i\alpha)}$$
$$= -\frac{i\pi}{2D} \qquad (K.1)$$

In order to get the quantities prescribed by equations (3.48) and (3.49) we calculate first the quantity

$$I = \int d\epsilon \frac{i\omega' i\omega + \epsilon^2}{[(i\omega')^2 - \epsilon^2][(i\omega)^2 - \epsilon^2]}$$
$$= \int d\epsilon \frac{(\omega + \epsilon)(\omega' + \epsilon) - \epsilon(i\omega' + i\omega)}{(\epsilon + \omega' + i\alpha)(\epsilon - \omega' - i\alpha)(\epsilon + \omega + i\alpha)(\epsilon - \omega - i\alpha)}$$

where we have used the fact that $i\omega' i\omega + \epsilon^2 = (\omega + \epsilon)(\omega' + \epsilon) - \epsilon(i\omega' + i\omega)$ so that

$$= \int d\epsilon \frac{1}{(\epsilon - \omega' - i\alpha)(\epsilon - \omega - i\alpha)}$$
$$- (i\omega' + i\omega)\int d\epsilon \frac{\epsilon}{(\epsilon + \omega' + i\alpha)(\epsilon - \omega' - i\alpha)(\epsilon + \omega + i\alpha)(\epsilon - \omega - i\alpha)}$$
$$I = 0 \qquad (K.2)$$

Note that in the third step of equation (K.2) the first term vanishes because both poles lie above the axis, and the second term has an odd integrand in ϵ. Similarly

$$\begin{aligned} II &= \int d\epsilon \frac{i\omega' i\omega^* + \epsilon^2}{[(i\omega')^2 - \epsilon^2][(i\omega^*)^2 - \epsilon^2]} \\ &= \int d\epsilon \frac{1}{(\epsilon - \omega' - i\alpha)(\epsilon - \omega + i\alpha)} \\ &\quad - (i\omega + i\omega^*) \int d\epsilon \frac{\epsilon}{(\epsilon + \omega' + i\alpha)(\epsilon - \omega' - i\alpha)(\epsilon + \omega - i\alpha)(\epsilon - \omega + i\alpha)} \\ II &= \frac{i\pi}{\omega' - \omega + i\alpha} \end{aligned} \tag{K.3}$$

where the second term at the second step above also vanishes.

Now equations (3.48) and (3.49) can be evaluated to be

$$\sum_k \frac{<d_s^\dagger F_{k\bar{s}}>}{[(i\omega')^2 - \epsilon_k^2]} = -\frac{V}{2D} \int d\omega f(\omega) \frac{G(d_{\bar{s}})^*}{\omega - \omega' - i\alpha} \tag{K.4}$$

and

$$\begin{aligned} \sum_{k,k'} \frac{<A_{k'\bar{s}}^\dagger F_{k\bar{s}}>}{[(i\omega')^2 - \epsilon_k^2]} &= -\frac{1}{2D} \int d\omega f(\omega) \frac{1}{\omega - \omega' - i\alpha} \\ &\quad - \frac{i\pi V^2}{4D^2} \int d\omega f(\omega) \frac{G(d_{\bar{s}})^*}{\omega - \omega' - i\alpha} \end{aligned} \tag{K.5}$$

We will only consider here the non-magnetic case where $G(d_{\bar{s}}) = G(d_s)$ and take $<n_{d\bar{s}}>=<n_d>/2$. Defining $\Delta \equiv \frac{\pi V^2}{2D}$ and

$$A(\omega') \equiv -\frac{V^2}{2D} \int d\omega f(\omega) \frac{G(d_{\bar{s}})^*}{\omega - \omega' - i\alpha} \tag{K.6}$$

we obtain using (K.1), (K.4), and (K.5) into (3.36) that

$$\boxed{G(d_s, d_s^\dagger; \omega') = \frac{1 - \frac{1}{2} <n_d> - A(\omega')}{i\omega' - E_d + i\Delta + \frac{\Delta}{\pi} \int d\omega f(\omega) \frac{1}{\omega - \omega' - i\alpha} - 2i\Delta A(\omega')}} \tag{K.7}$$

where

$$<n_d>= -\frac{2}{\pi} \int f(\omega') \mathrm{Im} G(d_s, d_s^\dagger; \omega') d\omega'. \tag{K.8}$$

Equation (K.7) is equation (16) in reference 42 of chapter 3. Thus, reducing to the expression obtained for normal metals.

K.2. Using the DOS from a 1-d chain with a Gap.

Now we will evaluate equation (3.36) using (3.5). First of all lets calculate (3.50).

$$\begin{aligned} I &\equiv \sum_k \frac{i\omega'}{[(i\omega')^2 - \epsilon_k^2]} \\ &= \frac{\omega' L}{\pi v_f} \int d\epsilon \frac{\mid \epsilon \mid}{\sqrt{\epsilon^2 - \Delta_o^2}} \frac{1}{[(i\omega')^2 - \epsilon^2]} \\ &= \frac{\omega' L}{\pi v_f} \left[- \int_{-D}^{-\Delta_o} + \int_{\Delta_o}^{D} d\epsilon \frac{\epsilon}{\sqrt{\epsilon^2 - \Delta_o^2}} \frac{1}{\omega'^2 - \epsilon^2} \right] \\ &= -\frac{2L\omega'}{\pi v_f} \frac{1}{\sqrt{\Delta_o^2 - \omega'^2}} \tan^{-1} \sqrt{\frac{D^2 - \Delta_o^2}{\Delta_o^2 - \omega'^2}} \end{aligned} \tag{K.9}$$

for $\mid \omega' \mid < \Delta_o$.

$$\begin{aligned} I &= -\frac{\omega' L}{\pi v_f} \left[- \int_{-D}^{-\Delta_o} + \int_{\Delta_o}^{D} d\epsilon \frac{\epsilon}{\sqrt{\epsilon^2 - \Delta_o^2}} \mathcal{P} \frac{1}{\epsilon + \omega'} \mathcal{P} \frac{1}{\epsilon - \omega'} \right] - i \frac{L\omega'}{v_f \sqrt{\omega'^2 - \Delta_o^2}} \\ &= -\frac{\omega' L}{\pi v_f \sqrt{\omega'^2 - \Delta_o^2}} \ln \frac{\sqrt{D^2 - \Delta_o^2} - \sqrt{\omega'^2 - \Delta_o^2}}{\sqrt{D^2 - \Delta_o^2} + \sqrt{\omega'^2 - \Delta_o^2}} - i \frac{\omega' L}{v_f \sqrt{\omega'^2 - \Delta_o^2}} \end{aligned}$$

for $\omega' > \Delta_o$, where we have used

$$\frac{1}{x + i\alpha} = \mathcal{P} \frac{1}{x} - i\pi\delta(x).$$

And, finally,

$$\begin{aligned} I = -\frac{\omega' L}{\pi v_f} \Bigg[&- \int_{-D}^{-\Delta_o} d\epsilon \frac{\epsilon}{\sqrt{\epsilon^2 - \Delta_o^2}} \frac{1}{\epsilon + \omega'} \mathcal{P} \frac{1}{\epsilon - \omega'} \\ &+ \int_{\Delta_o}^{D} d\epsilon \frac{\epsilon}{\sqrt{\epsilon^2 - \Delta_o^2}} \frac{1}{\epsilon - \omega'} \mathcal{P} \frac{1}{\epsilon + \omega'} \Bigg] + i \frac{\omega' L}{v_f} \frac{1}{\sqrt{\omega'^2 - \Delta_o^2}} \\ = -\frac{\omega' L}{\pi v_f} \frac{1}{\sqrt{\omega'^2 - \Delta_o^2}} &\ln \frac{\sqrt{D^2 - \Delta_o^2} - \sqrt{\omega'^2 - \Delta_o^2}}{\sqrt{D^2 - \Delta_o^2} + \sqrt{\omega'^2 - \Delta_o^2}} + i \frac{\omega' L}{v_f \sqrt{\omega'^2 - \Delta_o^2}} \end{aligned}$$

for $\omega' < -\Delta_o$. Also of importance will be the quantities

$$II \equiv \sum_k \frac{i\omega'^*}{i\omega'^{*2} - \epsilon_k^2}$$
$$= \frac{\omega' L}{\pi v_f} \int d\epsilon \frac{\mid \epsilon \mid}{\sqrt{\epsilon^2 - \Delta_o^2}} \frac{1}{(i\omega'^*)^2 - \epsilon^2} \qquad (K.10)$$

$$III \equiv \int d\epsilon \rho(\epsilon) \frac{i\omega' i\omega + \epsilon^2}{[(i\omega')^2 - \epsilon^2][(i\omega)^2 - \epsilon^2]} \qquad (K.11)$$

$$IV \equiv \int d\epsilon \rho(\epsilon) \frac{i\omega' i\omega^* + \epsilon^2}{[(i\omega')^2 - \epsilon^2][(i\omega^*)^2 - \epsilon^2]} \qquad (K.12)$$

The details of the calculation follow the same procedure as done above for equation (K.9). Thus, the results of all of these integrals will only be stated. The definitions

$$\frac{L}{\pi v_f} \equiv \frac{1}{\epsilon_o} \qquad (K.13)$$

$$f_1^D(\omega) \equiv \tan^{-1} \frac{\sqrt{D^2 - \Delta_o^2}}{\sqrt{\Delta_o^2 - \omega^2}} \qquad (K.14)$$

$$f_2^D(\omega) \equiv \ln \frac{\sqrt{D^2 - \Delta_o^2} - \sqrt{\omega^2 - \Delta_o^2}}{\sqrt{D^2 - \Delta_o^2} + \sqrt{\omega^2 - \Delta_o^2}} \qquad (K.15)$$

will be of use. The quantity ϵ_o has a significance of the bare effective energy per site in the chain.

Thus, we proceed to enumerate them as follows:

$$I, II = -\frac{2}{\epsilon_o} \frac{\omega'}{\sqrt{\Delta_o^2 - \omega'^2}} f_1^D(\omega') \qquad ; \text{for} \mid \omega' \mid < \Delta_o$$

$$I, II^* = -\frac{1}{\epsilon_o} \frac{\omega'}{\sqrt{\omega'^2 - \Delta_o^2}} f_2^D(\omega') \mp \frac{i\pi}{\epsilon_o} \frac{\omega'}{\sqrt{\omega'^2 - \Delta_o^2}} \qquad ; \text{for} \begin{cases} \omega' > \Delta_o \\ \omega' < -\Delta_o \end{cases}$$

$$III, IV = \frac{2}{\epsilon_o} \frac{1}{\omega - \omega'} \left[\frac{\omega}{\sqrt{\Delta_o^2 - \omega^2}} f_1^D(\omega) \right.$$
$$\left. - \frac{\omega'}{\sqrt{\Delta_o^2 - \omega'^2}} f_1^D(\omega') \right] \qquad ; \text{for} \begin{cases} \mid \omega' \mid, \mid \omega \mid < \Delta_o, \\ \text{same sign,} \\ \text{and } \omega' \neq \omega \end{cases}$$
$$= \frac{2}{\epsilon_o} \frac{1}{\Delta_o^2 - \omega'^2} \left[\frac{\sqrt{D^2 - \Delta_o^2}}{D^2 - \omega'^2} \omega'^2 \right.$$

$$+\frac{\Delta_o^2}{\sqrt{\Delta_o^2-\omega'^2}}f_1^D(\omega')\Bigg] \quad ;\text{for}\begin{cases}|\,\omega'\,|,|\,\omega\,|<\Delta_o\\ \text{and } \omega'=\omega\end{cases}$$

$$III,IV=\frac{2}{\epsilon_o}\frac{1}{\omega'-\omega}\left[\frac{\omega'}{2\sqrt{\omega'^2-\Delta_o^2}}f_2^D(\omega')-\frac{\omega}{2\sqrt{\omega^2-\Delta_o^2}}f_2^D(\omega)\right]$$

$$\pm\frac{i\pi}{\epsilon_o}\frac{1}{\omega'-\omega}\left[\frac{\omega'}{\sqrt{\omega'^2-\Delta_o^2}}(-)(+)\frac{\omega}{\sqrt{\omega^2-\Delta_o^2}}\right] \quad ;\text{for}\begin{cases}\omega',\omega>\Delta_o\\ \omega',\omega<-\Delta_o\\ \text{both } \omega'\neq\omega\end{cases}$$

$$III,IV=-\frac{2}{\epsilon_o}\frac{1}{\omega'-\omega}\left[\frac{\omega}{\sqrt{\Delta_o^2-\omega^2}}f_1^D(\omega)-\frac{\omega'}{2\sqrt{\omega'^2-\Delta_o^2}}f_2^D(\omega')\right]$$

$$\pm\frac{i\pi}{\epsilon_o}\frac{1}{\omega'-\omega}\frac{\omega'}{\sqrt{\omega'^2-\Delta_o^2}} \quad ;\text{for}\begin{cases}\omega>\Delta_o,|\,\omega\,|<\Delta_o\\ \omega'<-\Delta_o,|\,\omega\,|<\Delta_o\end{cases}$$

$$III,IV^*=-\frac{2}{\epsilon_o}\frac{1}{\omega-\omega'}\left[\frac{\omega'}{\sqrt{\Delta_o^2-\omega'^2}}f_1^D(\omega')-\frac{\omega}{2\sqrt{\omega^2-\Delta_o^2}}f_2^D(\omega)\right]$$

$$\pm\frac{i\pi}{\epsilon_o}\frac{1}{\omega-\omega'}\frac{\omega}{\sqrt{\omega^2-\Delta_o^2}} \quad ;\text{for}\begin{cases}\omega>\Delta_o,|\,\omega'\,|<\Delta_o\\ \omega<-\Delta_o,|\,\omega'\,|<\Delta_o\end{cases}$$

$$III,IV=\frac{2}{\epsilon_o}\frac{1}{\omega'-\omega}\left[\frac{\omega'}{2\sqrt{\omega'^2-\Delta_o^2}}f_2^D(\omega')-\frac{\omega}{2\sqrt{\omega^2-\Delta_o^2}}f_2^D(\omega)\right]$$

$$\pm\frac{i\pi}{\epsilon_o}\frac{1}{\omega'-\omega}\left[\frac{\omega'}{\sqrt{\omega'^2-\Delta_o^2}}\right.$$

$$\left.(+)(-)\frac{\omega}{\sqrt{\omega^2-\Delta_o^2}}\right] ;\text{for}\begin{cases}\omega'>\Delta_o,\omega<-\Delta_o\\ \omega'<-\Delta_o,\omega>\Delta_o\end{cases}$$

$$III=0 \qquad ;\text{for}|\,\omega'\,|,|\,\omega\,|>\Delta_o,\omega'=\omega$$

$$IV=\pm\frac{2\pi^2}{\epsilon_o}\frac{\omega'}{\sqrt{\omega'^2-\Delta_o^2}}\delta(\omega'-\omega) \quad ;\text{for}\begin{cases}\omega',\omega>\Delta_o,\omega'=\omega\\ \omega',\omega<-\Delta_o,\omega'=\omega\end{cases}$$

For simplicity of expressions and calculations we will take the limit of large bandwidth such that

$$f_1^\infty(\omega)=\frac{\pi}{2} \quad \text{and} \quad f_2^\infty(\omega)=0.$$

Using these results now we have

$$I,II=-\frac{\pi}{\epsilon_o}N(\omega') \qquad ;\text{for}\ |\,\omega'\,|<\Delta_o$$

$$I, II^* = -i\frac{\pi}{\epsilon_o}M(\omega') \qquad ;\text{for } |\omega'| > \Delta_o$$

$$III, IV = \frac{\pi}{\epsilon_o}[N(\omega) - N(\omega')]\mathcal{P}\frac{1}{\omega - \omega'} + \frac{\pi}{\epsilon_o}Z(\omega')\delta(\omega' - \omega) \qquad ;\text{for } \begin{cases} |\omega'|, |\omega| < \Delta_o \\ \text{of same sign} \end{cases}$$

$$III = i\frac{\pi}{\epsilon_o}[M(\omega') - M(\omega)]\mathcal{P}\frac{1}{\omega' - \omega} \qquad ;\text{for } \begin{cases} \omega', \omega > \Delta_o \\ \omega', \omega < -\Delta_o \end{cases}$$

$$IV = i\frac{\pi}{\epsilon_o}[M(\omega') + M(\omega)]\mathcal{P}\frac{1}{\omega' - \omega} + \frac{2\pi^2}{\epsilon_o}M(\omega')\delta(\omega' - \omega) \qquad ;\text{for } \begin{cases} \omega', \omega > \Delta_o \\ \omega', \omega < -\Delta_o \end{cases}$$

$$III, IV = -\frac{\pi}{\epsilon_o}[N(\omega) - iM(\omega')]\frac{1}{\omega' - \omega} \qquad ;\text{for } |\omega'| > \Delta_o, |\omega| < \Delta_o$$

$$III, IV^* = -\frac{\pi}{\epsilon_o}[N(\omega') - iM(\omega)]\frac{1}{\omega - \omega'} \qquad ;\text{for } |\omega| > \Delta_o, |\omega'| < \Delta_o$$

$$III, IV = i\frac{\pi}{\epsilon_o}[M(\omega') \; (-)(+)M(\omega)]\frac{1}{\omega' - \omega} \qquad ;\text{for } \begin{cases} \omega' > \Delta_o, \omega < -\Delta_o \\ \omega' < -\Delta_o, \omega > \Delta_o \end{cases}$$

where $N(\omega) \equiv \omega g(\omega)$, $M(\omega) \equiv |\omega| g(\omega)$, $g(\omega) \equiv 1/\sqrt{|\Delta_o^2 - \omega^2|}$. Also,

$$Z(\omega') \equiv \frac{\Delta_o^2 \epsilon_o}{(\Delta_o^2 - \omega'^2)^{3/2}}.$$

The inclusion of the previous results into equations (3.49) through (3.50) yields the equations (3.51) through (3.53) that are used to further calculate the Green function for the system with a gap.